Universidad de Oviedo

Programa de Doctorado

Energía y Control de Procesos

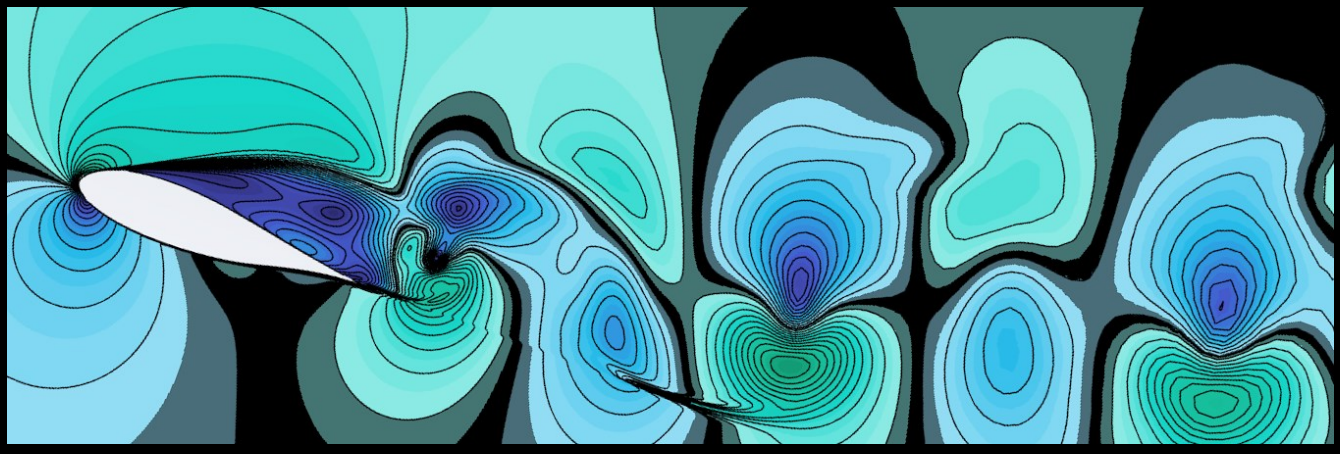

DESARROLLO Y APLICACIÓN DE PROCEDIMIENTOS EXPERIMENTALES PARA EL ENSAYO EN TÚNEL DE VIENTO DE MODELOS A ESCALA DE TURBINAS EÓLICAS DE EJE VERTICAL (VAWT)

2023

Autor:
Luis Santamaría Bertolín

Directores:
Sandra Velarde Suárez
Jesús Manuel Fernández Oro

Universidad de Oviedo

Programa de Doctorado en
Energía y Control de Procesos

DESARROLLO Y APLICACIÓN DE PROCEDIMIENTOS EXPERIMENTALES PARA EL ENSAYO EN TÚNEL DE VIENTO DE MODELOS A ESCALA DE TURBINAS EÓLICAS DE EJE VERTICAL (VAWT)

Luis Santamaría Bertolín

Directores:
Sandra Velarde Suárez
Jesús Manuel Fernández Oro

2023

AGRADECIMIENTOS

En primer lugar, me gustaría dar las gracias a **Sandra Velarde Suárez**, codirectora de esta tesis, por seleccionarme en su momento para un modesto proyecto del IUTA relacionado con las VAWT y dirigir mi TFG en esa temática. Por ofrecerme poco después el contrato de investigador, que me condujo primero al Máster de Ingeniería Energética y luego a este Doctorado. Y finalmente, por incluirme en el proyecto de TKE que ayudó en la falta de financiación de esta tesis en los últimos años. Sin duda su papel ha sido clave en la orientación de mi carrera y de no haber sido por ella, esta hubiera seguido un camino muy distinto, gracias por la confianza y por apostar por mí.

Seguidamente, me gustaría dar las gracias a **Jesús M. Fernández Oro**, también codirector de esta tesis, por sus enseñanzas, su orientación y su consejo. Por trabajar las publicaciones conmigo mano a mano, planteando los aspectos formales, poniendo el tono de catedrático y elevando la calidad de éstas. Por hacer incontables mallas, casos y simulaciones, indispensables en este trabajo. Por incluirme en el proyecto del tundish de Hyperion. Pero, sobre todo, por compartir el trabajo y el día a día conmigo tratándome como un igual, como un compañero, como un amigo. Sin su apoyo esta hubiera sido otra tesis inacabada.

Asimismo, me gustaría agradecer a **Katia M. Argüelles Díaz** su gran papel de gestión de la investigación, siempre atenta a las convocatorias de financiación, elaborando las propuestas, coordinando las reuniones del equipo y gestionando todas las compras de equipamiento y material. Y, pese a ello, ofreciendo siempre una disposición absoluta para todo, ya sea para bajar al laboratorio, o para leer bibliografía.

También me gustaría dar las gracias al resto de miembros del equipo de investigación, **Mónica Galdo**, **Bruno Pereiras**, **José González**, y, más recientemente, **Adrián Pandal**, por vuestras aportaciones y por hacerme sentir uno más del equipo, tanto en el laboratorio, como en las comidas de celebración.

Igualmente, gracias a **Eduardo Blanco**, por ser el padre de la disciplina experimental en el Área, desde los túneles de viento a las sondas, y por transmitirme tanto la devoción a esta temática, como el conocimiento y la experiencia. Así como a **Andrés Meana**, con quien di los primeros pasos en la investigación, y con quien pasé innumerables horas trabajando en el laboratorio. Por último, dentro del Departamento, me gustaría agradecer a aquellos con los que compartí la sala de becarios y mucho más; **Celia**, **Manu**, **Ahmed**, **Lee**, **Angie**, **Eva**, **Andrés**, **Alain**, y a los a los encargados de taller **Fran**, **Germán** y **Charo**, su disposición, amabilidad y cercanía.

Además, dentro de la propia Universidad de Oviedo, me gustaría dar las gracias a **Fernando Peña**, doctor próximamente también, y que ha sido mi referencia, compañero y amigo desde la carrera, con todo lo que ello implica. También, agradecer a sus compañeros del **Área de Ingeniería de Fabricación**, todo el trabajo y material que han aportado desinteresadamente a esta investigación.

En el plano personal, en primer lugar, me gustaría dar las gracias a mi pareja **Isabel Aramburu**, con quien voy de camino a cumplir 9 años, por su apoyo incondicional, por animarme en lo peor y poder ir de su mano en la más absoluta incertidumbre. Por ver las figuras de esta tesis más veces que los propios codirectores, porque pocos biólogos habrán escuchado en su vida tanto sobre ingeniería como ella. Gracias por estar ahí siempre.

Seguidamente, me gustaría dar las gracias a mis padres, **Jose Luis** y **María Luisa** por darme literalmente todo, su apoyo, un sustento, y facilitarme incluso crear mi propio hogar. Así como al resto de **Familia**, incluida la política, por su respaldo y por preocuparse tanto por mí. Finalmente, agradecer a mis **Amigos**, sobre todo a los que siguen ahí después de una pandemia y una tesis falta de financiación (que no son muchos), su apoyo también y su amistad.

RESUMEN

Tras un comienzo pausado y falto de seguimiento, la transición energética se sitúa hoy en un primer plano, siendo sus principales metas la minimización del uso de los combustibles fósiles, alcanzar un escenario de cero emisiones netas y disponer de un suministro de energía resiliente, independiente y seguro. Dentro de las acciones que se están llevando a cabo, centradas en el despliegue de energías renovables, la eólica supone un componente fundamental, siendo su principal tecnología las turbinas eólicas de eje horizontal (HAWT). Sin embargo, los desafíos actuales en este campo (despliegues en entornos offshore de aguas profundas y turbinas de gran capacidad superando los 10MW), así como las mejoras de la red eléctrica (digitalización, sistemas de almacenamiento, etc.) y las últimas tendencias de arquitectura sostenible, autoconsumo y smart-cities, abren la puerta a tecnologías alternativas como las turbinas eólicas de eje vertical (VAWT). Estas turbinas, y especialmente las VAWT de sustentación con palas rectas (H-rotor) cuentan con características muy ventajosas para este contexto, pero todavía se encuentran en desarrollo y existe una evidente falta de proyectos a escala real. Para alcanzar un estado de desarrollo que permita el despliegue comercial los ensayos experimentales en túnel de viento son una herramienta imprescindible. Sin embargo, trabajar con prototipos a pequeña escala de VAWT es especialmente difícil, debido principalmente a la reducción de un par que es ya de por sí variable. En cambio, los costes e infraestructura necesaria para trabajar con prototipos de mayor tamaño se disparan, limitando enormemente la investigación en este campo. Por ello, el desarrollo de metodología y equipamiento que permitan el estudio de estas turbinas mediante ensayos experimentales a escala en túnel de viento resulta considerablemente interesante y es el objetivo principal de esta tesis. Aunque se trata de una tesis por compendio de publicaciones, existe una clara línea conductora en este sentido, que liga las tres publicaciones presentadas, así como el resto de la tesis y las ponencias de congreso y trabajos en curso presentados en los anexos.

En primer lugar, se ha expuesto el trabajo realizado sobre prestaciones de perfiles típicos de VAWT, centrado en la evaluación y aplicación de un diseño novedoso de balanza aerodinámica para el ensayo experimental de perfiles en túnel de viento. Mediante el ensayo de diferentes prototipos y la comparación con datos de la bibliografía y simulaciones fluidodinámicas computacionales (CFD) realizadas con modelos de turbulencia recientemente desarrollados, se han comprobado sus capacidades, y se ha validado su uso para la mencionada aplicación. Además, se ha encontrado una notable concordancia en la comparación de los datos y se han proporcionado resultados interesantes sobre el flujo no estacionario. Por último, se han identificado los factores críticos que afectan a las medidas y se han propuesto mejoras para trabajos futuros.

A continuación, se ha presentado el trabajo sobre el desarrollo de una metodología innovadora para la caracterización de prestaciones de prototipos de VAWT a pequeña escala en túnel de viento, utilizando un enfoque mecánico. Este trabajo, publicado en una revista de muy alto nivel, incluye el desarrollo de una instalación experimental y la aplicación de la novedosa metodología, basada en el modo de conducción activa (ADM), al estudio de un prototipo a escala. Mediante este trabajo se ha demostrado que la metodología desarrollada muestra interesantes ventajas sobre la determinación convencional del rendimiento de la turbina mediante el modo de conducción pasiva (PDM). Asimismo, se consigue un profundo nivel de caracterización y un alto control de los ensayos con un sencillo montaje experimental, siendo aspectos clave el aislamiento de las pérdidas mecánicas del arrastre de las palas y la cuantificación del arrastre parásito de los soportes de la turbina. Los resultados experimentales se han comparado con simulaciones CFD y modelos analíticos obteniendo una notable correspondencia. Adicionalmente, se ha propuesto una corrección analítica de los modelos CFD para incluir el efecto 3D y una corrección semi-empírica del bloqueo, basada en trabajos de la bibliografía.

Finalmente, se ha presentado el trabajo sobre determinación de prestaciones de VAWT en túnel de viento a partir de medidas aerodinámicas mediante la aplicación de la teoría de Volúmenes de Control (VC), superando los típicos problemas mecánicos derivados de la pequeña escala, ya que además se trata de medidas sin contacto. Se han realizado medidas completas para varios TSR distintos, de la presión de entrada y el perfil de velocidades de la estela, así como el perfil de velocidades en el hueco inferior entre la turbina y el túnel, proporcionando información interesante sobre la naturaleza del flujo. Se ha presentado un desarrollo formal de la teoría de VC aplicada a este estudio, consiguiendo estimar a partir de estas medidas aerodinámicas, el empuje, el par y el rendimiento de la turbina estudiada. Se ha obtenido, una buena concordancia con los datos experimentales anteriores y una precisión razonable. Además, se ha realizado un análisis detallado sobre la incertidumbre, para comprobar la validez del método y prever variables críticas que requieren una precisión especial.

Adicionalmente, se han incluido 3 comunicaciones en Congresos relacionadas con la tesis. La primera, se centra en la fabricación de prototipos experimentales, donde se trata el desarrollo del prototipo de VAWT estudiado. La segunda, relacionada con las medidas aerodinámicas preliminares que condujeron al posterior trabajo sobre la teoría de VC. Y la tercera, desarrollando la corrección de flujo 3D propuesta anteriormente. Además, en esta tesis se hace una breve mención a los trabajos en curso dentro de la línea de investigación actual. Estos trabajos tratan sobre el desarrollo de un sistema modular automatizado de posicionamiento de sondas (MAPPS) de hilo caliente para la caracterización del flujo no estacionario aguas abajo de la turbina, sobre la optimización del proceso de medida con la balanza aerodinámica previamente validada y sobre la caracterización y optimización de un prototipo a escala real para entornos urbanos.

A través de los trabajos presentados, se han cumplido los objetivos de la investigación, proveyendo las herramientas necesarias para realizar ambiciosas investigaciones experimentales en este campo. Asimismo, se ha afianzado la actual línea de investigación, justificando la financiación anterior y consiguiendo nueva financiación, ambas vinculadas a proyectos de Plan Nacional. Además, los trabajos realizados han alcanzado un notable reconocimiento, siendo publicados en revistas de alto nivel, expuestos en congresos internacionales y difundidos hacia la industria en webinarios internacionales. Finalmente, gracias al amplio conocimiento generado y adquirido en el campo, se han podido proponer nuevas líneas de investigación vinculadas, para continuar el progreso hacia el desarrollo comercial de las VAWT.

ABSTRACT

After a slow start and lack of follow-up, the energy transition is now at the forefront, with its main goals being to minimize the use of fossil fuels, achieve a net-zero emissions scenario and have a resilient, independent and secure energy supply. Within the actions that are being carried out, focused on the deployment of renewable energies, wind energy is a fundamental component, with horizontal axis wind turbines (HAWT) as its main technology. However, the current challenges in this field (deployments in deep water offshore environments and large capacity turbines over 10MW), as well as improvements in the electrical grid (digitalization, storage systems, etc.) and the latest trends in sustainable architecture, self-consumption and smart-cities, open the door to alternative technologies such as vertical axis wind turbines (VAWT). These turbines, and especially the straight-bladed (H-rotor) VAWTs, have very advantageous characteristics for this context, but they are still under development and there is a clear lack of full-scale projects. To reach a state of development that allows commercial deployment, experimental wind tunnel tests are an essential tool. However, working with small-scale VAWT prototypes is particularly difficult, mainly due to the reduction of an already variable torque. On the other hand, the costs and infrastructure required to work with larger prototypes are massive, greatly limiting research in this field. Therefore, the development of methodology and equipment that allow the study of these turbines through experimental tests at wind tunnel scale is of considerable interest and is the main objective of this thesis. Although this is a thesis by compendium of publications, there is a clear guiding line in this sense, which links the three publications presented, as well as the rest of the thesis and the conference papers and works in progress presented in the appendices.

Firstly, the work carried out on the performance of typical VAWT airfoils has been presented, focused on the evaluation and application of a novel aerodynamic balance design for the experimental testing of airfoils in wind tunnels. By testing different prototypes and comparing the results with data from the literature and computational fluid dynamic (CFD) simulations performed with recently developed turbulence models, its capabilities have been verified, and its use for the aforementioned application has been validated. Furthermore, a remarkable agreement has been found in the comparison and interesting results on non-stationary flow have been provided. Finally, critical factors affecting the measurements have been identified and improvements have been proposed for future works.

Following, the work performed on the development of an innovative methodology for performance characterization of small-scale VAWT prototypes in wind tunnel, using a mechanical approach, has been presented. This work, published in a very high-level journal, includes the development of an experimental set-up and the application of the novel methodology, based on the active driving mode (ADM), to the study of a scaled prototype. Through this work it has been demonstrated that the developed methodology shows interesting advantages over the conventional determination of the turbine performance by means of the passive driving mode (PDM). Also, a deep level of characterization and a high control of the tests is achieved with a simple experimental set-up, being key aspects the isolation of the mechanical losses of the blade drag and the quantification of the parasitic drag of the turbine supports. The experimental results have been compared with CFD simulations and analytical models obtaining a remarkable correspondence. Additionally, an analytical correction of the CFD models to include the 3D effect, and a semi-empirical correction of the blockage based on works in the literature, have been proposed.

Finally, the work on determination of VAWT performance in wind tunnel from aerodynamic measurements by applying the Control Volumes (CV) theory has been presented, overcoming the typical mechanical problems derived from the small scale, since these are also non-contact measurements. Complete measurements have been performed for several different TSRs, of the

inlet pressure and wake velocity profile, as well as the velocity profile in the lower gap between the turbine and the tunnel, providing interesting information on the nature of the flow. A formal development of the VC theory applied to this study has been presented, achieving to estimate from these aerodynamic measurements, the thrust, torque and efficiency of the studied turbine. A good agreement with the previous experimental data and a reasonable accuracy have been obtained. In addition, a detailed uncertainty analysis has been carried out to check the validity of the method and to foresee critical variables that require special precision.

Additionally, 3 international conference works have been included related to this thesis. The first one is focused on the manufacturing of experimental prototypes, where the development of the VAWT prototype studied is discussed. The second one, related to the preliminary aerodynamic measurements that led to the subsequent work on the VC theory. And the third one, developing the 3D flow correction proposed above. In addition, in this thesis a brief mention is made of the work in progress within the current line of research. These works deal with the development of an automated modular hot-wire probe positioning system (MAPPS) for the characterization of non-stationary flow downstream of the turbine, with the optimization of the measurement process with the previously validated aerodynamic balance, and with the characterization and optimization of a full-scale prototype for urban environments.

Through the work presented, the research objectives have been fulfilled, providing the necessary tools to carry out ambitious experimental research in this field. Likewise, the current line of research has been strengthened, justifying previous funding and obtaining new funding, both linked to National Plan projects. In addition, the work carried out has achieved notable recognition, being published in high-level journals, presented at international conferences and disseminated to the industry through international webinars. Finally, thanks to the extensive knowledge generated and acquired in the field, it has been possible to propose new lines of research, to continue progressing towards the commercial development of VAWTs.

ÍNDICE

ÍNDICE DE FIGURAS

ÍNDICE DE FIGURAS (ANEXOS)

ÍNDICE DE TABLAS

ÍNDICE DE PUBLICACIONES

Capítulo 2:

[1] Santamaría L, Galdo Vega M, Pandal A, González Pérez J, Velarde-Suárez S, Fernández Oro JM. Aerodynamic Performance of VAWT Airfoils: Comparison between Wind Tunnel Testing Using a New Three-Component Strain Gauge Balance and CFD Modelling. *Energies* **2022**; 15 9351. https://doi.org/10.3390/en15249351

Capítulo 3:

[2] Santamaría L, Fernández Oro JM, Argüelles Díaz KM, Meana-Fernández A, Pereiras B, Velarde-Suárez S. Novel methodology for performance characterization of vertical axis wind turbines (VAWT) prototypes through active driving mode. *Energy Conversion and Management* **2022**; 258 115530. https://doi.org/10.1016/j.enconman.2022.115530.

Capítulo 4:

[3] Santamaría L, Argüelles Díaz KM, Galdo Vega M, González Pérez J, Velarde-Suárez S, Fernández Oro JM. Performance assessment of vertical axis wind turbines (VAWT) through control volume theory. Sustainable *Energy Technologies and Assessments* **2022**; 54 102811. https://doi.org/10.1016/j.seta.2022.102811.

Anexo I:

[4] Santamaría L, García M, Gharib A, Galdo Vega M, Blanco E, Fernández Oro JM, Velarde-Suárez S. Training Program for Researchers in Design and Manufacturing of Experimental Prototypes for Fluids Engineering using Additive Technologies. IOP Conference Series: Material Science and Engineering 2021; 1193 012096:1–8. https://doi.org/10.1088/1757-899X/1193/1/012096.

[5] Santamaría L, Argüelles Díaz KM, Vega MG, Velarde-Suárez S, Pereiras B, Pérez JG. Preliminary flow measurements of a small-scale, vertical axis wind turbine for the analysis of blockage influence in wind tunnels. Journal of Physics: Conference Series 2022; AICFM16. https://doi.org/10.1088/1742-6596/2217/1/012039.

[6] Santamaría L, Argüelles Díaz KM, Vega MG, Velarde-Suárez S, Pereiras B, Pérez JG. 3D flow compensation for a 2D CFD numerical model of a VAWT in confined environments with high blockage. *1st Spanish Fluid Mechanics Conference* **2022**; 139. https://sfmc22.uca.es/bookofabstracts/

CAPÍTULO 1

INTRODUCCIÓN

1.1. El panorama energético actual y el papel de las VAWT

En los últimos 20 años el contexto energético ha cambiado de manera sustancial. La transición energética hacia las energías renovables y la descarbonización empezaron de manera lenta y paulatina. Sin embargo, en los últimos años los proyectos de energías renovables se incrementaron exponencialmente, motivados por las políticas internacionales y la creciente concienciación sobre el cambio climático. Cabe mencionar, que los objetivos OB7 y OB11 de los objetivos de desarrollo sostenible (ODS) de Naciones unidas están directamente relacionados con la energía sostenible y el "European Green Deal" establece el objetivo de cero emisiones netas en EU para 2050. En 2020, la pandemia Covid-19 forzó una pausa global en la actividad y causó una importante crisis económica. Mientras que esto afectó notablemente a la demanda de combustibles fósiles, el avance de las renovables no fue detenido, sino estimulado, gracias en su mayoría, a las condiciones de los fondos de recuperación otorgados por los gobiernos de Europa y las otras grandes potencias. No obstante, aunque la capacidad renovable ha aumentado significativamente en los últimos años, también ha ido aumentado la demanda total de energía. De esta manera, aunque se ha frenado el aumento en el consumo de combustibles fósiles, la proporción de energía que proviene de este sector sigue siendo ampliamente predominante. En la Figura 1.1 se puede apreciar este recorrido, desde el panorama del año 2000 hasta el 2021, distinguiendo la progresión en el consumo mundial de los distintos tipos de energía. Además de lo anterior, resalta que en 20 años el consumo de energía nuclear apenas ha variado.

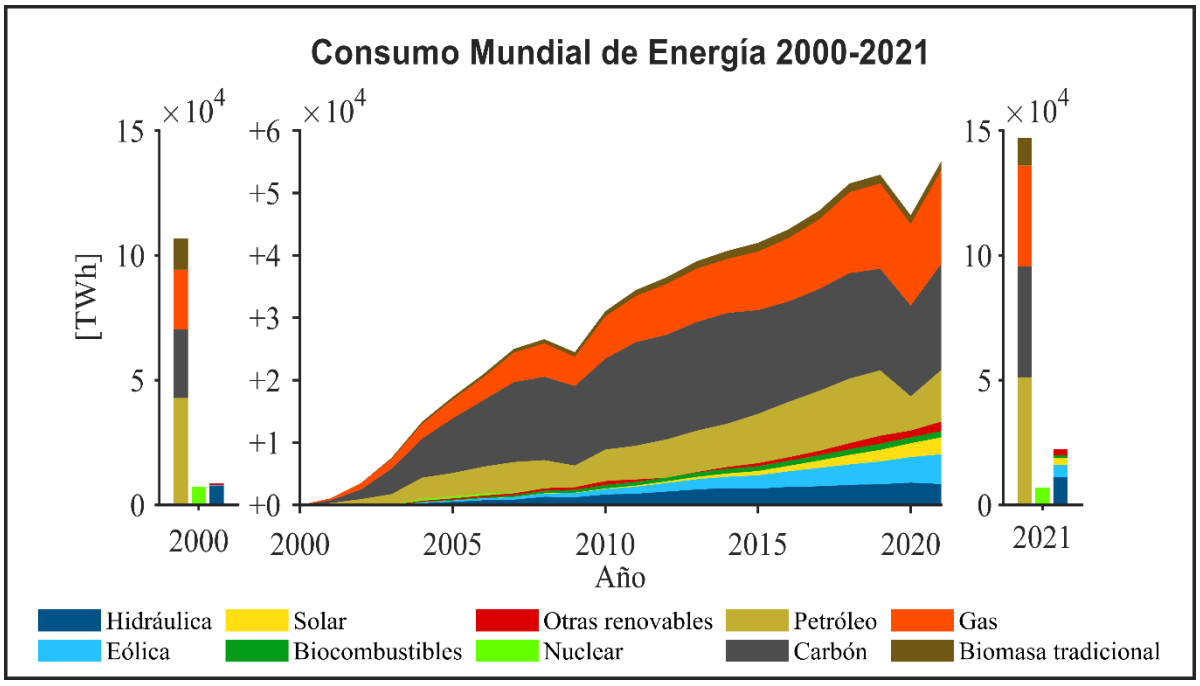

Figura 1.1. Evolución del consumo mundial de energía entre 2000 y 2021 por fuente de energía. *Datos de* [1].

En el ámbito más reciente, 2022, la complicada situación geopolítica mundial derivada de la invasión de Ucrania por parte Rusia, ha desembocado en una crisis energética de múltiples dimensiones; con los precios del petróleo, y sobre todo del gas, disparados, así como problemas para asegurar los suministros de comida y energía [2]. Esto ha provocado que la transición energética pase a un primer plano y al objetivo de fondo de la descarbonización y mitigación del cambio climático se le ha unido el importante desafío de conseguir una producción energética diversificada, independiente y segura.

Dentro de las acciones que se están llevando a cabo, lideran los despliegues de energía solar fotovoltaica y eólica. Esta última producida por turbinas eólicas de eje horizontal (HAWT) tanto en tierra como offshore, debido principalmente a la madurez de la tecnología, su fiabilidad y su bajo coste. Sin embargo, con el importante incremento de instalaciones de energía de este tipo (cuya producción es variable) la red necesita ser mejorada. Para ello, además de una importante digitalización, es necesario incluir otros sistemas que permitan estabilizarla y ajustar las curvas de oferta y demanda [3]. Así, se aprovecharían los periodos de exceso de energía para el almacenamiento, mediante centrales de bombeo, super baterías y baterías de gravedad y para la conversión a otros vectores energéticos, como hidrógeno o calor. Esta adaptación de la red abre las puertas a otras tecnologías alternativas, cuya integración en la rígida red existente resultaba poco atractiva hasta el momento. Por otro lado, estrategias como la poli-generación y los procesos energéticos integrados son cada vez más comunes, no sólo en el sector industrial [4], sino también en el residencial [5]. En este ámbito, las tecnologías alternativas de generación de energía pueden encontrar sinergias y proporcionar soluciones interesantes y rentables.

Dentro del sector eólico existen distintas tecnologías que permiten aprovechar la energía del viento, mediante su conversión a energía eléctrica. Aunque existen otras alternativas poco convencionales, como la energía eólica aerotransportada con generación en suelo (GAWE) (**Figura 1.2 (a)**) que utiliza el movimiento de cometas transmitido por cuerdas para mover un generador, comúnmente la energía eólica se obtiene mediante turbinas.

(a) (b) (c) (d)

Figura 1.2. (a) GAWE de 200kW PN-14 de SKYSAILS POWER. (b) HAWT de 4MW de Vestas. (c) Savonius de 3kW LS Helix 3.0 de LUVSIDE. (d) Darrieus original de 4MW Project Éole.

Las turbinas convencionales y con mayor desarrollo son las ya mencionadas HAWT. Particularmente, las HAWT basadas en sustentación, con: rotor tripala upwind, palas afinadas y torsionadas y mecanismos de orientación tanto del rotor, como de las palas. En estas turbinas el rotor se monta con el eje de giro paralelo al plano de la base (i.e. en la dirección de referencia del viento) y por delante de la góndola (upwind), que gira sobre la torre (**Figura 1.2, (b)**). En estas turbinas las palas se disponen con la longitud en la dirección radial, lo que causa que los momentos de flexión se concentran en la base, y que la punta de la pala experimenta velocidades de giro mucho más altas que la base. El cociente entre la velocidad de punta y la velocidad del viento se denomina TSR por sus siglas en inglés o λ y es el parámetro adimensional frente al cual se representa el rendimiento para definir la curva de prestaciones de los aerogeneradores.

Asimismo, existen también turbinas eólicas de eje vertical (VAWT), las cuales tienen su eje de giro perpendicular a la base y sus palas tienen la longitud paralela a la dirección axial. Estas turbinas a su vez pueden estar basadas: en arrastre (Savonius y derivados), o en sustentación (Darrieus y derivados). Los Savonius tienen como palas grandes superficies curvas expuestas al flujo, lo cual les proporciona un mayor par en relación a su tamaño, facilitando el autoarranque. Sin embargo, sus TSR de operación son mucho más bajos, así como su eficiencia. Aunque la aplicación convencional de estas turbinas no es la generación eléctrica si no el transporte de fluidos (por ejemplo, en sistemas de riego), existen algunos diseños con palas más complejas que sí están diseñados para este fin y se aplican en entornos urbanos e instalaciones de autoconsumo (**Figura 1.2 (c)**). Por el contrario, las turbinas Darrieus tienen palas de sección constante con forma de perfil aerodinámico, separadas del eje mediante soportes o mediante los extremos de las propias palas cuando éstas son curvas (**Figura 1.2 (d)**). Este tipo de turbinas sí está concebido para generación eléctrica y tienen TSR de operación y eficiencias notablemente superiores a los Savonius. No obstante, sus TSR de operación, y generalmente su eficiencia también, son inferiores a la de las HAWT.

Aunque las VAWT comenzaron su desarrollo en los 70, el interés por esta tecnología ha resurgido en los últimos años y sigue creciendo, principalmente en el entorno académico (**Figura 1.3**). No obstante, el colapso de varios prototipos de VAWT con potencias entre 100 y 500 kW en las décadas de los 80 y 90 propició una falta de confianza por parte de posibles inversores, que ha supuesto (y actualmente sigue suponiendo) un verdadero impedimento para el desarrollo comercial de esta tecnología [5]. De esta manera, aunque empiezan también a surgir en los últimos años proyectos de cierto calibre, todavía son muy escasos (**Figura 1.4**). Como se puede ver en esta figura, los diseños de turbinas Darrieus originales con radio variable han ido perdiendo popularidad, en favor de los diseños con palas rectas, como el que es objeto de estudio en esta tesis.

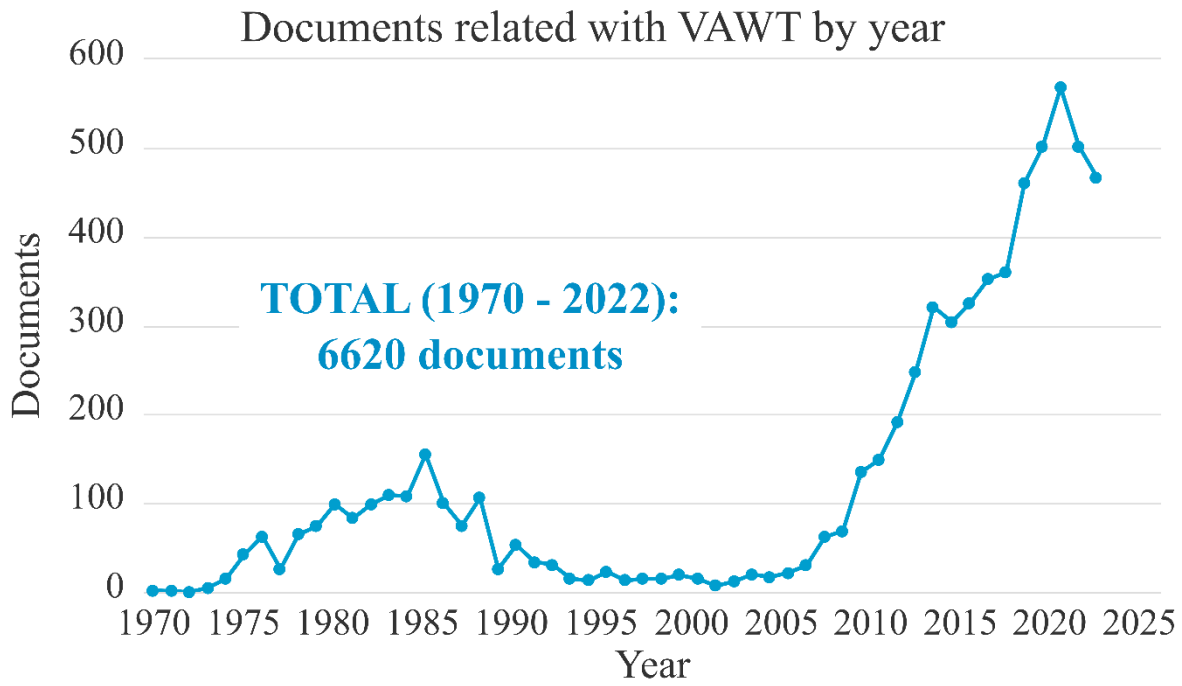

Figura 1.3. Documentos científicos indexados en la base de datos Scopus de Elsevier, relacionados con VAWT.

Tradicionalmente, al compararlas con las HAWT estas turbinas resultaban menos atractivas debido a su menor eficiencia. Sin embargo, gracias a toda la investigación que se ha llevado a cabo, se ha demostrado que se trata más de una cuestión de ámbito de uso y que estas turbinas pueden resultar competitivas en ciertas aplicaciones.

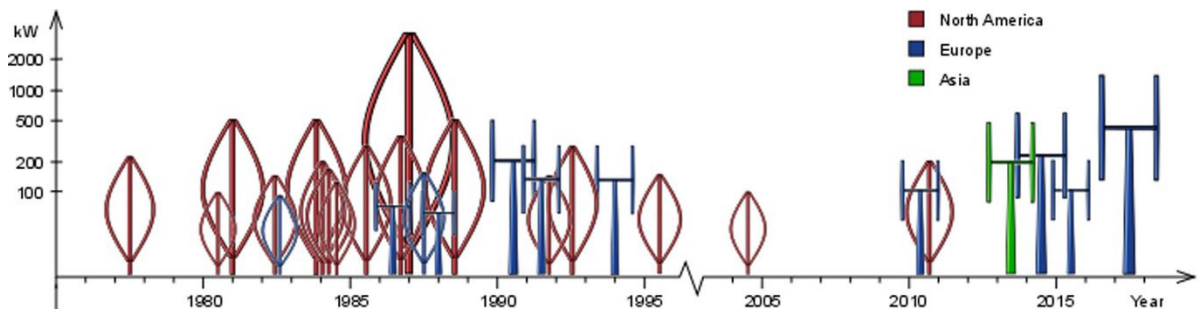

Figura 1.4. Proyectos de VAWT con potencias por encima de los 100kW desde 1970 a 2018. *Extraído de* [6].

Las VAWT gozan de omnidireccionalidad, por lo que no sólo no necesitan mecanismos de orientación si no que son capaces de funcionar mejor en condiciones de viento variable. Asimismo, su punto de funcionamiento óptimo se encuentra a menores velocidades de punta, por lo que generan menor ruido aerodinámico [7]. Por tanto, en un emplazamiento típico eólico de HAWT, como puede ser un risco descubierto, donde el viento tiene una dirección predominante y a su alrededor no hay fauna, ni personas, su aplicación no tiene sentido. Sin embargo, sus peculiaridades hacen a las VAWT especialmente interesantes para entornos urbanos o instalaciones de autoconsumo [8]. En este contexto, al tratarse de baja potencia, la eficiencia no es tan relevante como sus otras características positivas.

De igual manera, cuando se trata de diseños a mayor escala, las VAWT tienen su caja de engranajes (si la hay) y su generador a nivel del suelo, presentan un menor momento de vuelco y un centro de gravedad más bajo [9]. Estas son características interesantes para entornos offshore de aguas profundas, ya que hacen que las estructuras de soporte sean más económicas y facilitan enormemente las labores de despliegue y mantenimiento. Además, las últimas tendencias en eólica buscan aumentar la escala todo lo posible para reducir costes, lo cual supone un problema para las HAWT. A estas escalas, el perfil de velocidad del viento incidente no tiene la misma dirección en toda la altura, por lo que (al ser direccionales) estas turbinas pierden eficiencia. Además, con el incremento del tamaño del rotor, las velocidades de punta y los momentos flectores crecen notablemente, dificultando el diseño de las palas y aumentando su coste. Por último, las estelas también crecen, requiriendo una mayor área de ocupación cuando se disponen en parques eólicos [10]. Por el contrario, las VAWT no tienen estos problemas, ya que son omnidireccionales, su radio de pala es constante y su velocidad de punta menor y tienen comportamientos sinergéticos cuando se disponen cerca unas de otras [11], resultando ideales para densos parques eólicos marinos.

A pesar de su notable interés para las citadas aplicaciones, existen muy pocos ejemplos de instalaciones reales, sobre todo en entornos offshore. En entornos urbanos la comercialización de este tipo de turbinas se lleva a cabo por pequeñas y medianas empresas, ya que la baja calidad del recurso eólico, la falta de acuerdo en un diseño de máquina óptimo y la complejidad de la normativa hacen que las grandes empresas energéticas no estén interesadas [12]. No obstante, es necesario mencionar que la generación en entornos urbanos tiene otras ventajas, como la disponibilidad de infraestructuras e instalaciones aprovechables y la disminución de pérdidas en transformación y transporte debido a la cercanía del consumidor. Algunos ejemplos de empresas fabricantes y comercializadoras de VAWT para entornos urbanos, activas en 2022, son: Quietrevolution (Reino Unido), V-Air (China), Wuxi Flyt New Energy Technology (China), Hi-VAWT (Taiwán) (**Figura 1.5**).

(a) (b) (c) (d)

Figura 1.5. (a) Qr6 de Quietrevolution. (b) VisionAIR 5 de V-Air. (c) FH 2kW de FLTXNY (También comercializada en Europa por Aeolos). (d) DS-700 de Hi-VAWT.

Por el contrario, en el caso de las turbinas offshore, la falta de proyectos se debe a la gran inversión inicial necesaria y a la escasez de precedentes [6,13]. No obstante, en la actualidad el proyecto de 1MW S2x de SeaTwirl (Suecia) está en marcha, con instalación prevista en 2023 y con muy buenas perspectivas. Además, hay al menos otros tres proyectos ya en desarrollo o trabajando para conseguir inversores suficientes para salir adelante. Es el caso de: ARCUS de SNL (Estados Unidos), WorldWideWind (Noruega) y VertAx Wind (Reino Unido). Los diseños conceptuales de estas turbinas offshore se muestran en la **Figura 1.6**.

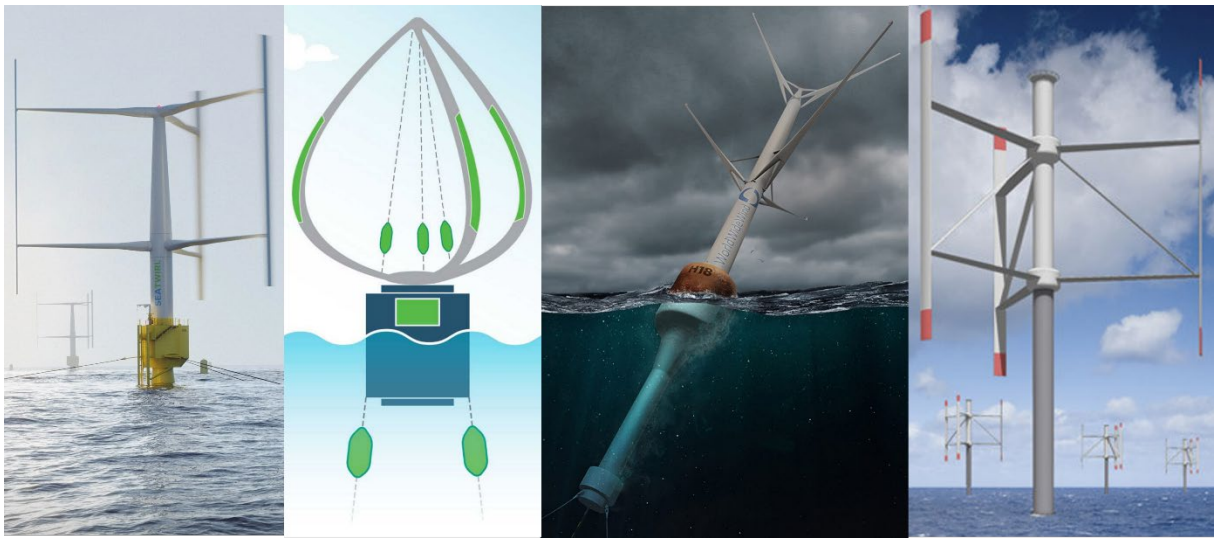

(a) (b) (c) (d)

Figura 1.6. (a) S2x de SeaTwirl. (b) ARCUS de SNL. (c) WorldWideWind. (d) VertAx Wind.

1.2. Aerodinámica y diseño de VAWT

Como se ha mencionado previamente las VAWT son una tecnología aún en desarrollo, principalmente debido a su complicada aerodinámica. Estas turbinas funcionan con flujo cruzado, por lo que pueden extraer energía del flujo, tanto en la parte de aguas arriba del eje como en la parte de aguas abajo. Sin embargo, esto viene asociado a inconvenientes como la generación de interacciones entre los álabes y las estelas de los álabes anteriores y la presencia de un factor de inducción en el flujo, que causa una desigualdad entre las velocidades percibidas en la mitad aguas arriba y aguas abajo.

Adicionalmente, los perfiles de sus palas perciben ángulos de ataque fluctuantes en función de la posición azimutal de la pala (**Figura 1.7, (a)**). Asimismo, la fluctuación de estos ángulos varía con el TSR ($\lambda = \omega R/U_\infty$, donde λ es el TSR, ω la velocidad de rotación y U_∞ la velocidad de referencia del flujo). A bajos TSR es aún mayor, llegando a alcanzar zonas de desprendimiento del flujo (**Figura 1.7, (b)**). Por el contrario, a altos λ los ángulos de ataque son muy pequeños, lo cual produce bajos ratios entre sustentación y arrastre y hace caer las prestaciones ($C_P = \frac{\omega T}{\frac{1}{2}\rho D H U_\infty^3}$, donde C_P son las prestaciones o rendimiento, T es el par producido, ρ la densidad del aire, D el diámetro de la turbina y H la altura del rotor) (**Figura 1.8**) [14–18].

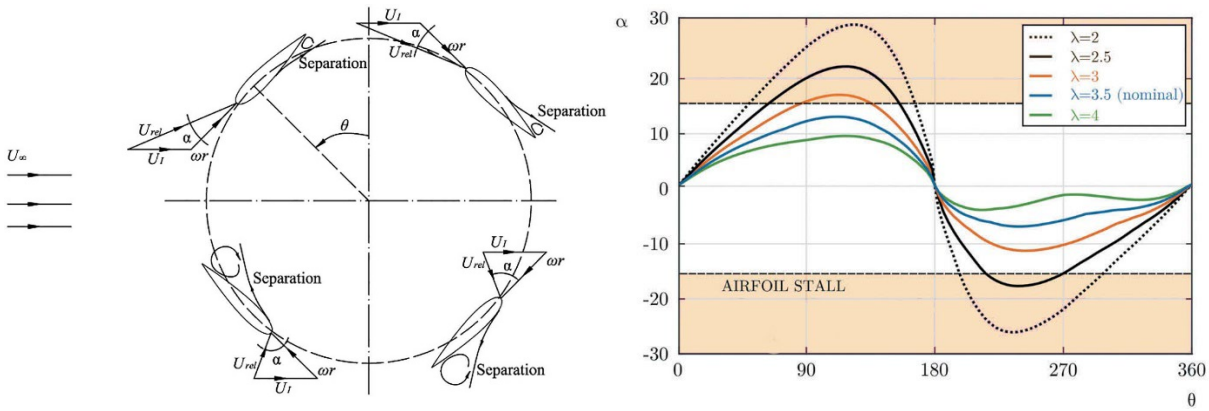

(a) (b)

Figura 1.7. (a) Angulos de ataque en función de la posición azimutal. *Extraído de* [17]. (b) Angulos de ataque en función de la posición azimutal para varios λ y zona de desprendimiento. *Adaptado de* [14].

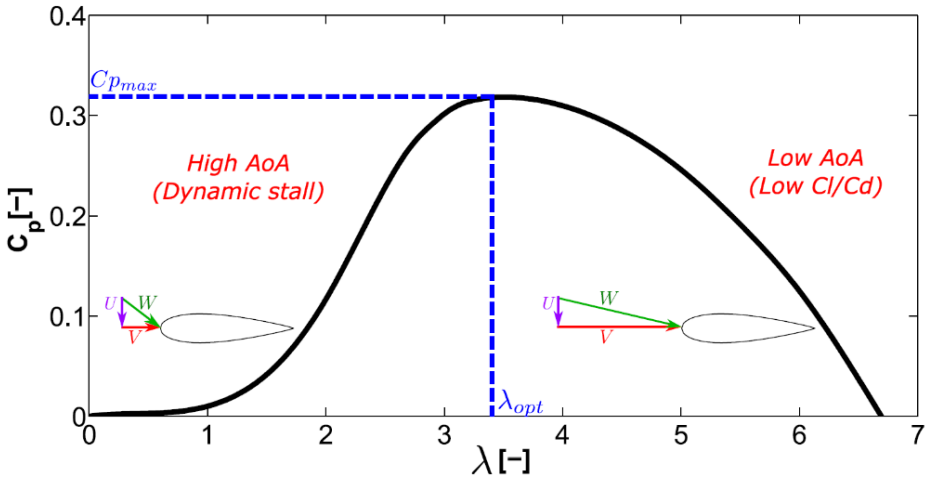

Figura 1.8. Curva de prestaciones típica de VAWT con ilustración de los triangulos de velocidades a bajos y altos λ. *Extraído de* [16].

El par se genera a partir de la suma de las contribuciones de cada pala y su promedio se obtiene a partir de la integración de las contribuciones a lo largo de la evolución angular. Mecánicamente, estos complejos aspectos del flujo se traducen en una producción de par fluctuante que dificulta la generación eléctrica y el autoarranque de la propia máquina [19]. Además, se traduce también en unos importantes esfuerzos alternativos en la estructura del rotor, que hacen a estas máquinas muy susceptibles a problemas de fatiga [18]. Por ello, un buen diseño aerodinámico es crucial para obtener una turbina fiable, eficiente y competente en las aplicaciones previamente mencionadas.

A lo largo de los últimos 20 años se ha construido una modesta base teórica sobre el diseño de VAWT y, aunque todavía existe falta de acuerdo [20] y controversia sobre el diseño óptimo, los parámetros de diseño se encuentran ya relativamente acotados [16].

De las múltiples configuraciones de VAWT basadas en sustentación, las más comunes son: palas curvas (Darrieus), palas helicoidales (Gorlov) y palas rectas (H-rotor) siendo estas últimas las que resultan más interesantes para la producción a gran escala, debido a su simplicidad, su mayor eficiencia y su capacidad para implementar estrategias de control de frenado por desprendimiento [16].

Dentro de esta configuración las principales características y parámetros de la máquina son:

- **Perfil aerodinámico.** Típicamente se elegían simétricos (por el desprendimiento alternativo entre las caras de succión y presión), pero actualmente también se adoptan no simétricos (por la diferencia de velocidades entre la zona aguas arriba y aguas abajo debido al factor de inducción) [21]. No existe consenso sobre una opción óptima, se emplean perfiles de muchas familias (NACA, DU, SAND, SELIG, FX, etc.). No obstante, en particular interesan grosores entre el 18 y el 21% y con muy poca curvatura (máx. 3%) [22]. En cuanto a sus prestaciones, es conveniente que tengan un valor modesto de coeficiente de sustentación máximo, una zona de desprendimiento abrupta y un amplio rango de bajo arrastre en función del ángulo de ataque (**Figura 1.9**) [16]. Las dos primeras características permiten un mejor control de la turbina a altas velocidades de viento, mientras que la tercera contribuye a una eficiencia competitiva. También se busca que haya flujo laminar en la mayor parte del perfil. Sin embargo, se ha sugerido que, en entornos reales, debido a problemas como la suciedad o el hielo, es difícil que se dé esta situación [23].

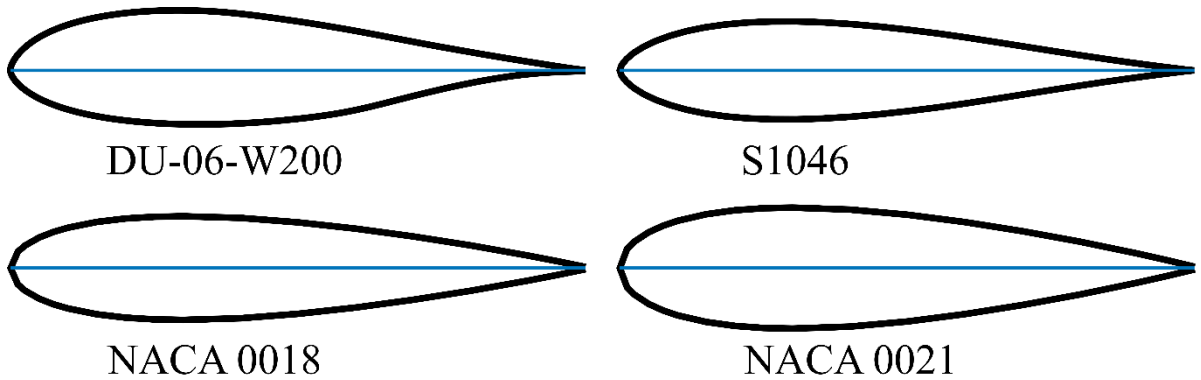

Figura 1.9. Perfiles típicos de VAWT.

- **Solidez (σ).** Determina el nivel de bloqueo al flujo de la turbina. Por un lado, este parámetro depende del número de palas (N), que en los mejores diseños puede ser 2 o 3. Los diseños bipala cuentan con mayor eficiencia, mayor rigidez estructural y menores costes de fabricación [23], mientras que los diseños con 3 palas producen un par por vuelta más constante y se ven sometidas a esfuerzos alternativos más leves [24]. Por otro lado, la solidez depende también del cociente entre cuerda (c) y radio (R), que además del bloqueo

tiene que ver con la curvatura del flujo que perciben las palas, por lo que se recomiendan valores bajos (<0.1). En consecuencia, en la mayoría de los trabajos se define la solidez de las turbinas VAWT como: $\sigma = Nc/R$. Valores elevados de solidez (>0.5) favorecen el autoarranque, pero sufren de mucho desprendimiento (TSR baja) y se reduce la eficiencia (además de tener un rango operativo mucho más estrecho) con mayor interacción entre álabes y estelas. Valores bajos de solidez (<0.2) presentan rangos más amplios de funcionamiento, pero sufren de peor autoarranque hasta llegar a TSR=3. Asimismo, experimentan mayores velocidades de rotación y por tanto más pérdidas en los soportes y las puntas de la pala. Los valores óptimos se encuentran entre 0.2 y 0.3 [22,25].

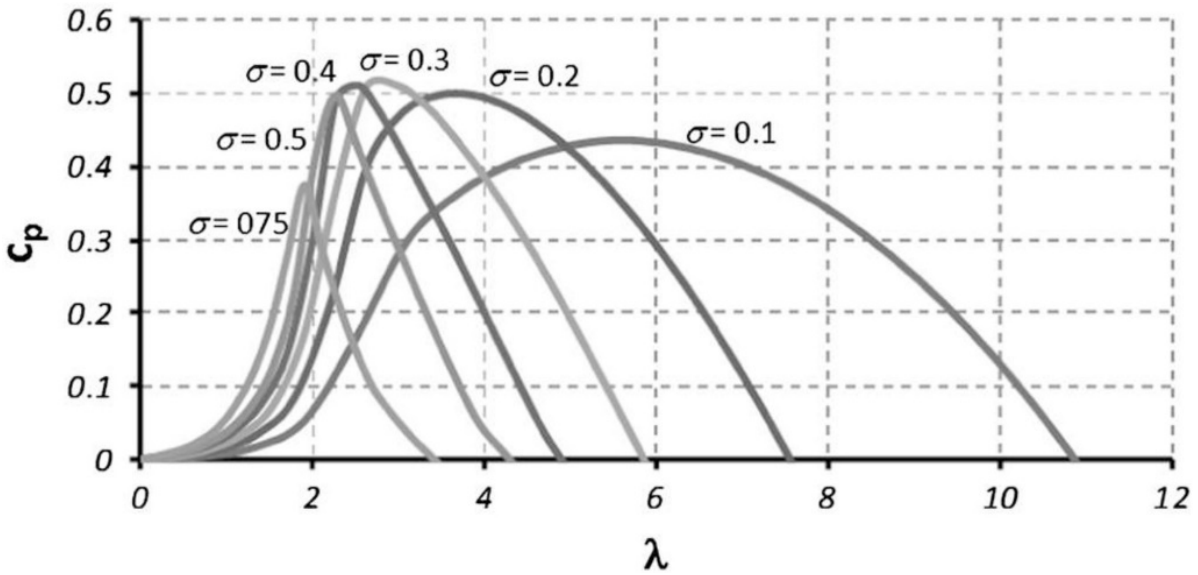

Figura1.10. Efecto de la solidez en la curva de prestaciones de una VAWT. *Extraído de* [16].

- **Relación de aspecto de la turbina (H/R).** Está interrelacionada con el ya mencionado cociente entre cuerda y radio (c/R) y la esbeltez de la pala (c/H, donde H es la longitud de la pala). A primera vista pequeños valores de H/R maximizarían el valor local del Reynolds en la pala, resultando positivo para las prestaciones de los perfiles. Sin embargo, en la realidad debido a la gran importancia de las pérdidas en la punta de la pala y la influencia de los vórtices de punta en el desprendimiento dinámico, resulta más relevante apostar por palas lo más esbeltas posibles, lo cual implica valores altos de H/R. No obstante, los momentos flectores causados por las fuerzas centrífugas aumentan con la esbeltez si no se aumenta el número de soportes, por lo que se suele buscar un compromiso, recomendándose valores de 2 a 3 [26]. También es común encontrar este parámetro definido como H/D, donde D es el diámetro, aunque los valores son proporcionales.
- **Soportes y conexión a las palas.** El diseño más recomendable utiliza dos soportes alabeados por pala, ya que éstos penalizan notablemente la eficiencia, pero son necesarios para limitar los momentos flectores, para lo cual su posición óptima se encuentra en el 20.7% de la longitud de la pala [27]. La conexión con las palas se recomienda, tanto por motivos estructurales como aerodinámicos, en el centro de presiones del perfil, que se localiza en el 25% de la cuerda. Además, esta conexión puede realizarse de manera que exista un ángulo entre la cuerda y la tangente a la circunferencia que traza la pala, encontrándose los mejores resultados cuando este ángulo es de 2º con el borde de ataque del perfil hacia fuera [28]. También hay diseños que cuentan con un sistema de ángulo variable con el que se consigue un notable aumento de la eficiencia. No obstante, esto se produce a base de incrementar sustancialmente la complejidad y los costes del diseño. Además, este tipo de sistemas puede comprometer la resistencia mecánica de la turbina y por lo tanto su capacidad de escalado, así como incrementar las necesidades de

mantenimiento [16]. Por último, es muy recomendable que esta conexión se realice de manera perpendicular a la longitud de la pala y con una transición suave entre el perfil del soporte y el de la pala.

Finalmente, a modo de resumen se incluye en la **Figura 1.9** un ejemplo de turbina que cumpliría estas recomendaciones de diseño. Nótese la similitud del diseño con la turbina S2x de SeaTwirl de la **Figura 1.6**.

Palas (N)	3
Solidez (σ)	0.25
H/R	2.6
Perfil	DU 06-W-200
Pitch (β)	-2º (borde de ataque hacia fuera)
Punto de unión pala-soporte	25% *c*

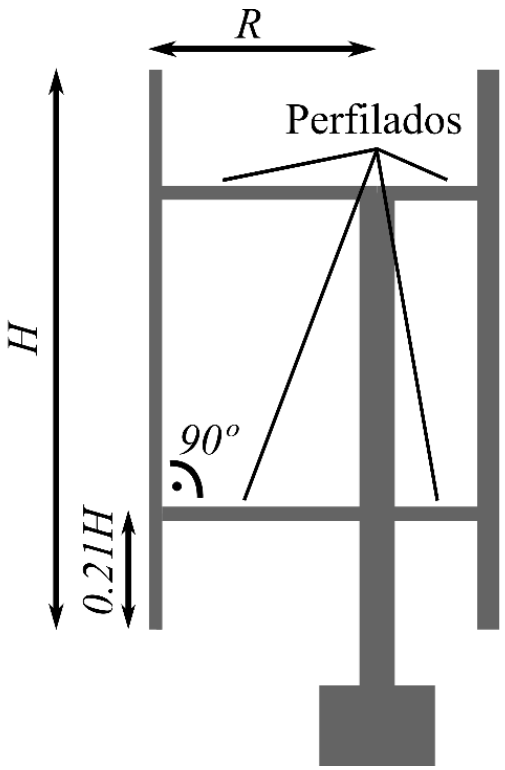

Figura 1.11. Ejemplo de diseño que cumple las recomendaciones recogidas en la bibliografía.

En cuanto a las tendencias más actuales en diseño de VAWT, éstas siguen tres vías principales [18]:

- **Dispositivos de control de flujo (FCDs).** Buscan el control de las prestaciones y especialmente del desprendimiento dinámico, mediante actuaciones sobre las palas. Pueden ser activos: sistemas de chorros, sistemas de succión de la capa límite y palas y perfiles adaptables (morphing wings); o pasivos: Gurney Flaps (GF) [29], ranuras (Dimples) [18], Generadores de vórtices (VG) [30], Winglets y puntas de pala afinadas y palas aserradas [31]. Los primeros consiguen una notable mejora de la eficiencia, pero son sistemas complejos y de coste muy elevado. Los segundos consiguen mejoras más modestas, pero son más fáciles de implementar, siendo los más susceptibles de ser incorporados a turbinas de aplicación real.
- **Dispositivos de aceleración del flujo (FADs).** Sirven para aumentar la extracción de energía, mediante la aceleración del flujo de entrada hacia la turbina empleando elementos convergentes de flujo. Pueden ser unidireccionales (lo cual limita una de las características básicas de las VAWTs) como: toberas, ductos, difusores, deflectores o directrices de entrada (IGV); u omnidireccionales (aunque aumenta notablemente su complejidad y coste) como directrices direccionales (reorientables con el viento), directrices omnidireccionales (cubren todo el perímetro) o dispositivos de flujo cruzado (aprovechando los soportes alabeados como turbina de eje horizontal) [18,32]. Adicionalmente, en entornos urbanos se buscan elementos arquitectónicos que produzcan este mismo efecto, mejorando la calidad del recurso eólico [33].

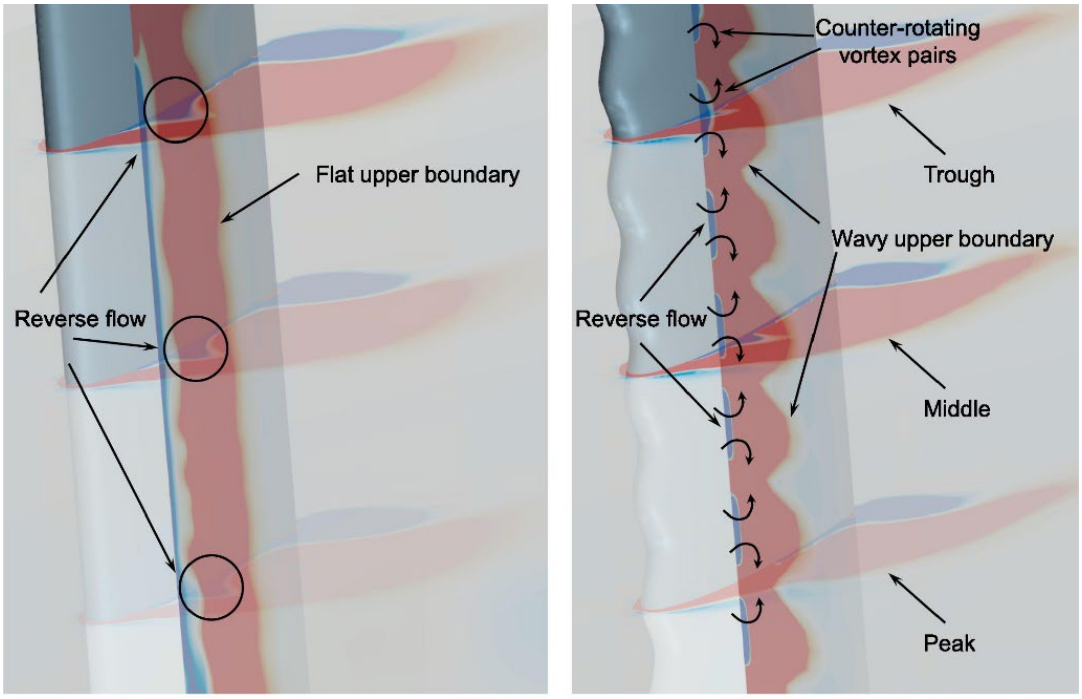

Figura 1.12. Ejemplo de FCD, puntas de pala aserradas y su efecto en el flujo. *Extraído de* [31].

Figura 1.13. (a) Ejemplo de FAD adaptado a un entorno urbano, turbina Crossflex. *Extraído de* [33]. (b) Ejemplo de FAD turbina con directrices omnidireccionales, turbina McCamley.

- **Diseños híbridos o sinergéticos.** Atacan problemas de estas turbinas, como el par fluctuante y la dificultad de autoarranque o tratan de aumentar la eficiencia. Algunos ejemplos de diseños híbridos son: turbinas que utilizan Savonius para facilitar el autoarranque o el X-rotor que genera energía mediante dos HAWT a partir de la velocidad inducida por la rotación de una VAWT. En cuanto a los diseños sinergéticos, los más conocidos son: los rotores coaxiales contrarrotantes [34], los rotores con varias etapas y los rotores contrarrotantes paralelos [11]. Estos últimos son notablemente interesantes para los parques eólicos, ya que producen un alto factor de energía por área ocupada, superior al de los convencionales parques eólicos de VAWT.

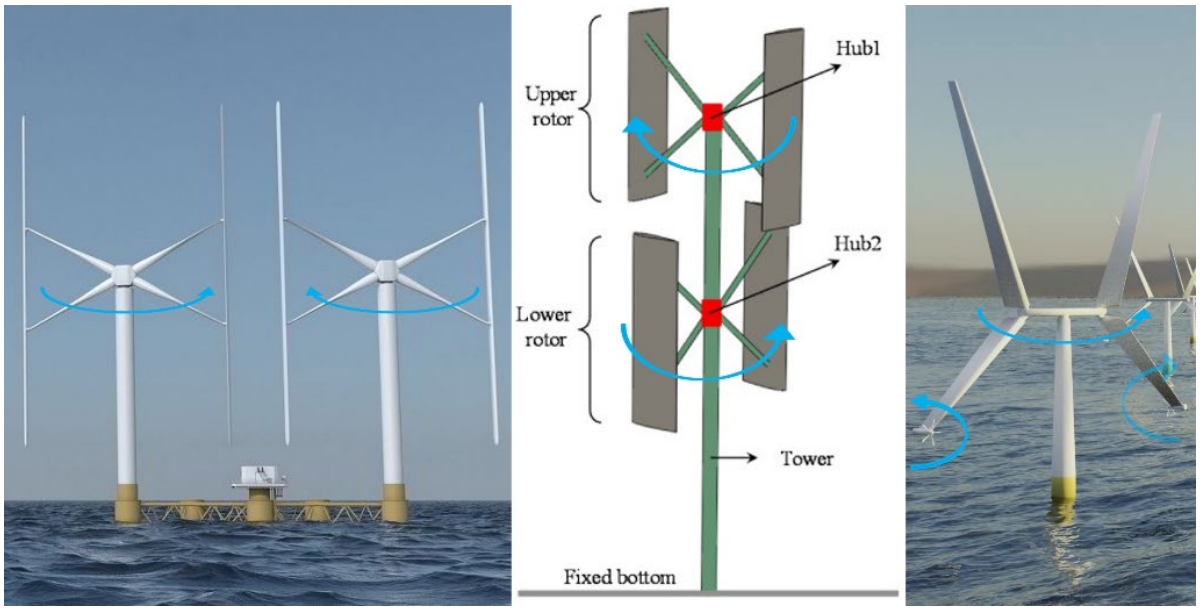

(a) (b) (c)

Figura 1.14. (a) Rotores paralelos contrarrotantes, turbina INFLOW. (b) Rotores coaxialoes contrarrotantes. *Extraído de* [34]. (c) Diseño híbrido de VAWT, X-Rotor.

1.3. El reto de la investigación sobre VAWT

El desarrollo de VAWT se lleva a cabo por tres vías principales: los modelos analíticos, los modelos fluidodinámicos computacionales (CFD) y los ensayos experimentales.

Los modelos analíticos son la opción más económica y rápida y se suelen utilizar para cálculos preliminares, ya que se basan en importantes simplificaciones. De éstos, el modelo de doble disco actuador y múltiples tubos de corriente (DMST) es el más utilizado, y cuando se combina con la teoría BEM, ofrece resultados bastante acertados [15]. Sin embargo, este recurso necesita como dato de partida las curvas de prestaciones de los perfiles aerodinámicos y proporciona poca información sobre el flujo, por lo que su aplicación es limitada. Además, para conocer el nivel de aproximación ofrecido por estos modelos es necesario contar con algún tipo de contrastación experimental.

Por otro lado, las simulaciones CFD permiten estudiar el flujo sobre un perfil independiente o sobre el conjunto de la turbina. No obstante, la precisión de las simulaciones CFD depende significativamente de la calidad de la malla computacional y de las características numéricas (esquemas temporales y espaciales) [25,35], por lo que la simulación de turbinas completas suele limitarse a las etapas avanzadas de los proyectos por sus altos costes computacionales. Así es que la dinámica típica de trabajo consiste en comenzar el estudio con simulaciones 2D de varios tipos de perfiles o por ejemplo dispositivos de control de flujo pasivo, para centrar

posteriormente el estudio en unos pocos casos y evaluar su comportamiento en un modelo 2D de la turbina completa. Finalmente, si procede, se realizaría un modelo 3D de media turbina para incluir los efectos de los soportes y los vórtices de punta. Las simulaciones CFD proporcionan información de gran valor sobre el flujo, permitiendo incluso estudiar fenómenos no estacionarios como el desprendimiento, el cual es muy relevante en las VAWT. Sin embargo, hay aspectos de las simulaciones, como la selección del modelo de turbulencia, que inevitablemente necesitan de una base bibliográfica que haya validado su uso en una aplicación similar, o en su defecto requieren validación experimental.

Los ensayos experimentales se pueden realizar al aire libre o en túnel de viento. Los experimentos al aire libre se realizan en condiciones más realistas, pero es complicado obtener datos fiables debido a la falta de control sobre las condiciones de los ensayos. Además, la fabricación de prototipos experimentales a escala real es altamente costosa y su ensayo conlleva asociados importantes riesgos. Por ello esta etapa se suele reservar para cuando ya se cuenta con un diseño muy pulido y un gran bagaje de investigación.

Finalmente, los ensayos experimentales en túnel de viento son una parte crucial del desarrollo de este tipo de turbinas. Al igual que sucedía con las simulaciones, se pueden ensayar tanto los perfiles de manera independiente como las turbinas completas. No obstante, esta técnica tiene algunos problemas intrínsecos, como la interacción prototipo-túnel (bloqueo). Para poder conseguir las condiciones requeridas en el flujo (velocidad, turbulencia) el tamaño total del túnel debería ser mucho mayor que el de su sección de ensayo. Además, los costes crecen exponencialmente con el tamaño de la sección de ensayo, lo que comúnmente fuerza a reducir la escala de los prototipos. En el ensayo de perfiles esto provoca una mayor relevancia de la rugosidad superficial [36] y una mayor dificultad para medir la resistencia aerodinámica en ángulos de incidencia bajos [37]. Asimismo, en el ensayo de turbinas, variables como la potencia o el par se reducen sustancialmente, mientras que resulta necesario aumentar otras como la velocidad de giro para alcanzar condiciones dinámicas semejantes. Debido a la reducción de escala, tanto las pérdidas mecánicas como las parásitas aerodinámicas se suelen encontrar en un orden de magnitud relevante, lo que dificulta la medida [38]. Además, las turbinas VAWT son especialmente sensibles a este problema ya que suelen presentar dificultades de autoarranque. El resultado es que la investigación experimental de calidad sobre VAWT con diseños competitivos, ha quedado típicamente limitada a los pocos laboratorios en los que se dispone de túneles de gran tamaño.

Por todo lo anterior, el desarrollo de metodologías y equipamientos experimentales que permitan ensayar prototipos a escala, tanto de perfiles como de turbinas, en túneles de viento convencionales, resulta notablemente interesante. Esto permitiría ampliar y reforzar la base de conocimiento sobre el diseño de VAWTs, además de impulsar nuevos estudios que permitan producir turbinas competitivas en las aplicaciones mencionadas anteriormente.

1.4. Objetivos de la tesis

El objetivo general de esta investigación se puede formular de la manera siguiente: desarrollar y aplicar procedimientos experimentales efectivos para el ensayo en túnel de viento de modelos a escala de turbinas de viento de eje vertical (VAWT).

Este objetivo general se puede desglosar en los siguientes objetivos específicos:

1. Diseñar y construir un montaje experimental que permita caracterizar las prestaciones de un modelo a escala de VAWT en túnel de viento, con unos costes de infraestructura e instrumentación moderados.
2. Cuantificar los efectos de bloqueo que se producen al ensayar modelos de turbinas en un túnel de viento, obteniendo unos valores adecuados para los coeficientes de corrección

que deban aplicarse en cada caso.

3. Obtener experimentalmente los coeficientes aerodinámicos asociados a los perfiles habitualmente empleados en turbinas VAWT en sus rangos típicos de funcionamiento, que no suelen estar disponibles en la bibliografía.
4. Caracterizar en detalle el flujo no estacionario aguas abajo de un modelo de VAWT ensayado en túnel de viento.
5. Aplicar las metodologías experimentales desarrolladas para la contrastación de modelos analíticos y numéricos (CFD) de VAWT desarrollados por el equipo investigador.

1.5. Estructura del documento

Este documento está estructurado de la siguiente manera:

El Capítulo 2 aborda el ensayo de perfiles de VAWT en túnel de viento, centrándose en el trabajo de validación de una balanza desarrollada para este fin. En este capítulo se presentan resultados tanto de simulaciones CFD de perfiles como experimentales de placas planas y un perfil típico de VAWT.

Posteriormente, el Capítulo 3 comprende la caracterización de prestaciones de turbinas VAWT de forma mecánica, presentando una novedosa metodología. Además, se estudia el flujo no estacionario mediante simulaciones CFD y se propone una corrección para compensar el flujo 3D y una corrección experimental para el bloqueo.

Más adelante, en el Capítulo 4 se presenta el trabajo sobre medidas aerodinámicas de la turbina y la estimación de prestaciones a partir de éstas aplicando el método de volúmenes de control. Este trabajo incluye una detallada caracterización del flujo a la salida de la turbina en relación al TSR, además de un notable desarrollo teórico y una contrastación experimental de los resultados.

A continuación, en el Capítulo 5 se recopilan y discuten los resultados obtenidos y los principales descubrimientos realizados, se argumenta el grado de consecución de los objetivos, las principales implicaciones e impacto del trabajo realizado y se plantean posibles líneas de investigación y trabajos futuros.

Finalmente, se encuentran los Anexos I y II. En el Anexo I se incluyen 3 comunicaciones en Congresos relacionadas con la tesis. La primera, se centra en la fabricación de prototipos experimentales, donde se trata el desarrollo del prototipo de VAWT cuyos resultados se presentan en los capítulos 3 y 4. La segunda, relacionada con las medidas aerodinámicas preliminares que condujeron al posterior trabajo presentado en el capítulo 4. Y la tercera, desarrollando la corrección de flujo 3D propuesta en el capítulo 2. En el Anexo II, se incluye una breve descripción de los trabajos en curso relacionados con esta tesis. Estos trabajos tratan sobre el desarrollo de un sistema modular automatizado de posicionamiento de sondas (MAPPS) de hilo caliente para la caracterización del flujo no estacionario aguas abajo de la turbina, sobre la optimización del proceso de medida con la balanza aerodinámica validada en el capítulo 2, y sobre la caracterización y optimización de un prototipo a escala real para entornos urbanos.

Los capítulos 2, 3 y 4, que incluyen las publicaciones JCR que conforman el compendio, siguen el siguiente esquema: en primer lugar, se presenta un resumen de la publicación en español, después se incluye el artículo en su versión publicada y finalmente se proveen las métricas de la revista donde han sido publicados.

1.6. Bibliografía

[1] BP. BP Statistical Review of World Energy 2022,(71st edition). [Online] London: BP Statistical Review of World Energy 2022:1–60.

[2] Agency IE. World Energy Outlook 2022. 2022.

[3] Gür TM. Review of electrical energy storage technologies, materials and systems: Challenges and prospects for large-scale grid storage. Energy and Environmental Science 2018;11:2696–767. https://doi.org/10.1039/c8ee01419a.

[4] Calise F, de Notaristefani di Vastogirardi G, Dentice d'Accadia M, Vicidomini M. Simulation of polygeneration systems. Energy 2018;163:290–337. https://doi.org/10.1016/j.energy.2018.08.052.

[5] Pinto ES, Serra LM, Lázaro A. Optimization of the design of polygeneration systems for the residential sector under different self-consumption regulations. International Journal of Energy Research 2020;44:11248–73. https://doi.org/10.1002/er.5738.

[6] Möllerström E, Gipe P, Beurskens J, Ottermo F. A historical review of vertical axis wind turbines rated 100 kW and above. Renewable and Sustainable Energy Reviews 2019;105:1–13. https://doi.org/10.1016/j.rser.2018.12.022.

[7] Balduzzi F, Bianchini A, Carnevale EA, Ferrari L, Magnani S. Feasibility analysis of a Darrieus vertical-axis wind turbine installation in the rooftop of a building. Applied Energy 2012;97:921–9. https://doi.org/10.1016/j.apenergy.2011.12.008.

[8] Chabaud A, Eynard J, Grieu S. A rule-based strategy to the predictive management of a grid-connected residential building in southern France. Sustainable Cities and Society 2017;30:18–36. https://doi.org/10.1016/j.scs.2016.12.016.

[9] Borg M, Collu M. A comparison between the dynamics of horizontal and vertical axis offshore floating wind turbines. Philosophical Transactions of the Royal Society A: Mathematical, Physical and Engineering Sciences 2015;373. https://doi.org/10.1098/rsta.2014.0076.

[10] Tjiu W, Marnoto T, Mat S, Ruslan MH, Sopian K. Darrieus vertical axis wind turbine for power generation II: Challenges in HAWT and the opportunity of multi-megawatt Darrieus VAWT development. Renewable Energy 2015;75:560–71. https://doi.org/10.1016/j.renene.2014.10.039.

[11] Hezaveh SH, Bou-Zeid E, Dabiri J, Kinzel M, Cortina G, Martinelli L. Increasing the Power Production of Vertical-Axis Wind-Turbine Farms Using Synergistic Clustering. Boundary-Layer Meteorology 2018;169:275–96. https://doi.org/10.1007/s10546-018-0368-0.

[12] Kumar R, Raahemifar K, Fung AS. A critical review of vertical axis wind turbines for urban applications. Renewable and Sustainable Energy Reviews 2018;89:281–91. https://doi.org/10.1016/j.rser.2018.03.033.

[13] Hand B, Cashman A. A review on the historical development of the lift-type vertical axis wind turbine: From onshore to offshore floating application. Sustainable Energy Technologies and Assessments 2020;38. https://doi.org/10.1016/j.seta.2020.100646.

[14] Meana-Fernández A, Díaz-Artos L, Fernández Oro JM, Velarde-Suárez S. An optimized airfoil geometry for vertical-axis wind turbine applications. International Journal of Green Energy 2020;17:181–95. https://doi.org/10.1080/15435075.2020.1712211.

[15] Sanvito AG, Dossena V, Persico G. Formulation, validation, and application of a novel 3d bem tool for vertical axis wind turbines of general shape and size. Applied Sciences (Switzerland) 2021;11. https://doi.org/10.3390/app11135874.

[16] Hand B, Kelly G, Cashman A. Aerodynamic design and performance parameters of a lift-type vertical axis wind turbine: A comprehensive review. Renewable and Sustainable Energy Reviews 2021;139:110699. https://doi.org/10.1016/j.rser.2020.110699.

[17] Zhong J, Li J, Guo P, Wang Y. Dynamic stall control on a vertical axis wind turbine aerofoil using leading-edge rod. Energy 2019;174:246–60. https://doi.org/10.1016/j.energy.2019.02.176.

[18] Zhao Z, Wang D, Wang T, Shen W, Liu H, Chen M. A review: Approaches for aerodynamic performance improvement of lift-type vertical axis wind turbine. Sustainable Energy Technologies and Assessments 2022;49:101789. https://doi.org/10.1016/j.seta.2021.101789.

[19] Bianchini A, Ferrari L, Magnani S. Start-up behavior of a three-bladed H-darrieus vawt: Experimental and numerical analysis. Proceedings of the ASME Turbo Expo, vol. 1, 2011, p. 811–20. https://doi.org/10.1115/GT2011-45882.

[20] Barnes A, Marshall-Cross D, Hughes BR. Towards a standard approach for future Vertical Axis Wind Turbine aerodynamics research and development. Renewable and Sustainable Energy Reviews 2021;148:111221. https://doi.org/10.1016/j.rser.2021.111221.

[21] Danao LA, Qin N, Howell R. A numerical study of blade thickness and camber effects on vertical axis wind turbines. Proceedings of the Institution of Mechanical Engineers, Part A: Journal of Power and Energy 2012;226:867–81. https://doi.org/10.1177/0957650912454403.

[22] Meana-Fernández A, Solís-Gallego I, Fernández Oro JM, Argüelles Díaz KM, Velarde-Suárez S. Parametrical evaluation of the aerodynamic performance of vertical axis wind turbines for the proposal of optimized designs. Energy 2018;147:504–17. https://doi.org/10.1016/j.energy.2018.01.062.

[23] Sutherland HJ, Berg DE, Ashwill TD. A Retrospective of VAWT Technology. Security 2012:1–64.

[24] Bedon G, Schmidt Paulsen U, Aagaard Madsen H, Belloni F, Raciti Castelli M, Benini E. Computational assessment of the DeepWind aerodynamic performance with different blade and airfoil configurations. Applied Energy 2017;185:1100–8. https://doi.org/10.1016/j.apenergy.2015.10.038.

[25] Rezaeiha A, Montazeri H, Blocken B. Towards accurate CFD simulations of vertical axis wind turbines at different tip speed ratios and solidities: Guidelines for azimuthal increment, domain size and convergence. Energy Conversion and Management 2018;156:301–16. https://doi.org/10.1016/j.enconman.2017.11.026.

[26] Paraschivoiu I. Wind Turbine Design: With Emphasis on Darrieus Concept. 2002.

[27] Hand B, Cashman A. Conceptual design of a large-scale floating offshore vertical axis wind turbine. Energy Procedia 2017;142:83–8. https://doi.org/10.1016/j.egypro.2017.12.014.

[28] Rezaeiha A, Kalkman I, Blocken B. Effect of pitch angle on power performance and aerodynamics of a vertical axis wind turbine. Applied Energy 2017;197:132–50. https://doi.org/10.1016/j.apenergy.2017.03.128.

[29] Yang J, Yang H, Wang X, Li N. Experimental Study of a Gurney Flap on a Pitching Wind Turbine Airfoil under Turbulent Flow Conditions. Journal of Marine Science and Engineering 2022;10. https://doi.org/10.3390/jmse10030371.

[30] Fernandez-Gamiz U, Zulueta E, Boyano A, Ansoategui I, Uriarte I. Five megawatt wind turbine power output improvements by passive flow control devices. Energies 2017;10. https://doi.org/10.3390/en10060742.

[31] Wang Z, Zhuang M. Leading-edge serrations for performance improvement on a vertical-axis wind turbine at low tip-speed-ratios. Applied Energy 2017;208:1184–97. https://doi.org/10.1016/j.apenergy.2017.09.034.

[32] Wong KH, Chong WT, Sukiman NL, Poh SC, Shiah YC, Wang CT. Performance enhancements on vertical axis wind turbines using flow augmentation systems: A review. Renewable and Sustainable Energy Reviews 2017;73:904–21. https://doi.org/10.1016/j.rser.2017.01.160.

[33] Sharpe T, Proven G. Crossflex: Concept and early development of a true building integrated wind turbine. Energy and Buildings 2010;42:2365–75. https://doi.org/10.1016/j.enbuild.2010.07.032.

[34] Poguluri SK, Lee H, Bae YH. An investigation on the aerodynamic performance of a co-axial contra-rotating vertical-axis wind turbine. Energy 2021;219. https://doi.org/10.1016/j.energy.2020.119547.

[35] Castelli MR, Masi M, Battisti L, Benini E, Brighenti A, Dossena V, et al. Reliability of numerical wind tunnels for VAWT simulation. Journal of Physics: Conference Series 2016;753. https://doi.org/10.1088/1742-6596/753/8/082025.

[36] Howell R, Qin N, Edwards J, Durrani N. Wind tunnel and numerical study of a small vertical axis wind turbine. Renewable Energy 2010;35:412–22. https://doi.org/10.1016/j.renene.2009.07.025.

[37] Selig MS, McGranahan BD. Wind tunnel aerodynamic tests of six airfoils for use on small wind turbines. Journal of Solar Energy Engineering, Transactions of the ASME 2004;126:986–1001. https://doi.org/10.1115/1.1793208.

[38] Santamaría L, Fernández Oro JM, Argüelles Díaz KM, Meana-Fernández A, Pereiras B, Velarde-Suárez S. Novel methodology for performance characterization of vertical axis wind turbines (VAWT) prototypes through active driving mode. Energy Conversion and Management 2022;258. https://doi.org/10.1016/j.enconman.2022.115530.

CAPÍTULO 2

ENSAYO DE PERFILES AERODINÁMICOS EN TÚNEL DE VIENTO

2.1. Resumen

Como se ha mencionado anteriormente, las turbinas eólicas de eje vertical son una tecnología emergente y en desarrollo que se caracteriza por su complicada aerodinámica. Las condiciones de flujo desprendido, que suelen aparecer en TSR operativas, exigen una caracterización rigurosa de los perfiles aerodinámicos para una predicción precisa del rendimiento de la turbina. Además, en el desarrollo de nuevos perfiles o dispositivos de control de flujo, el estudio individual de las geometrías constituye una etapa preliminar esencial. Para ello, el ensayo de perfiles en túneles de viento es ampliamente utilizado. No obstante, los problemas de escala, la gran diferencia entre la magnitud de las fuerzas de arrastre y sustentación y la necesidad de caracterizar las prestaciones en amplios rangos angulares donde hay condiciones de flujo desprendido, hacen que ésta sea una tarea complicada y que requiera de equipamiento especializado.

Recientemente, investigadores del Departamento de Energía de la Universidad de Oviedo han propuesto un nuevo diseño de balanza externa multi-pieza de galgas extensométricas con 3 componentes, concebida inicialmente para el estudio de los fenómenos de galloping/fluttering de placas solares con seguidores sometidas a cargas de viento. Debido a sus relevantes características, como los distintos rangos de carga en diferentes direcciones y la alta respuesta en frecuencia, esta balanza ha sido identificada como potencialmente atractiva para ensayar perfiles aerodinámicos de VAWT. Además, su reducido tamaño, escalabilidad y facilidad de fabricación, la hacen aún más interesante. En esta investigación se presenta una nueva aplicación de la mencionada balanza, incluyendo la comprobación de sus capacidades, y la validación de su uso para la mencionada aplicación.

En este trabajo se han ensayado en un túnel de viento placas planas 2D y 3D, así como el perfil aerodinámico DU06-W-200, obteniendo los coeficientes de sustentación y arrastre y los momentos de cabeceo para un amplio rango angular a Re = 200,000. Los resultados se han comparado con los datos de la bibliografía y simulaciones CFD, realizadas con el modelo de turbulencia GEKO (Generalized k-omega) recientemente desarrollado, logrando una notable concordancia. También se han analizado las fuerzas instantáneas mediante técnicas experimentales y CFD, proporcionando resultados interesantes sobre el flujo no estacionario. Por último, se han identificado los factores críticos que afectan a las medidas y se han propuesto mejoras para trabajos futuros.

energies

MDPI

Article

Aerodynamic Performance of VAWT Airfoils: Comparison between Wind Tunnel Testing Using a New Three-Component Strain Gauge Balance and CFD Modelling

Luis Santamaría, Mónica Galdo Vega, Adrián Pandal, José González Pérez, Sandra Velarde-Suárez and Jesús Manuel Fernández Oro *

Fluid Mechanics Area, Department of Energy, University of Oviedo, C/Wifredo Ricart s/n, Gijon, 33204 Asturias, Spain

* Correspondence: jesusfo@uniovi.es

Abstract: Vertical axis wind turbines are an emerging and in-development wind energy technology which are characterized by their complicated aerodynamics. Detached flow conditions, which are typically developed at operational tip speed ratios, demand a rigorous characterization of the airfoils for an accurate prediction of the turbine performance. In this work, a custom-built, three-component external strain gauge balance, specifically developed for airfoil testing, is validated. The physical reasons responsible for discrepancies with reference data are also analyzed. Two- and three-dimensional flat plates, as well as the DU06-W-200 airfoil, are tested in a wind tunnel. Lift and drag coefficients and pitching moments are obtained for a wide angular range at Re = 200,000. The results are compared with data from the bibliography and CFD simulations, performed with the recently developed GEKO (generalized k-omega) turbulence model, achieving remarkable agreement. Instantaneous forces are also analyzed with both experimental and CFD techniques, providing interesting results of the unsteady fluid dynamics. Finally, critical factors affecting the measurements are identified and enhancements are proposed for future works. In summary, a thorough evaluation of this new balance design is provided, showing its valuable potential for VAWT applications.

Keywords: airfoil testing; strain gauge balance; wind tunnel; GEKO turbulence model; vertical axis wind turbine; VAWT

Citation: Santamaría, L.; Galdo Vega, M.; Pandal, A.; González Pérez, J.; Velarde-Suárez, S.; Fernández Oro, J.M. Aerodynamic Performance of VAWT Airfoils: Comparison between Wind Tunnel Testing Using a New Three-Component Strain Gauge Balance and CFD Modelling. *Energies* **2022**, *15*, 9351. https://doi.org/10.3390/en15249351

Academic Editors: Artur Bartosik and Dariusz Asendrych

Received: 28 October 2022
Accepted: 8 December 2022
Published: 10 December 2022

1. Introduction

At the present time, humanity is focused on the achievement of a reliable, affordable, and decarbonized energy system. The accomplishment of this goal involves undoubtedly the use of renewable energy, with wind energy harvested through horizontal axis wind turbines (HAWTs) leading the way due to their mature development.

However, such objectives start to require rapid actions and deeper strategies to fulfill the established deadlines (such as a net-zero-emissions scenario by 2050 [1]). These may even include the consideration of the real-time demand curves and on-site production for self-consumption. In this regard, wind energy production in urban environments is gaining much attention. In such restrictive placements, the lift-type vertical axis wind turbines (VAWT) seem to be the best candidates for wind energy extraction [2,3] due to their omnidirectionality, avoiding the need for orientation mechanisms; their ability to work better in variable wind conditions; and their lower noise emission [4].

Nevertheless, in contrast with the well-established HAWTs, which present higher efficiencies and superior rated power, the VAWT turbines are machines still requiring a vast amount of research to overcome the crucial issues that prevent them from achieving a profitable and efficient development status [5]. First of all, their aerodynamics are far

more complicated than conventional turbines and there is no agreement yet on the best reference rotor design [6]; additionally, the application on urban environments means facing very-poor-quality wind resources [2,7]. As a result, recent efforts in this field have been directed towards increasing performance and overall energy production through the development of both flow augmentation and control devices [8]; although, the latter are even more attractive for higher-size turbines such as those for deep-water offshore environments. Therefore, a necessary first stage comprises the study of new airfoil designs (which include these characteristics) or existing airfoils in new set-ups, both requiring a precise determination of the aerodynamic properties.

To that extent, CFD methods are a highly valuable tool to improve understanding of the airflow around the turbine blades, the interactions with the flow control devices, and the effect of power augmentation devices. Moreover, they allow the analysis of different types of geometries at a lower cost. However, the accuracy of CFD simulations depends significantly on the selection of the appropriate turbulence model, computational grid construction, and numerical characteristics (temporal and spatial schemes). For that reason, experimental validation is always required. Wind tunnel testing is widely employed, although this technique faces some intrinsic problems such as prototype–tunnel interaction (blockage) which usually forces downscaling. This in turn derives from other issues, as an intensified relevance of surface roughness [9] and the increased difficulty of measuring airfoil drag at low incidence angles [10]. Furthermore, unsteady phenomena may arise due to complex aerodynamics in cases of highly loaded airfoils. This is especially relevant for VAWT turbines where high angles of attack occur, even when flow control devices are used [11]. During the regular operation of a VAWT, i.e., during a complete rotor turn, the blade angle of attack varies continuously going from positive to negative incidences of the relative incoming flow. Thus, in the pursuit of VAWT performance enhancement, or to properly design passive flow control devices, the understanding of airfoil behavior at different angles of attack is essential. To this effect, the development of accurate, reliable and affordable equipment, useful for this purpose, is inherently interesting.

Aerodynamic performance can be estimated from the integration of the pressure distributions measured with pressure taps [12] or directly with an aerodynamic balance. The first method provides more information but limits the number of geometries that can be tested, as every prototype has to be complexly manufactured to include the pressure tabs and tubes. On the other hand, while there are a wide variety of balance designs, external balances (placed outside the test section) are the most common for airfoil testing. Within external balances, two types are distinguished, single-piece (with multi-component load cells) and multi-piece (with several load cells) [13]. Single-piece aerodynamic balances are usually expensive and not commercial, as each application usually requires a specific range distribution; thus, they are custom-manufactured [14]. Meanwhile, multi-piece balances typically need more space, although in external balances, that is not commonly problematic and, thus, they are widely used [13,14].

Recently, a new design of a three-component external multi-part strain gauge balance, intended for studying the galloping of solar trackers, has been proposed [15,16]. Due to its relevant characteristics, as different load ranges in different directions and high-frequency response, this balance has been identified as potentially attractive to test airfoils. Furthermore, its reduced size, scalability and ease of manufacturing make it even more interesting for this application.

This work presents a brand-new application of the aforementioned balance, including the testing of its capabilities, and the validation of its use for the evaluation of aerodynamic performance of VAWT airfoils. For that purpose, several prototypes have been tested in a wind tunnel using the balance, including a typical airfoil (DU06-W-200) developed for VAWT applications. Moreover, CFD simulations have been performed with recently developed turbulence models for complementary analysis and comparison.

The paper is structured as follows. Firstly, the experimental set-up used is presented in Section 2, including the description of the wind tunnel, the aerodynamic balance, and measurement procedures. Then, Section 3 describes the main characteristics of the CFD numerical modeling. Afterwards, the validation procedure is presented in Section 4. Two- and three-dimensional flat plates and the DU06-W-200 airfoil are used for comparison, taking advantage of the available data in the open literature. In Section 5, the results are provided: the validation of the balance against bibliographic results is firstly presented for both the flat plates and the airfoil. In the following section, a deeper analysis is carried out with the help of CFD modelling, including the unsteady phenomena with respect to the pitching angle. Finally, after the presentation of the results, relevant conclusions and future works are provided in Section 6.

2. Experimental Methodology

2.1. Set-Up

This research was conducted in the facilities of the Energy Department of the University of Oviedo (Viesques University Campus at Gijón, Spain). In particular, a subsonic open-loop wind tunnel of 13.75 m in length and powered by a 30 kW axial fan with a diameter of 1.2 m was used for this research. It has a nozzle with a 1:12 area ratio, which provides a squared test section of 0.68 × 0.68 m^2 and allows wind velocities up to 35.5 m/s. A characteristic turbulence intensity of 0.7% for an averaged integral length scale of 0.1 m was obtained at the nozzle discharge. Although its typical configuration is arranged in an atmospheric, fully opened test section, an additional enlargement of the nozzle sidewalls was made to guarantee planar flow over the tested prototypes (discussed later in detail). A sketch of the wind tunnel is shown in Figure 1a. The test wind velocity is measured from the pressure difference in the nozzle, with a 1 in the $H_2O \pm 0.25\%$ differential pressure sensor. Note that, given the contraction ratio, velocities in the settling chamber were considered negligible.

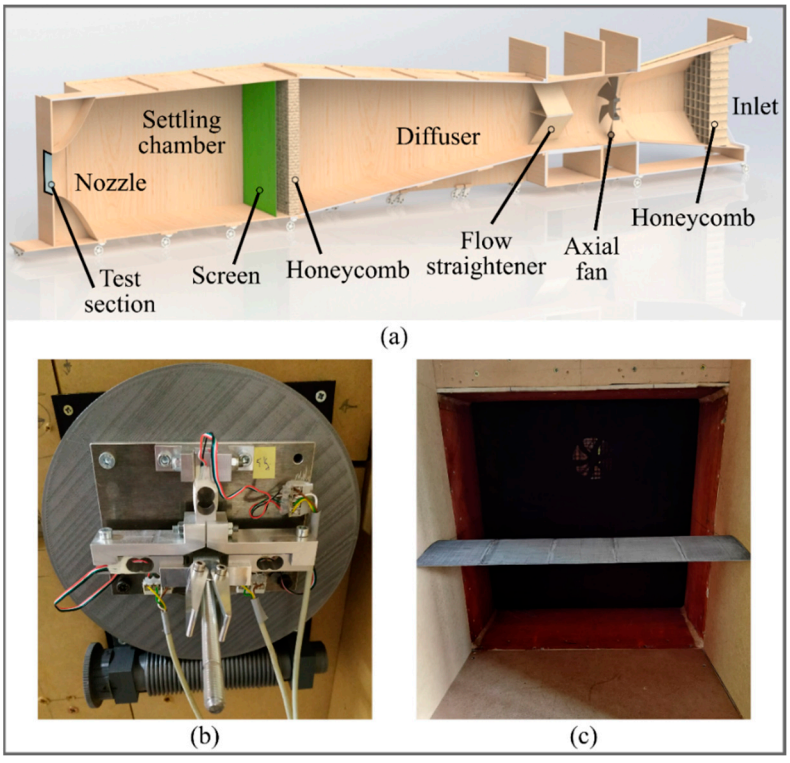

Figure 1. (**a**) Sketch of the wind tunnel (Courtesy of Angie L. Ramírez Celis). (**b**) Aerodynamic balance mounted on the mechanical orientation system. (**c**) DU06-W-200 airfoil prototype in the test section.

The custom-built aerodynamic balance under study is a strain gauge force balance with 3 components, which provides lift and drag forces and pitching moment. This balance was originally conceived to measure unsteady forces and torques on small-scale single-axis solar trackers, and successfully employed for recent aeroelastic investigations in our research group [15,16]. Precisely, the balance was designed to provide a larger range in one direction with respect to the other, which is also a very useful feature for testing airfoils where lift forces are much greater than drag forces. The balance, which rotates with the prototype to be tested, is composed of a floating axis supported by two symmetrically placed load cells, which are attached to a frame supported by the third load cell. The assembly is designed so that forces and moments outside of the measuring plane are minimized. Two different balances were built for measuring ranges within 0.75 kg and 5 kg, respectively (ranges of the single load cell direction), although the design can be easily scaled to any other quantity. Each load cell has two strain gages that are connected to the same Wheatstone bridge circuit to provide an amplified output. The voltage from the bridges is measured with a data acquisition card, which allows a measuring frequency up to 20 kHz. Note that this is especially relevant when unsteady phenomena are to be studied with this kind of device. The rotation of the balance was performed with a mechanical orientation system which granted the variation in the pitching angle using a worm gear pair (Figure 1b). The system was manufactured by fused deposition modelling (FDM) and allowed a minimum angular step of 0.5°. Finally, measurement data analysis and calculations were performed with custom MATLAB codes in a computer.

Three different prototypes were tested in the aerodynamic balance for this work: two flat plates (of different dimensions) and the DU06-W-200 airfoil (Figure 1c). One of the flat plates was designed to perform as a theoretical 3D plate, featuring an aspect ratio (L/c, where L is the span and c is the chord or width) of 3.2, which was proved to be sufficient for the purpose. On the other hand, the 2D plate had a span as wide as the wind tunnel test section (a clearance of tenths of a millimeter was left so that there is no contact with the walls) and the same width of the 3D flat plate. Note that this allowed testing both at the same wind velocity with an equal Reynolds number. Hence, the 2D flat plate had an aspect ratio of 7.2. The airfoil prototype also had a span as wide as the wind tunnel, but the chord was chosen so that, at the objective Reynolds, the obtained forces were coherent with the range of the aerodynamic balance used. Thus, the resultant aspect ratio was 3.8, which, given the results obtained, proved to be sufficient to obtain 2D airfoil coefficients over this wall-to-wall prototype. The dimensions of the tested prototypes are included in Table 1.

Table 1. Tested prototypes and dimensions.

Prototype	Span [mm]	Chord/Width [mm]	Aspect Ratio [-]
Flat plate 3D	300	95	3.2
Flat plate 2D	680	95	7.2
DU06-W-200	680	180	3.8

The three models were made of PLA and manufactured with FDM, requiring subsequent sanding and polishing to achieve an adequate final roughness. The prototypes have in their core a steel rod to increase their stiffness. This rod has a fixed support connection to the balance and cylindrical joint in the wall of the other end, avoiding movements in the measurement plane and prototype bending. The balance calibration procedure already accounts for the effect of the second support.

2.2. Balance Calibration

In order to provide quality measurements, the aerodynamic balance was calibrated before each experiment. The calibration routine employed for this work assumed a linear response of the load cells, so a direct (exact solution) method was chosen to determine the

correlation coefficients. The calibration, which implied a two-stage procedure to determine the calibration matrix, was completed under "no wind" conditions. In the first stage, the prototype was just mounted in the balance and a measurement was performed at free load, defining the zero-loading state. In the second stage, several measurements were performed with the balance loaded with known weights. Specifically, 3 load cases (LC) were carried out:

- Single load, F_{x_1}, in the horizontal direction (LC1).
- Single load, F_{y_2}, in the vertical direction (LC2).
- Combined load, obtained through a vertical load, F_{y_3}, displaced a known distance b from the axis (LC3).

From each load case, three outputs (one for each load cell) were obtained providing a 9 equation and 9 unknowns system to represent the direct correlation between loads and measured components. Matrix algebra can be applied to streamline this process in the following way.

First, a force matrix F_{LC} is defined with the three load cases, with one column for each component and one row for each load case.

$$F_{LC} = \begin{pmatrix} F_{x_1} & 0 & 0 \\ 0 & F_{y_2} & 0 \\ 0 & F_{y_3} & F_{y_3} b \end{pmatrix} \quad (1)$$

where F is the applied load, x and y are the horizontal and vertical directions, respectively, in the balance coordinate system, and b is the horizontal distance to the axis in load case 3.

With the output of the single load cell being associated with the measurements in the horizontal direction in these experiments, referred to as "signal 1" (s_1), and the other two, associated with the measurements in the vertical direction, referred to as "signal 2" (s_2) and "signal 3" (s_3), the output of the balance in the zero-loading state can be posed as a vector S_{LC_0} containing the values recorded in each load cell.

$$S_{LC_0} = (s_{1_0} \quad s_{2_0} \quad s_{3_0}) \quad (2)$$

Following this, the matrix S_{LC} is defined with the load cells' output for the three load cases, yielding:

$$S_{LC} = \begin{pmatrix} s_{1,1} & s_{1,2} & s_{1,3} \\ s_{2,1} & s_{2,2} & s_{2,3} \\ s_{3,1} & s_{3,2} & s_{3,3} \end{pmatrix} \quad (3)$$

Then, the calibration matrix K with the coefficients that relate the output of the three load cells with the forces and moment is:

$$K = \begin{pmatrix} k_{1,1} & k_{1,2} & k_{1,3} \\ k_{2,1} & k_{2,2} & k_{2,3} \\ k_{3,1} & k_{3,2} & k_{3,3} \end{pmatrix} \quad (4)$$

Finally, applying the linear response assumption, the equation system is thus stated as:

$$F_{LC} = \left[S_{LC} - S_{LC_0}\right] \cdot K \quad (5)$$

where the no-load signals are discounted as the system offset. From this matrix system, matrix K can be directly deduced as $K = [S - S_0]^{-1} \cdot F_{xyz}$, thus obtaining the direct relation between load cell outputs and measured forces.

Once the calibration matrix is determined, it can be employed to obtain the forces acting on the models from the signals measured during the operation of the wind tunnel using a generalization of Equation (5) for a single-point measurement:

$$F_{xyz} = [S - S_0] \cdot K \quad (6)$$

where F_{xyz} and S are now row vectors with three columns.

As the calibration used is a linear, two-point method, the balance was additionally tested before the aerodynamic measurements' campaign to evaluate its accuracy. Figure 2 shows the response of the calibrated balance (y-axis) to 5 different known weights in the lower part of the balance range (x-axis), where the linearity of these types of sensors is mostly critical.

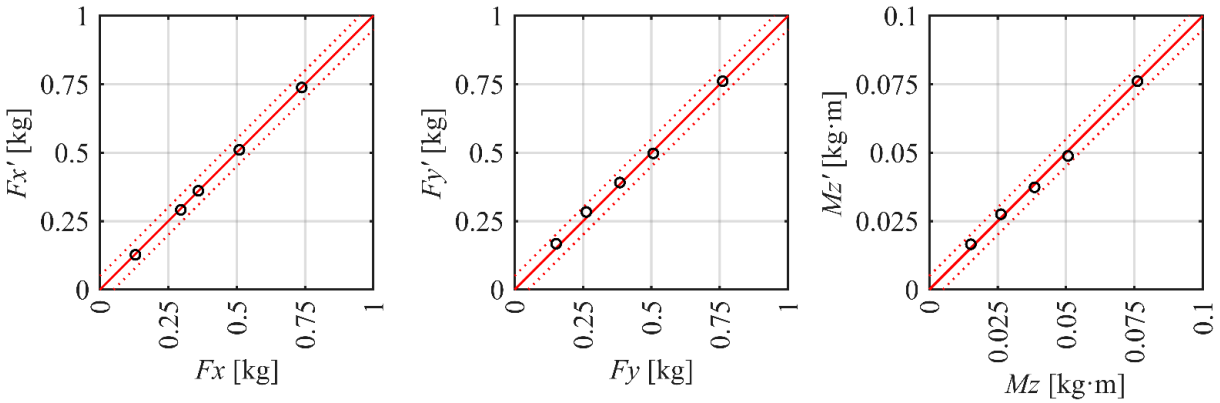

Figure 2. Balance response to a range of known weights using a two-point, linear calibration method.

The figure shows that the calibration method used provides a sufficiently accurate linear response, even for the lower part of the balance range. The response in this range is better in the horizontal direction because its range is half than the others, so it is better prepared to measure small forces. This is especially interesting to the case of airfoil testing, as drag forces are much lower than lift ones.

During the aerodynamic measurements campaign, the balance was calibrated before each experiment and tested after with known weights to validate the balance calibration. This reduces the influence of random errors produced by differences in the testing environment temperature, differences in the set-up assembly, etc. Up to 13 calibrations were performed during the campaign, providing useful statistical data of the balance performance. Table 2 shows the mean, standard deviation, maximum and median value of the relative errors between the known weights and the measured weights those 13 calibrations.

Table 2. Relative error statistics of 13 calibrations performed during the measurements campaign.

Component	Fx	Fy	Mz
$\bar{e}$ [%]	1.31	0.83	1.11
$s(e)$ [%]	1.13	0.86	1.41
e_{max} [%]	3.48	2.74	4.31
$\tilde{e}$ [%]	0.81	0.40	0.29

The mean relative error obtained was around 1%, slightly higher in the horizontal direction and slightly lower in the vertical direction. However, as the standard deviation reveals, there was some variability in the quality of the calibrations; hence, the mean is not very representative of the real performance of the balance. Note that although all 13 calibrations have been included in this analysis, a quality requirement was established in 1%. Thus, calibrations with errors above this, such as the one that achieved the maximum error shown in Table 2, were discarded and repeated. Nevertheless, as the median indicates, these discarded cases were not common and the typical balance calibration errors were about 0.8% for the horizontal direction, 0.4% for the vertical direction, and 0.3% for the moment. In these calibrations, the loads were adjusted to the expected measured

forces; hence, in contrast with the previous figure, the vertical and moment errors are lower. The higher error in the horizontal force is probably due to the higher difficulty to produce a pure horizontal load, as opposed to the simplicity of vertical loading.

2.3. Aerodynamic Measurements

With the balance already calibrated, the procedure for the aerodynamic measurements is as follows. The offset signals S_0 can be equal to S_{LC_0} or not, depending on the chosen zero-load state of reference. This aspect is especially relevant when a given pitching angle α is fixed for the prototype–balance assembly because S_0 must be measured for every particular pitch. In addition, to obtain the forces F_{DLz} in the wind coordinate system (drag and lift, see Figure 3), a base–change matrix, M_{BC}, must be applied in the following way:

$$M_{BC} = \begin{pmatrix} \cos\alpha & -\sin\alpha & 0 \\ \sin\alpha & \cos\alpha & 0 \\ 0 & 0 & 1 \end{pmatrix} \quad (7)$$

$$F_{DLz} = F_{xyz} \cdot M_{BC} \quad (8)$$

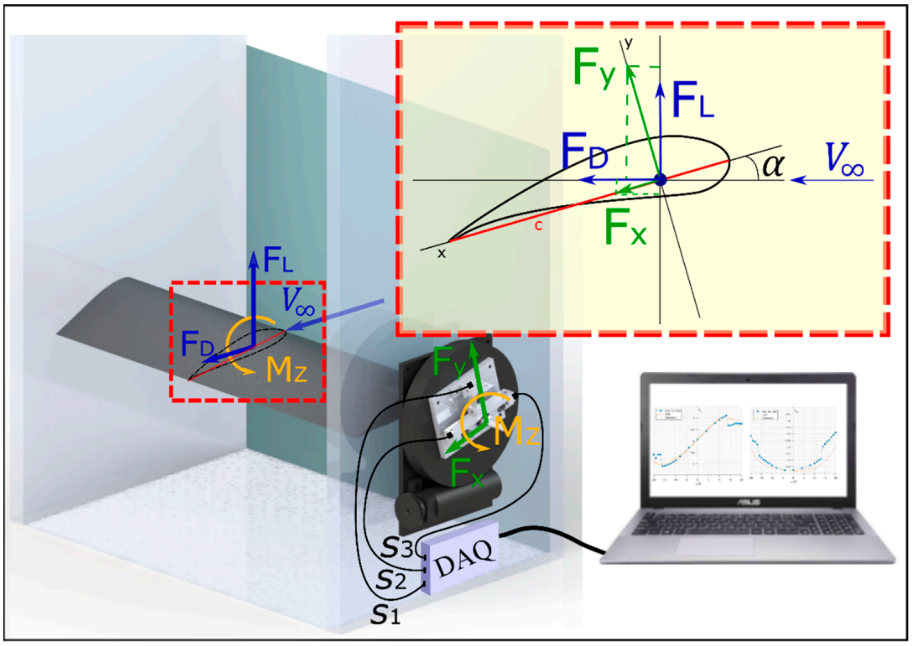

Figure 3. Diagram of the set-up with the variables and the different coordinate systems involved in the measuring procedure.

The aerodynamic coefficients can be finally obtained if the measured forces are made non-dimensional with the upstream dynamic pressure expressed as a force exerted on the prototype:

$$F_\infty = \frac{1}{2}\rho v_\infty^2 cL \quad (9)$$

leading to:

$$C_{DLM} = F_{DL} \cdot \begin{pmatrix} 1/F_\infty & 0 & 0 \\ 0 & 1/F_\infty & 0 \\ 0 & 0 & 1/F_\infty c \end{pmatrix} \quad (10)$$

where ρ is the air density, v_∞ the reference wind velocity, c is the chord/width of the prototype and L its span. The moment component must also be divided by the

chord/width again to produce the non-dimensional moment coefficient. Hence, from Equation (10), the drag, lift and moment coefficients are retrieved directly.

The three aforementioned prototypes were tested following this procedure. Particularly, both flat plates were tested at a Reynolds number ($Re_c = v_\infty c/\nu$, where ν is the air kinematic viscosity) of 130,000 from 0° to 90° of the pitching angle using a constant angular step of 10°. Complementarily, the airfoil was tested at a Reynolds number of 200,000, going from −20° to 20° with a variable angular step, for a better characterization of the aerodynamic forces during the airfoil stall. The three gauge signals were recorded during almost 15 s at a typical acquiring rate of 20 kHz, which assured a sufficient number of points to guarantee correct repeatability and accuracy in the results.

3. Numerical Modelling

A 2D numerical model of the DU-06-W-200 airfoil was implemented in Ansys-FLUENT® v2020 to obtain the aerodynamic coefficients numerically. The Reynolds-averaged Navier–Stokes equations were resolved in an incompressible approach using eddy–viscosity turbulence modelling. Both Spalart–Allmaras (S-A) and new generalized k-ω (GEKO) models were used. The one-equation S-A model [17] is widely used for external aerodynamic applications. Although it is known to provide reasonable solutions for flows with adverse pressure gradients and separation, its accuracy to predict separation is lower than optimal two-equation models such as k-ω omega SST and GEKO. In addition, all k-ω models in Ansys are implemented with a $y+$-insensitive wall treatment, avoiding the discussion concerning the optimal selection of wall formulations in k-ε models [18].

GEKO is a recent turbulence model framework (based on the ω-equation) which introduces free parameters into the equations. The main advantage is that relevant parameters can be decided and tuned by the user for given operative ranges, and without a negative impact on the basic model calibration. The main tuning parameter for the GEKO model is the coefficient C_{SEP}, which controls the boundary layer separation, predicting a more aggressive detachment if its value is increased. In the case of airfoils, it is highly recommended to use a value between 2.0 and 2.5 [19]. Furthermore, the GEKO model has been executed also with the option for scale-adaptive simulation (SAS) activated, which deploys an improved URANS formulation for the resolution of the turbulent spectrum in unstable flow conditions. The SAS concept is based on the introduction of the von Kármán length scale into the turbulence scale equation, allowing the model to dynamically adjust to resolved structures in a URANS simulation, which results in an LES-like behavior in unsteady regions of the flow field (those with flow separation).

An extended domain, with a distance to the inlet of 12.5c and a distance to the outlet equal to 20c (domain size 32.5c × 25c), in line with typical values found in the literature, was considered accurate to avoid the effect of the boundaries on the development of the flow inside the domain region (see Figure 4). A C-mesh distribution has been employed around the airfoil, resulting in a [350 × 75] cell size for both pressure and suction sides of the airfoil. An averaged value of $y+ = 1.7$ (at $Re_c = 200{,}000$) has been achieved with the first mesh point located at roughly 0.05 mm from the wall. At the wake region, a structured mesh of [300 × 150] cells was also employed, resulting in 97,500 cells for the complete 2D model. Furthermore, an additional refined mesh with [525 × 150] nodes on the airfoil walls and 247,500 cells for the whole domain was also employed to check the solution sensitivity to the grid resolution.

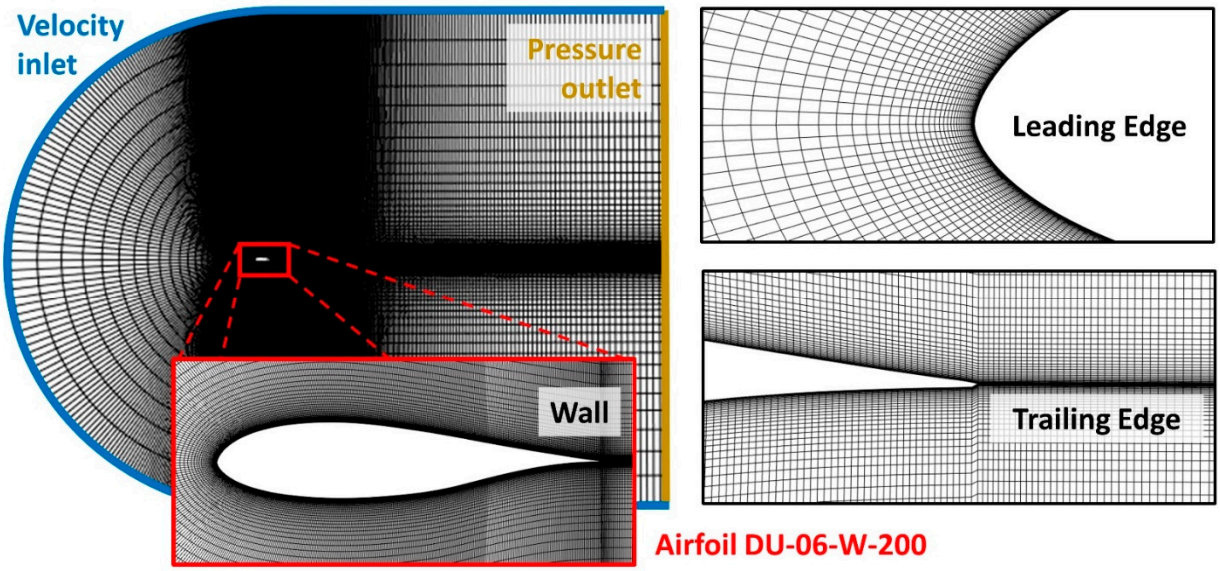

Figure 4. CFD simulation mesh detail views and boundary conditions.

The boundary conditions of the simulation domain are given in Figure 4 which includes details of the adopted mesh. A velocity inlet condition of 16.4 m/s was set at the domain inlet to match the Reynolds number (200,000) of the experimental measurements. Furthermore, up to 21 different angles of attack (*AoA*) were simulated to complete a detailed evolution of the aerodynamic coefficients, including negative and positive incidences: ±[0, 2, 4, 6, 8, 10, 12, 14, 16, 18, 20]. According to previous measurements, a turbulence intensity of 0.7% was fixed for a length scale one order of magnitude lower than the characteristic size of the test section in the wind tunnel. Both steady and unsteady simulations have been conducted, the latter necessary at high *AoA* for partially and fully detached flow conditions. A time-step size of 3×10^{-4} s was fixed in order to track the evolution of the vortex shedding with sufficient resolution. A time-averaged value of the airfoil coefficients was finally computed after periodically fluctuating regimes were achieved (typically, 50 times the airfoil chord flow-time).

The flow equations were discretized using the finite volume method with a second-order scheme for momentum and turbulent variables. Second-order accuracy was also selected in the transport equation for the pressure correction. The discretization of the temporal terms (when necessary) corresponds to a bounded second-order implicit formulation. The SIMPLE algorithm was used for the pressure–velocity coupling for all studied cases. Spatial discretization regarding gradient terms was selected to be the least-squares cell-based discretization. Finally, a convergence criterion of 10^{-6} was fixed for the velocity components of the momentum equation, while a minimum threshold of 10^{-5} was at least required for the rest of the equations. Simulations were performed using a four-node Intel Core i7-52820K at 3.3 GHz and 64 Gb RAM, with characteristic CPU times of 75 min for every execution (1 day of CPU time to complete the whole angular range) in the case of the refined mesh.

4. Validation Data Sources

4.1. Flat Plate Data

The available data in the bibliography for the lift and drag coefficients in 2D and 3D flat plates have been obtained from [20]. This reference shows how the force on a flat plate can be calculated from the aerodynamic coefficients. The different data are provided for Reynolds numbers greater than 10,000 with an estimated precision of ±5%. Specifically,

the aerodynamic coefficients on a flat plate of infinite span (2D) were obtained by applying the experimentally modified Kirchhoff and Rayleigh theory of discontinuous motion shown in the works of [21] and [22]. The coefficients for flat plates in three dimensions, presented in the equations shown by Blevins, were originally extracted from the experimental measurements presented by [23].

4.2. DU06-W-200 Airfoil

This airfoil was specifically designed for vertical axis wind turbine applications, with the objective of improving the self-starting abilities of this type of turbine. The available aerodynamic data of the DU06-W-200 airfoil in the literature, used to contrast the obtained results in the present database, are found in [24]. This source provides experimental work performed in the Low Turbulence Tunnel (LTT) at the Technical University of Delft. This wind tunnel has a 1.25 × 1.8 m test section and can achieve a maximum wind speed of 120 m/s. The tested model was made of solid aluminum with a 1.8 m span (the whole section width) and a chord of 0.25 m, and the aerodynamic coefficients were obtained with a six-component external balance. Two types of results are presented: "clean", corresponding to the bare airfoil in the wind tunnel with around 0.02% turbulence, and "dirty", which is the same testing conditions, but the airfoil features a zig-zag tape at 5% of the chord, simulating a much more turbulent test environment. From the available results, those corresponding to a Reynolds number of 300,000 have been chosen as a reference, as they are the closest to our experimental dataset.

5. Results

In this section, the results of the different tests are presented. Particularly, the results have been divided depending on the type of prototype used in the test: flat plate or DU06-W-200 airfoil.

5.1. Flat Plate

The aerodynamic coefficients (C_D, C_L) obtained with the flat plates are shown in Figure 5, compared with the data from the bibliography. Experimental curves are plotted with red discontinuous lines, using triangles for the 2D flat plate and squares for the 3D flat plate. On the other hand, 2D and 3D flat plate data from the bibliography are plotted with green and blue dotted lines, respectively.

The drag coefficient (top plot) exhibits a remarkable agreement for both flat plates in the whole angular range, with a very slight drift at high pitching angles. Complementarily, the lift coefficients (bottom plot) also show a good overall agreement, although with some overestimation for angles smaller than 20 degrees. This can be attributed to the lack of a complete symmetry between both pressure and suction sides of the plates. In fact, only the pressure sides are completely flat, because of a slight engrossment of the suction side at the mid-chord to accommodate a sufficiently robust shaft. Thus, at low pitching angles, when the flow is still attached, this geometrical defect raises the pressure difference between both sides leading to an increase in the lift force. However, at higher pitching angles, the flow in the suction side is completely detached and the experimental data matches the reference data with especially accurate results for the 3D flat plate. Despite the experimental lift coefficients for the 2D flat plate being slightly above the bibliography, the global trend is perfectly reproduced. The overall result suggests an accurate and precise performance of the balance, thus postulating it as a good candidate for airfoil testing.

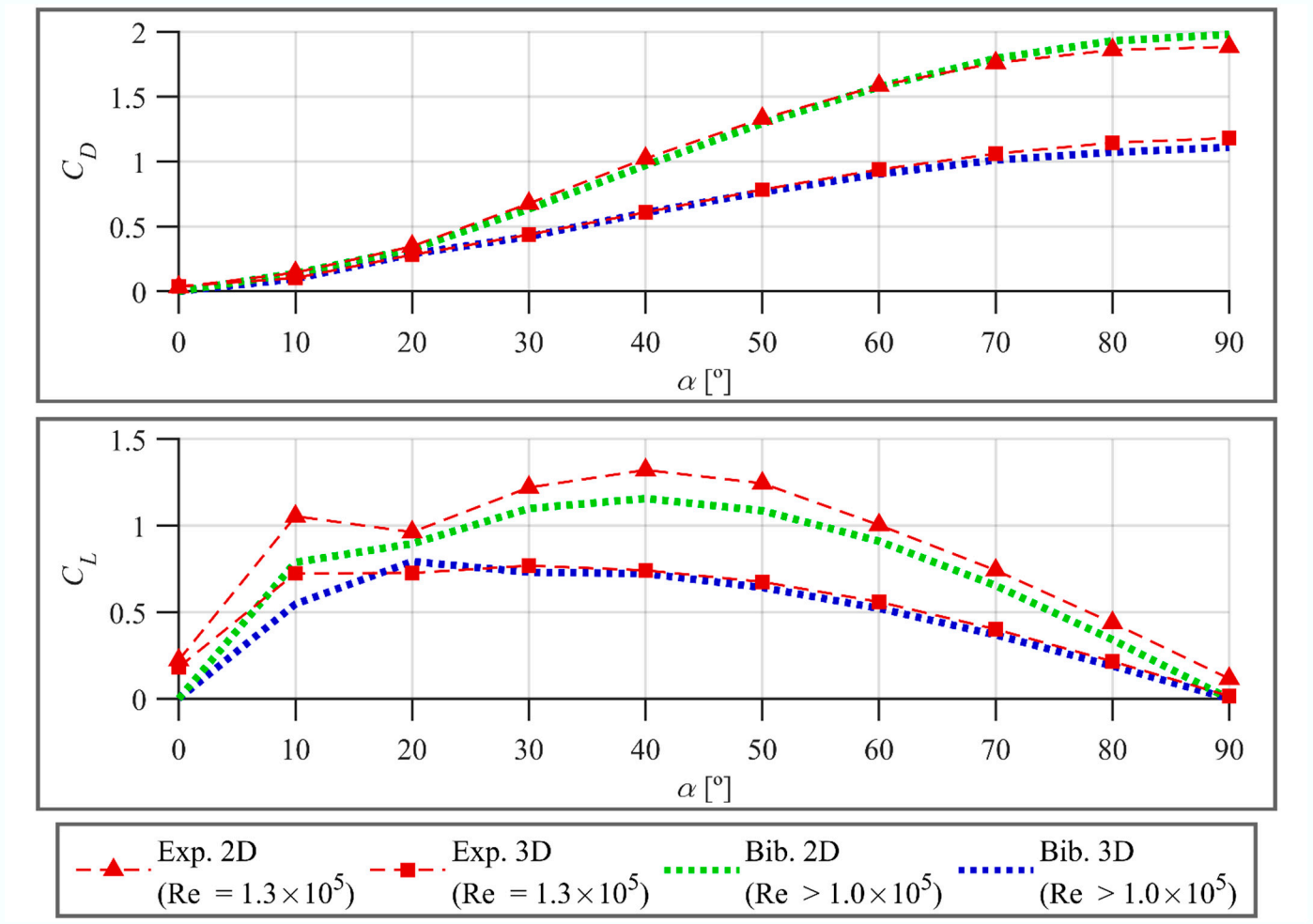

Figure 5. Experimental drag and lift coefficients from 2D and 3D flat plates compared with data from the bibliography.

5.2. DU06-W-200 Airfoil

Figure 6 shows the comparison of the experimental coefficients (C_D, C_L) of the airfoil measured with the aerodynamic balance and the data from the bibliography. Experimental data from this work are plotted with a red discontinuous line and triangle markers. Up to six complete tests were repeated in an effort to properly characterize the hysteresis zone related to the flow separation. Thus, in this figure, the markers and discontinuous line show the averaged coefficients from all the tests, while the light-red area bounds the maximum and minimum dispersion in the results.

Regarding the drag coefficient (left plot), the obtained results are significantly higher than those from the "clean" dataset. This can be easily related to the big difference in the mean turbulence level (about 35 times) between both wind tunnels. Nevertheless, the obtained results match remarkably well for the "dirty" dataset, with the exception of the range of low positive angles, in which the obtained coefficients are higher. The reason of this discrepancy may probably lie in the presence of a light dimple in the airfoil shape, close to the leading edge at the pressure side. This defect is a consequence of the deburring of the seam scar produced in the layer shift as the airfoil is 3D-printed. That irregularity may be triggering turbulence transition on the airfoil (precisely in the stagnation point) and, thus, increasing the drag artificially. Furthermore, additional polishing of the area has also slightly modified the local slope of the airfoil, leading to a mismatch with respect to the original geometry.

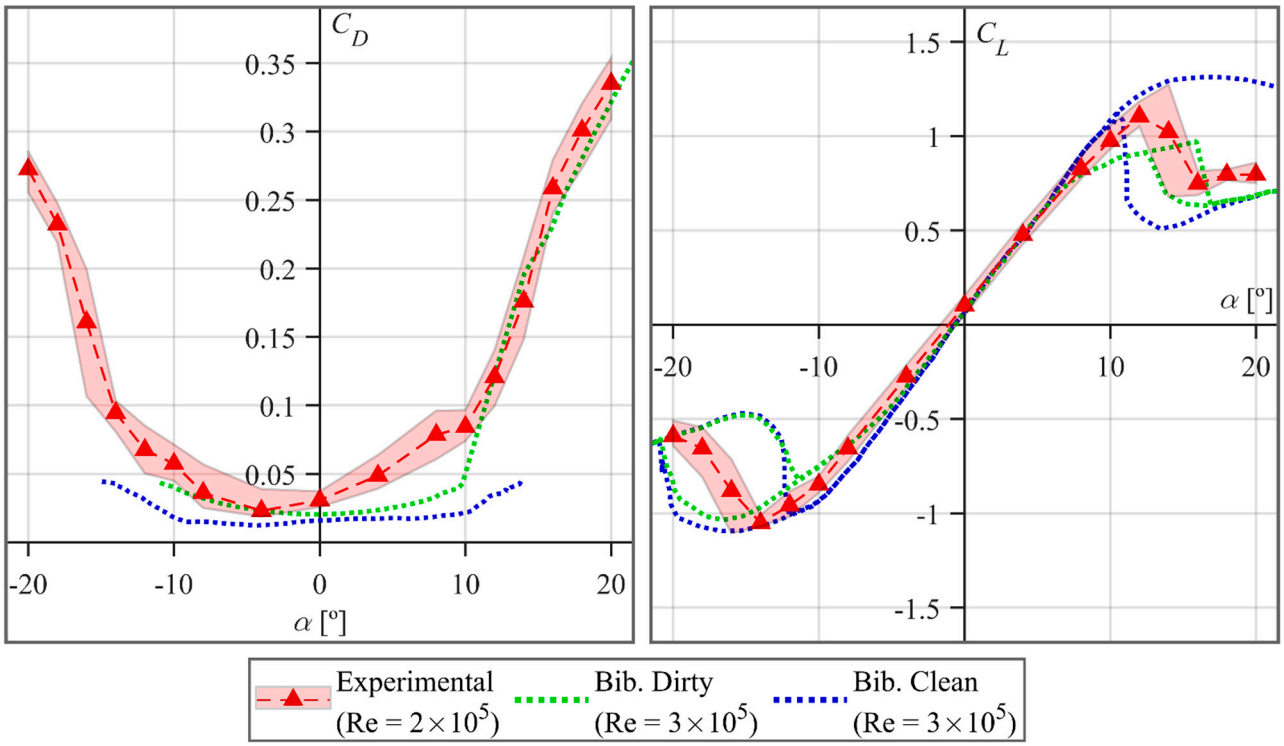

Figure 6. Experimental drag and lift coefficients from airfoil DU06-W-200 compared with data from the bibliography.

Meanwhile, the lift coefficient curves (right plot) overlap perfectly for all the datasets at low pitching angles (−6° to 6°), where the flow is completely attached, and the incoming flow turbulence is not relevant. However, at higher angles (−6° to −11° and 6° to 10°), the "clean" dataset bounds the maximum magnitude of the lift, with the obtained experimental results slightly below and the "dirty" dataset starting to decay due to the early flow separation. At negative angles of attack, both "clean" and "dirty" datasets maintain a slow and progressive detachment when the pitching angle is increased, until they finally drop at −20°. On the other hand, the experimental data from this work drops earlier at −16°, after achieving the maximum magnitude of the negative lift. Although our experiments have in fact not been performed to describe the hysteresis cycles, it is significant that the dispersion of the results resemble that phenomenon to some extent. Hence, the width of the hysteresis loop in the reference data is much higher than in the experiments, which practically crosses through the middle, dividing the others in half. This also occurs with the positive side of the curve. However, here, the difference between the lift drop of the "clean" dataset and the two others is much higher with the first one dropping outside the shown range (~22°) and the other two around 14°~15°. Furthermore, despite the experimental data achieving almost the same maximum lift coefficient as the "clean" dataset, the drop zone and hysteresis loop width match better the "dirty" dataset. The existence of a boundary layer on the side walls of the tunnel generating 3D effects at the ends of the tested wing may affect the hysteresis of flow separation on the wing. This could be the reason for the observed large differences between the experiment and CFD calculations at large angles of attack.

Considering the overall results, the aerodynamic balance used in this experiment clearly exhibits a notable accuracy, being able to reproduce the reference dataset both in drag and lift coefficients, and clearly characterizing the flow separation.

A further analysis of the experimental data obtained is discussed with the help of the CFD simulations performed. In Figure 7, the experimental coefficients are compared with the results from CFD simulations for different turbulence models and simulating condi-

tions. Specifically, results from the simulation with the Spalart–Allmaras (S-A) model executed in a steady fashion are represented in dark gray, those computed steadily but for a generalized k-ω (GEKO) model are shown in green, whereas the GEKO unsteady simulations are shown in blue, distinguishing between the coarse mesh (light-blue discontinuous line) and the extra refined mesh (dark-blue continuous line).

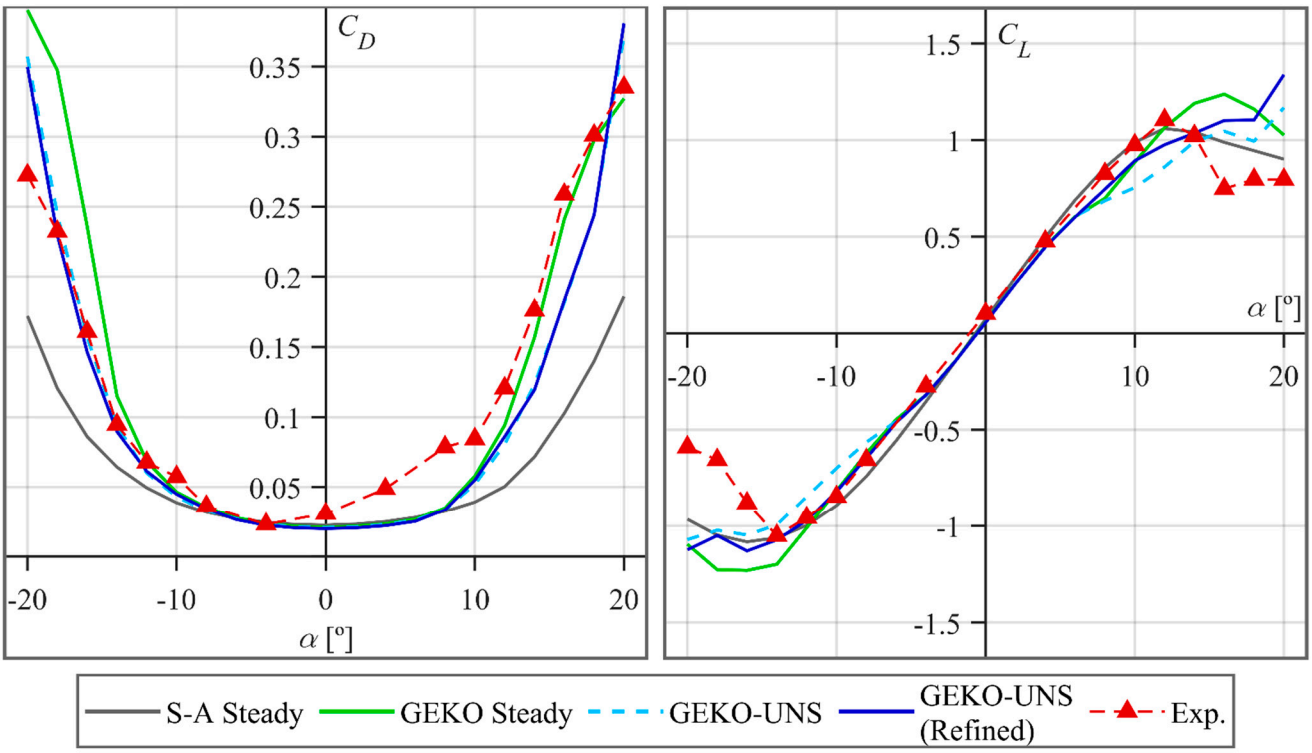

Figure 7. Experimental drag and lift coefficients from airfoil DU06-W-200 compared with results from CFD simulations for different turbulence models.

Despite the simplifications of the S-A steady simulation, it performs remarkably well in reproducing the lift curve, with only a slight underestimation of the maximum. However, it is clearly unable to predict an accurate drag overshoot. On the other hand, the set of GEKO simulations produce subtle different results among them. The GEKO steady simulation significantly improves the results compared with the S-A, accurately characterizing the drag overshoot as well as the lift curve. Nevertheless, it overestimates both drag and lift magnitude at negative wide angles (−12° to −20°). The results from the GEKO unsteady simulation and with the coarse mesh are enhanced, but show that the initial mesh is not sufficiently accurate to reproduce the lift curve when flow separation starts to be significant. In fact, it is still poorly predicting important flow features when the airfoil stalls, such as the instabilities of the boundary layers and the shedding of trailing vortexes. This is clearly improved with the extra-refined mesh, which produces the best results, especially for negative angles of attack. Yet, it still fails to predict accurate lift drops in the case of fully detached flow.

Since no data were found in the bibliography for the pitching moment, the experimental results have been directly compared with the GEKO unsteady simulation for the refined mesh in Figure 8. Furthermore, as a preliminary approach to evaluate unsteady capabilities of the aerodynamic balance, the RMS value of the fluctuations in the moment coefficient is also represented (dispersion bars) and compared in the figure. In this case, instead of presenting the averaged statistics of the whole dataset as before, only a single measurement has been used to ensure that these fluctuating results are consistent.

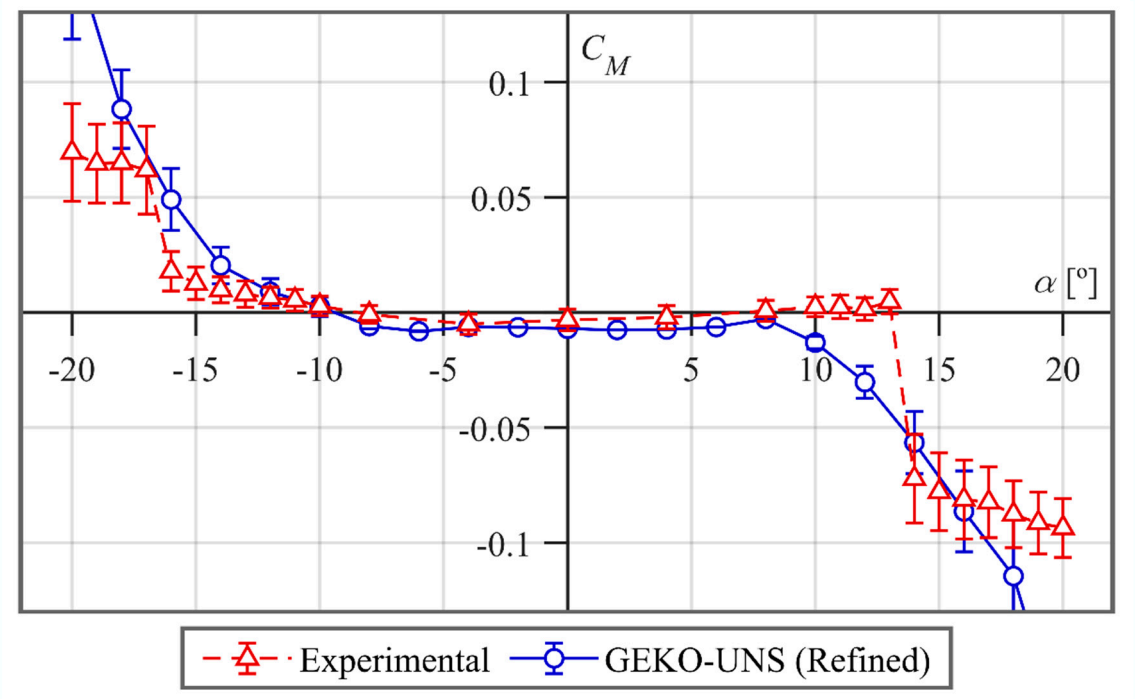

Figure 8. Experimental moment coefficient and fluctuating moment coefficient from airfoil DU06-W-200 compared with results from the best unsteady CFD model.

As expected, the moment coefficient for low pitching angles, which it is practically zero, matches perfectly between experiments and numerical results (solid and dashed lines). This is coherent with the hypothesis of the airfoil having the center of pressure approximately at 25% of the chord (the same location for the origin of coordinates in the CFD and for the center of the shaft in the experimental prototype). However, as pitching angles increase (both in negative and positive directions), the CFD model predicts a smooth, exponential-like rise in the coefficient magnitude, while the experimental results show a more drastic drop at −16° and 13°, followed by a moderate, linear-slope increase.

In the case of the RMS values, a very low level can be appreciated in the experimental data at low pitching angles. Likewise, the CFD model converges to a unique solution as there is no unsteadiness in the simulations. The flow separation can be easily identified in the figure by the sudden increase in the fluctuations in the experimental dataset, although in the CFD, there is a more progressive increase. Precisely, it was necessary to activate unsteady computations in the CFD model beyond ±8° of AoA to account for the inherent unsteadiness of the detached flow. This comparison also reveals that the dynamic sensitivity of the balance is enough to perceive the amplitude of the fluctuating forces, despite the structural damping of the wing model. Conversely, accurate frequency values are not feasible due to the high stiffness of the set-up, thus avoiding a complete fast response of the measurements.

For a deeper understanding of the unsteady phenomena involved in these fluctuating forces, the velocity field, pressure coefficient (defined as $C_p = 2(p - p_\infty)/\rho v_\infty^2$), and spectra of the fluctuating moment have been analyzed in detail for four positive pitching angles (8°, 12°, 16° and 20°) using the data from the refined GEKO unsteady simulation. The results are shown in Figure 9. The instantaneous velocity field at a particular instant in the simulation is represented on the left part of the figure in non-dimensional terms with respect to the upstream velocity. Meanwhile, on the upper-right plot, the pressure coefficient along the airfoil chord is represented for both suction and pressure sides at that same instant. In addition, shadowed areas have been introduced to illustrate how the coefficient is oscillating during a complete shedding cycle. Finally, on the right lower part,

the amplitude and oscillating frequency of the moment coefficient are shown, identifying the peak values.

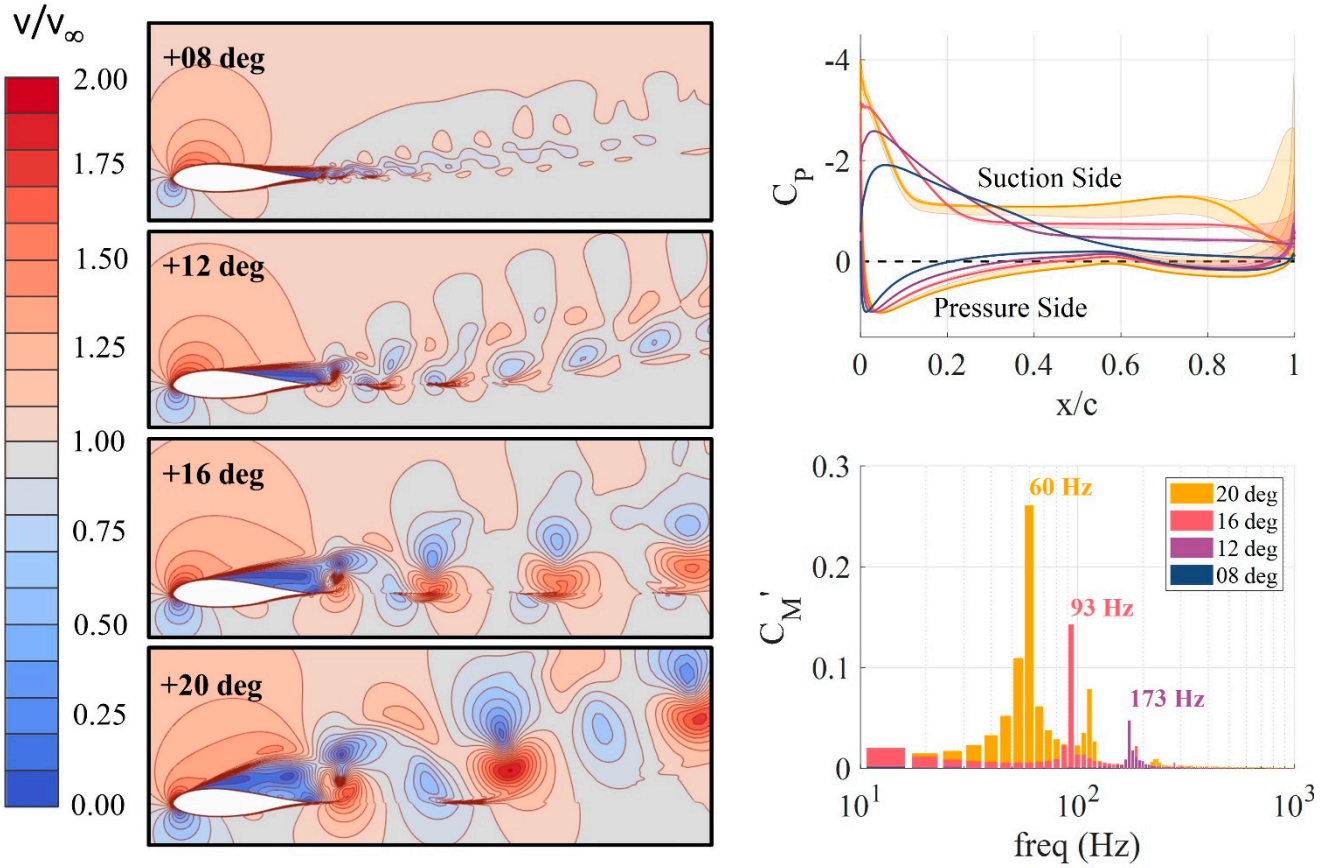

Figure 9. Velocity field, pressure coefficients and spectra of the fluctuating moment at AoA = 8°, 12°, 16° and 20°, obtained from the refined GEKO unsteady CFD simulation.

The maps with the representation of the velocity magnitude allow the identification of the stagnation points in the lower part of the leading edge and show an evident trend towards an early flow separation as the pitching angle is progressively increased, with a remarkable thickening of the boundary layer. A counter-rotating pair of vortices is shed from the airfoil, growing in size as the pitching angle is more pronounced. This vortex shedding is coherent with the frequencies of the fluctuating moment, which show high frequency but low size of the vortex shedding at the lower pitching angles. Conversely, lower frequencies and higher sizes of the vortices are observed at higher angles, once the flow is fully detached. As a consequence, the aerodynamic coefficients are intensively fluctuating with amplitudes up to three times larger than those formed at the separation onset. Regarding the pressure coefficient, there is also a notable increase in the oscillations with the pitching angle, revealed as a progressive build-up of the C_P value in the pressure side, and a shift towards the trailing edge of the airfoil in the suction side. Note that from 12° onwards, a wide fluctuation can be observed in the trailing edge due to an oscillatory partial reattachment, which it is also responsible for the periodic variations on both drag and lift coefficients.

Previous assertions are validated by means of the Strouhal number, $St = fL/v_\infty$, which relates the vortex shedding of the large turbulent scales and the frequencies of the fluctuating moment. The frequency values (f) correspond to the first (fundamental) harmonic in the power spectrum of the fluctuations for the torque coefficient (see plot in the bottom right in Figure 9). The characteristic length (L) has been adopted as the maximum

value of the integral length scale on the airfoil suction side (see Figure 10 below). The integral scale is estimated from the instantaneous values of the turbulent kinetic energy (k) and the turbulent dissipation rate (ε) according to $L = k^{3/2}/\varepsilon$ ([25]). Using the convective inlet velocity (v_∞=16.4 m/s), typical values around 0.2 are found (see Table 3) for all the situations considered between 10 deg (partial detachment) and 20 deg (fully detached flow), which is a characteristic value observed in separation of bluff-bodies at moderate-to-high Reynolds numbers.

Table 3. Strouhal numbers of the detached flow for different angles of attack.

AoA	f [Hz]	L [m]	St
10 deg	233	0.014	0.197
12 deg	173	0.019	0.199
14 deg	126	0.024	0.185
16 deg	93	0.032	0.180
18 deg	73	0.036	0.160
20 deg	60	0.039	0.143

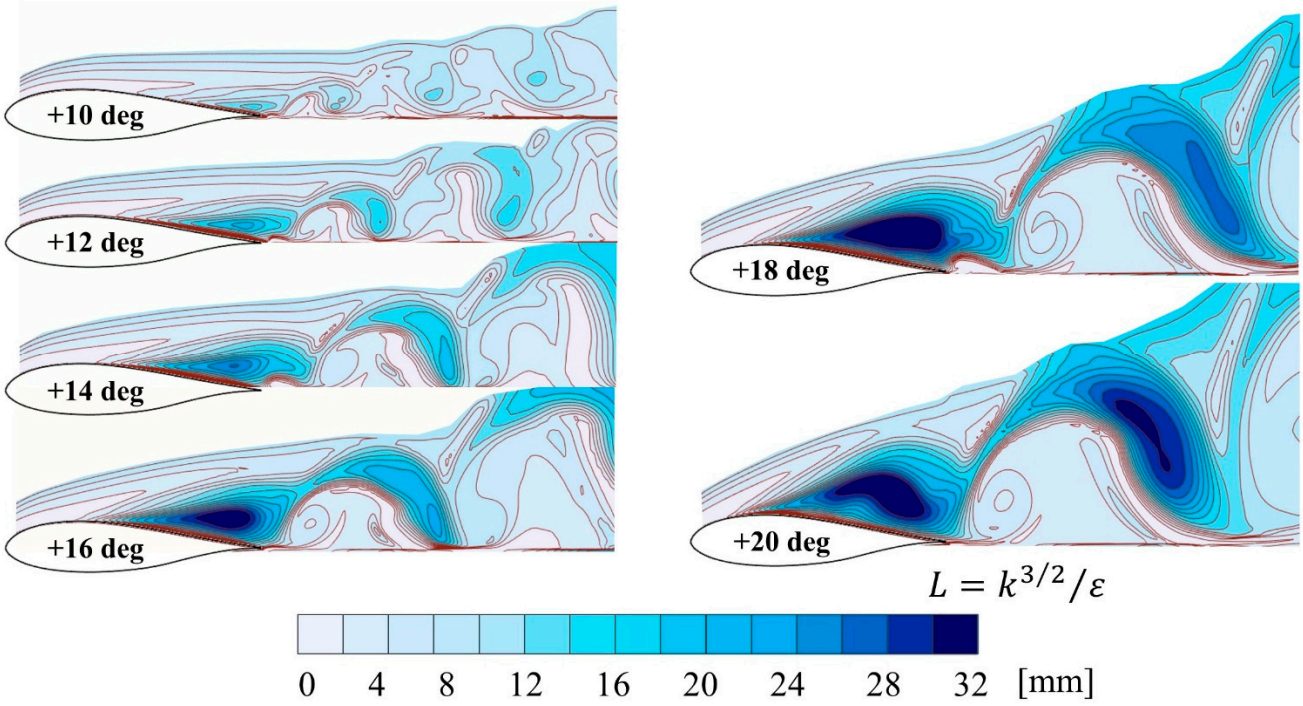

Figure 10. Integral length scales in the airfoil wake for positive AoA = 10°, 12°, 14°, 16°, 18° and 20°.

Figure 10 shows the computed values of integral length scales in the waked regions of the airfoil for different angles of attack. The figure reveals the vortical motion of the largest vortices, identified in a dark-blue color for an instantaneous snapshot, which illustrates the typical turn-out time of the vortices. At a low AoA, the size of the vortices is roughly in the order of magnitude of the airfoil thickness, with an intense vortex shedding (high frequency) revealed through the advection transport of the vortices street. For a high AoA, the vortices are progressively enlarged, now with a size in the order of magnitude of the airfoil chord, but with a lower shedding frequency (the generation rate of these large flow structures is significantly reduced as shown again in the convective transport along the airfoil wake).

Further insight is now provided with a closer look to the detached regions of the airfoil suction side during a complete oscillation cycle. For that purpose, the longitudinal distribution of the mean pressure coefficients on the suction side of the airfoil is shown in

a contour plot in Figure 11, for all the angles-of-attack simulated. A black dashed line identifies the averaged position of the separation point, revealing the severe engrossment of the detached region towards the leading edge for high pitching angles. Moreover, the contour map is complemented by a comprehensive view of the averaged detached regions over the airfoil, for AoA going from 6° to 20° (right plot), in order to illustrate the recirculation zones (identified with negative streamwise velocities).

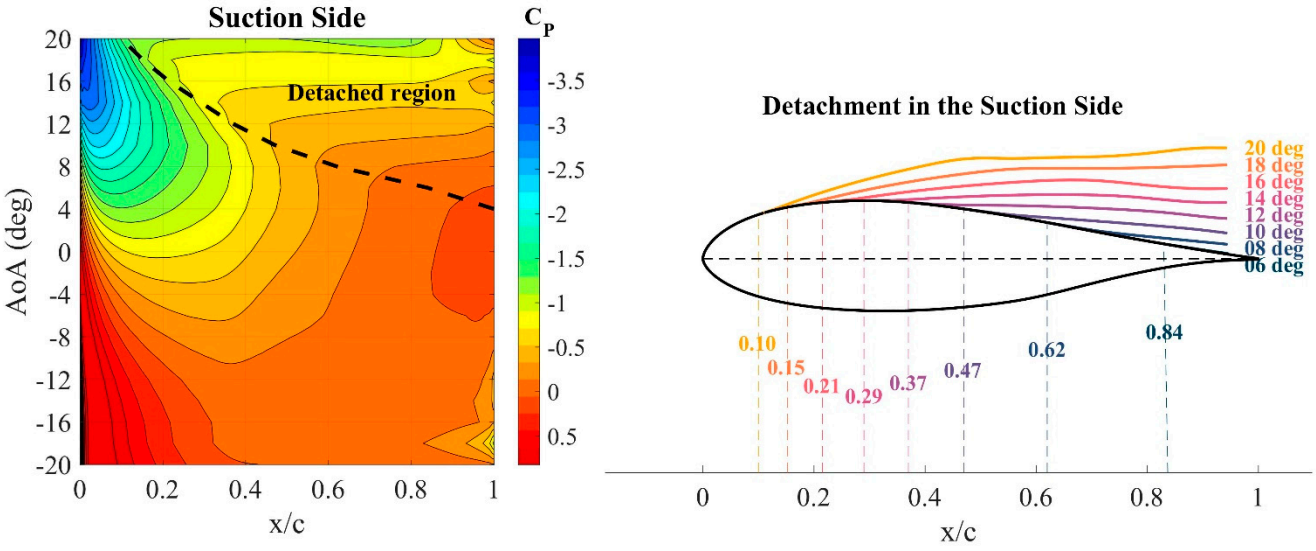

Figure 11. Pressure coefficient in the suction side, boundary layer and flow detachment point, for a wide set of pitching angles simulated with the refined GEKO unsteady model.

As expected, the position of the detachment point (where the wall shear stress equals zero) moves towards the leading edge, leaving a growing detached region. Note that at 20°, more than 80% of the suction face is exposed to fully detached flow. Although not shown here for brevity, a similar contour map is obtained for the pressure side, but symmetrically flipped with respect to the zero AoA and with a small shift, as detachment occurs at slightly higher angles for this side.

6. Conclusions

2D and 3D flat plates, in addition to the DU06-W-200 airfoil, have been tested in a wind tunnel equipped with a new external balance, designed for the measurement of aerodynamic forces. The inherent features of the balance make it suitable for an accurate characterization of VAWT airfoils, although specific validation has been required to ensure its performance. Furthermore, CFD simulations of the airfoil have been performed with different turbulence models and flow conditions, complementing the experimental results, and illustrating vividly the unsteady phenomena involved.

The experimental drag and lift coefficients obtained for both the flat plates and DU airfoil match the data available in the literature remarkably well, even at large angles of attack, when unsteady flow is rather relevant. The studied balance has proved its ability to capture fluctuating forces, although noise-filtering procedures must be implemented to obtain more reliable instantaneous data.

The new GEKO turbulence model used for this work offers accurate predictions of forces and moment, providing the best results when running unsteadily in the case of detached conditions, although the mesh requirements are significantly higher with respect to the steady simulations.

Finally, in light of the obtained results, the balance design as well as the CFD models have been successfully validated, and their integrated use has proved to be a highly recommendable and useful approach to test new airfoil geometries or airfoils featuring flow augmentation devices for VAWT applications.

Author Contributions: L.S., methodology, investigation, data curation, writing—original draft preparation; M.G.V., methodology, investigation; A.P., writing—original draft preparation; J.G.P., funding acquisition, resources; S.V.-S., supervision, resources; J.M.F.O., conceptualization, visualization, writing—review and editing, supervision. All authors have read and agreed to the published version of the manuscript.

Funding: This research was funded by the "Agencia Estatal de Investigación" (AEI) of the Spanish Ministry of Science and Innovation, in the context of the State Program to Promote Scientific-Technical Research and its Transfer, through the Project "Optimization through flow control techniques of a vertical axis wind turbine for urban environments" (ref. TED2021-131307B-I00), included in the NextGenerationEU funds of the European Community. Additionally, the support given by the University Institute for Industrial Technology of Asturias (IUTA) and the City Hall of Gijón, through the financed project SV-22-GIJON-1-04, is also recognized.

Acknowledgments: The authors would like to acknowledge the contribution of Katia Argüelles for her supervision and her administrative and technical support, as well as Bruno Pereiras for his advice and support during the measurement campaign.

Conflicts of Interest: The authors declare no conflict of interest. The funders had no role in the design of the study; in the collection, analyses, or interpretation of data; in the writing of the manuscript; or in the decision to publish the results.

References

1. IEA. *Net Zero by 2050—A Roadmap for the Global Energy Sector*; IEA: Paris, France, 2021.
2. Kumar, R.; Raahemifar, K.; Fung, A.S. A Critical Review of Vertical Axis Wind Turbines for Urban Applications. *Renew. Sustain. Energy Rev.* **2018**, *89*, 281–291.
3. Hand, B.; Kelly, G.; Cashman, A. Aerodynamic Design and Performance Parameters of a Lift-Type Vertical Axis Wind Turbine: A Comprehensive Review. *Renew. Sustain. Energy Rev.* **2021**, *139*, 110699. https://doi.org/10.1016/j.rser.2020.110699.
4. Balduzzi, F.; Bianchini, A.; Carnevale, E.A.; Ferrari, L.; Magnani, S. Feasibility Analysis of a Darrieus Verti-cal-Axis Wind Turbine Installation in the Rooftop of a Building. *Appl. Energy* **2012**, *97*, 921–929. https://doi.org/10.1016/j.apenergy.2011.12.008.
5. Du, L.; Ingram, G.; Dominy, R.G. A Review of H-Darrieus Wind Turbine Aerodynamic Research. *Proc. Inst. Mech. Eng. C J. Mech. Eng. Sci.* **2019**, *233*, 7590–7616. https://doi.org/10.1177/0954406219885962.
6. Barnes, A.; Marshall-Cross, D.; Hughes, B.R. Towards a Standard Approach for Future Vertical Axis Wind Turbine Aerodynamics Research and Development. *Renew. Sustain. Energy Rev.* **2021**, *148*, 111221. https://doi.org/10.1016/j.rser.2021.111221.
7. Micallef, D.; van Bussel, G. A Review of Urban Wind Energy Research: Aerodynamics and Other Challenges. *Energ. (Basel)* **2018**, *11*, 2204. https://doi.org/10.3390/en11092204.
8. Zhao, Z.; Wang, D.; Wang, T.; Shen, W.; Liu, H.; Chen, M. A Review: Approaches for Aerodynamic Performance Improvement of Lift-Type Vertical Axis Wind Turbine. *Sustain. Energy Technol. Assess.* **2022**, *49*, 101789.
9. Howell, R.; Qin, N.; Edwards, J.; Durrani, N. Wind Tunnel and Numerical Study of a Small Vertical Axis Wind Turbine. *Renew Energy* **2010**, *35*, 412–422. https://doi.org/10.1016/j.renene.2009.07.025.
10. Selig, M.S.; McGranahan, B.D. Wind Tunnel Aerodynamic Tests of Six Airfoils for Use on Small Wind Turbines. *J. Sol. Energy Eng. Trans. ASME* **2004**, *126*, 986–1001. https://doi.org/10.1115/1.1793208.
11. Wang, Z.; Zhuang, M. Leading-Edge Serrations for Performance Improvement on a Vertical-Axis Wind Turbine at Low Tip-Speed-Ratios. *Appl. Energy* **2017**, *208*, 1184–1197. https://doi.org/10.1016/j.apenergy.2017.09.034.
12. Kamliya Jawahar, H.; Alihan Showkat Ali, S.; Azarpeyvand, M.; Ilário da Silva, C.R. Aerodynamic and Aeroacoustic Performance of High-Lift Airfoil Fitted with Slat Cove Fillers. *J. Sound Vib.* **2020**, *479*, 115347. https://doi.org/10.1016/j.jsv.2020.115347.
13. Tropea, C.; Yarin, A.L.; Foss, J.F. *Handbook of Experimental Fluid Mechanics*; Springer: Berlin, Germany, 2007.

14. Tavakolpour-Saleh, A.R.; Setoodeh, A.R.; Gholamzadeh, M. A Novel Multi-Component Strain-Gauge External Balance for Wind Tunnel Tests: Simulation and Experiment. *Sens. Actuators A Phys.* **2016**, *247*, 172–186. https://doi.org/10.1016/j.sna.2016.05.035.
15. Martínez-García, E.; Marigorta, E.B.; Gayo, J.P.; Navarro-Manso, A. Experimental Determination of the Resistance of a Single-Axis Solar Tracker to Torsional Galloping. *Struct. Eng. Mech.* **2021**, *78*, 519–528. https://doi.org/10.12989/SEM.2021.78.5.519.
16. Martínez-García, E.; Blanco-Marigorta, E.; Parrondo Gayo, J.; Navarro-Manso, A. Influence of Inertia and Aspect Ratio on the Torsional Galloping of Single-Axis Solar Trackers. *Eng. Struct.* **2021**, *243*, 112682. https://doi.org/10.1016/j.engstruct.2021.112682.
17. Spalart, P.R.; Allmaras, S.R. One-Equation Turbulence Model for Aerodynamic Flows. *Rech. Aerosp.* **1994**, 5–21. https://doi.org/10.2514/6.1992-439.
18. Menter, F.; Sechner, R.; Germany GmbH Matyushenko, A.A.; Petersburg, S. Best Practice: RANS Turbulence Modeling in Ansys CFD. 2019. Available online: https://fluidcodes.ir/rans-turbulence-modeling/ (accessed on 27 July 2022).
19. Menter, F.R.; Matyushenko, A.; Lechner, R. Development of a Generalized K-ω Two-Equation Turbulence Model. *Notes Numer. Fluid Mech. Multidiscip. Des.* **2020**, *142*, 101–109. https://doi.org/10.1007/978-3-030-25253-3_10/COVER.
20. Blevins, R.D. *Applied Fluid Dynamics Handbook*; Van Nostrand Reinhold Co.: New York, NY, USA, 1984.
21. Bradford Wick, B.H.; June, W. *Study of the Subsonic Forces and Moments on an Inclined Plate of Infinite Span*; UNT Libraries Government Documents Department: Denton, TX, USA, 1954.
22. Fage A; Johansen, F.C. On the Flow of Air behind an Inclined Flat Plate of Infinite Span. *Proc. R. Soc. London. Ser. A Contain. Pap. A Math. Phys. Character* **1927**, *116*, 170–197. https://doi.org/10.1098/rspa.1927.0130.
23. Goldstein, S. (Ed.) *Modern Developments in Fluid Mechanics*; Oxford Univ. Press: London, UK, 1938.
24. Claessens, M.C. The Design and Testing of Airfoils for Application in Small Vertical Axis Wind Turbines. Master's Thesis, Delft University, Delft, The Netherlands, 2006.
25. Pope, S.B. *Turbulent Flows*; Cambridge Univ. Press: Cambridge, UK, 2000.

2.3. Métricas de la revista

Clarivate Analytics
Journal Citation Reports

Clarivate Web of Science™

Energies

Open Access since 2008

ISSN
N/A

EISSN
1996-1073

JCR ABBREVIATION
ENERGIES

ISO ABBREVIATION
Energies

Journal information

EDITION
Science Citation Index Expanded (SCIE)

CATEGORY
ENERGY & FUELS - SCIE

LANGUAGES	REGION	1ST ELECTRONIC JCR YEAR
English	SWITZERLAND	2010

Publisher information

PUBLISHER	ADDRESS	PUBLICATION FREQUENCY
MDPI	ST ALBAN-ANLAGE 66, CH-4052 BASEL, SWITZERLAND	24 issues/year

2021 JOURNAL IMPACT FACTOR	JOURNAL IMPACT FACTOR WITHOUT SELF CITATIONS
3.252	2.466
View calculation	View calculation

Journal Impact Factor Trend 2021 Export

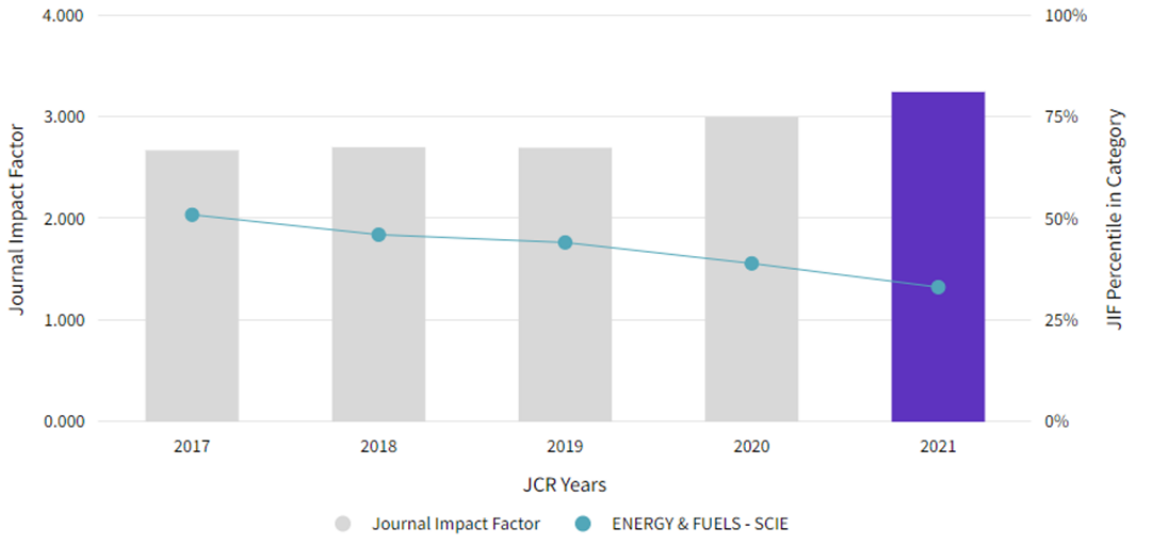

SJR
Scimago Journal & Country Rank

Scopus
ELSEVIER

Energies

Open Access

Scopus coverage years: from 1975 to 1976, from 2008 to Present

Publisher: Multidisciplinary Digital Publishing Institute (MDPI)

ISSN: 1996-1073

CiteScore 2021	SJR 2021	SNIP 2021	H-INDEX
5.0	0.653	1.104	111

Subject area: Mathematics: Control and Optimization | Engineering: Engineering (miscellaneous) | Engineering: Building and Construction | Energy: Energy (miscellaneous) | Engineering: Electrical and Electronic Engineering | Energy: Energy Engineering and Power Technology

CiteScore 2021

5.0 = 117.145 Citations 2018 - 2021 / 23.529 Documents 2018 - 2021

Calculated on 05 May, 2022

CiteScore rank 2021

Category	Rank	Percentile
Mathematics Control and Optimization	#18/118	85th
Engineering Engineering (miscellaneous)	#19/115	83rd

CiteScore trend

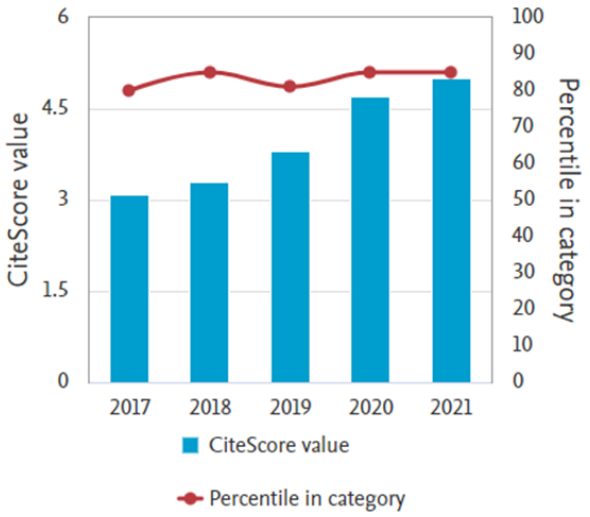

CAPÍTULO 3

CARACTERIZACIÓN DE PRESTACIONES DE FORMA MECÁNICA

3.1. Resumen

La caracterización de prestaciones de VAWT en túnel de viento es una parte crucial para su desarrollo. Normalmente, la escala de las turbinas tiene que reducirse considerablemente para mantener una elevada relación de tamaño entre el túnel y el prototipo. Esto conlleva reducciones sustanciales de las variables físicas que deben medirse (es decir, la potencia y el par), así como altas velocidades de rotación para mantener similitud dinámica. Las pérdidas mecánicas y los efectos inerciales dejan de ser marginales, por lo que el funcionamiento del prototipo puede verse comprometido y la medición de la potencia aerodinámica se complica.

Las metodologías convencionales de caracterización de prestaciones utilizan elementos pasivos, como frenos o generadores, para modificar el punto de funcionamiento de las turbinas. Esta metodología se denomina Modo de Conducción Pasiva (PDM). Asimismo, el par se mide con los propios frenos o de forma más precisa con torquímetros (que añaden pérdidas en la transmisión originadas por los acoplamientos). Además, para medir gradientes de par positivos en la curva de relación par-velocidad se necesitan sistemas adicionales de control del par, lo que restringe aún más el rango de funcionamiento de los ensayos.

En ensayos aerodinámicos, se suele utilizar el Modo de Conducción Activa (ADM) para superar estos problemas, accionando la turbina en condiciones cinemáticas equivalentes introduciendo un motor externo. Sin embargo, hasta ahora en la literatura no existe una metodología que permita caracterizar las prestaciones de forma mecánica utilizando ADM.

Este trabajo presenta el desarrollo y la aplicación de una metodología innovadora para el ensayo de prototipos de VAWT mediante ADM, mostrando interesantes ventajas sobre la determinación convencional del rendimiento de la turbina mediante PDM. Asimismo, se ha demostrado que se consigue un profundo nivel de caracterización y un alto control de los ensayos con un sencillo montaje experimental. En este trabajo se han identificado y estudiado en detalle los aspectos clave para la aplicación de esta metodología, como el aislamiento de las pérdidas mecánicas del arrastre de las palas o la cuantificación del arrastre parásito de los soportes de la turbina. Se han extraído conclusiones relevantes como el efecto del factor de inducción en el arrastre parásito, o la importancia de una correcta estimación del arrastre del álabe para el cálculo de las pérdidas mecánicas. Por último, la metodología se ha aplicado en un túnel de viento real, para la caracterización de una VAWT de 3 palas con un rotor H basado en el perfil DU 06-W-200. Los resultados de rendimiento obtenidos experimentalmente se han comparado con simulaciones CFD y modelos analíticos obteniendo una notable correspondencia. Adicionalmente, se ha propuesto una corrección analítica de los modelos CFD para incluir el efecto 3D y una corrección semi-empírica del bloqueo, basada en trabajos de la bibliografía.

Energy Conversion and Management 258 (2022) 115530

Contents lists available at ScienceDirect

Energy Conversion and Management

journal homepage: www.elsevier.com/locate/enconman

Novel methodology for performance characterization of vertical axis wind turbines (VAWT) prototypes through active driving mode

Luis Santamaría *, Jesús Manuel Fernández Oro, Katia María Argüelles Díaz, Andrés Meana-Fernández, Bruno Pereiras, Sandra Velarde-Suárez

Fluid Mechanics Area, Department of Energy, University of Oviedo, C/Wifredo Ricart s/n, Gijon, Asturias 33204, Spain

ARTICLE INFO

Keywords:
Vertical axis wind turbine
VAWT
Wind tunnel
Performance characterization
Active driving mode

ABSTRACT

Vertical axis wind turbines (VAWT) are called to have an important role in the definitive penetration of renewable energies in the near future. Although still under development, they are considered good candidates for urban environments and offshore generation in deep waters. For its experimental characterization, wind tunnel testing of small-scaled VAWTs is usually employed. However, self-starting issues, reduced aerodynamic torques -for reliable measurement- and high rotational speeds -imposed by similarity- emerge as inherent operative problems. To overcome these issues, Active Driving Mode (ADM) is commonly used to drive the turbine under equivalent kinematic conditions introducing an external motor. Up to now, an accurate characterization of the turbine performance, in terms of retrievable aerodynamic power, is not available for this methodology in the open literature.

This work presents the development and application of an innovative methodology for testing VAWT prototypes through ADM. Interesting advantages over the conventional determination of the turbine performance using Passive Driving Mode (PDM) are shown. It is demonstrated that a deep level of characterization and high-test control is achieved with a simple experimental set-up. In addition, the key aspects for the application of this methodology have been identified and studied in detail, like the isolation of the mechanical losses from the blade drag or the quantification of the parasitic drag of the turbine struts. Relevant conclusions have been revealed concerning the marginal effect of the induction factor on the parasitic drag, or the importance of a correct blade drag estimation for the computation of the mechanical losses. Finally, the methodology has been applied to a real wind tunnel set-up, for the characterization of a 3-bladed VAWT with a H-rotor based on the DU 06-W-200 profile. The performance results obtained experimentally have been accurately compared to CFD simulations.

1. Introduction

Nowadays, global energy models are increasingly focused on renewable energy sources and decentralized energy generation. Over the last two decades, wind energy has proven to be economical and reliable, being Horizontal Axis Wind Turbines (HAWT) one of the pillars of new energy policies due to its mature development. According to the International Energy Agency (IEA), by 2050, wind power will account for 19% (stated policies scenario STEPS) to 39% (net zero scenario NZE) of total world energy supply [1]. However, as the energy mix is more participated by renewable technologies, like solar PV or wind power, its variable power supply requires the development of new methods to adjust the production to the real-time demand curves. This issue is promoting the rise of a new energy economy based on microgrids and energy storage systems like batteries, small hydro reservoirs [2], CAES systems [3] or hydrogen, capable to provide distributed and variable energy integration. With those solutions, the energy supply is decoupled from the renewable sources, so local intermittencies, shortages due to weather conditions or occasional failures are also minimized. The adaptation of other types of variable renewable technologies, still under development and currently penalized by their difficult integration to the existing grid, can be even favored. Furthermore, in the current context, self-consumption for individual and collective installations is a growing approach in residential buildings, which has been proved profitable even without subsidies [4].

Lift-based Vertical Axis Wind Turbines (VAWT) have attracted renewed attention in recent times because they are particularly well-suited for this new scenario. Although they were already developed in

* Corresponding author.
E-mail address: santamarialuis@uniovi.es (L. Santamaría).

https://doi.org/10.1016/j.enconman.2022.115530
Received 13 January 2022; Received in revised form 23 February 2022; Accepted 21 March 2022
Available online 31 March 2022

the 70 s and 80 s, they were progressively abandoned due to the higher efficiencies and rated power provided by the HAWT family. Nevertheless, VAWTs characteristics make them better candidates than HAWTs for application in urban environments, due to their omnidirectionality, avoiding the need for orientation mechanisms; their ability to work better in variable wind conditions; and their lower noise emission [5]. In the case of wind turbines for offshore generation in deep waters, VAWTs are also a considerable option and specifically tailored to floating devices, due to their superior energy density for wind farming. In addition, VAWTs present a lower inclining moment, lower turbine mass and lower center of gravity which leads to more economical supporting structures [6]. Furthermore, they present their gearbox and generator at ground level which makes the operation easier and safer [7]. This is very important for offshore applications where deployment and maintenance labors in a sea environment are extremely difficult.

However, despite the valuable potential of VAWTs, their current state of development is still limited [8], mainly due to their complex aerodynamics. For its further study, wind tunnel testing is an essential tool to obtain reliable data. It allows direct visualization of flow-turbine interactions and provides experimental data for validation of both analytical and computational fluid dynamics (CFD) models. From an engineering point of view, wind tunnel data is also used to retrieve performance curves which are further extrapolated to real scale turbines.

Typically, the scale of the turbines has to be significantly downsized in order to preserve high tunnel-to-prototype size ratios. This leads to substantial reductions in the physical variables to be measured (i.e., power and torque), and high rotational speeds to match dynamic similarity. The mechanical losses and inertial effects are no longer marginal, so the prototype operation is compromised and the measurement of the aerodynamic power complicated. Moreover, conventional methodologies for performance characterization use passive elements such as brakes or generators to modify the operating point of the wind-driven turbines. The torque is measured directly with torquemeters [9] or other passive elements like Prony [10] or electromagnetic brakes [11] which over-increase the mechanical resistance. Additional torque control systems are also required to measure positive torque gradients in the torque-speed ratio curve, thus restricting the testable operating range even more [12]. As a result, the experimental wind tunnel tests of small-scale turbines in a passive driving mode (PDM) suffer from severe inconveniences and are not fully operational, being even aggravated with the self-starting issues of these kinematic turbines.

As a feasible alternative, active driving mode (ADM) tests, also called motor-driven, may be employed to avoid all these self-starting problems and small-scale issues. This option emerges when the turbine is not able to generate net power at the required rotating velocity, so the operating point is artificially achieved with an external energy input. The aerodynamic performance can be retrieved from that deficit, assuming that both situations are similar. Although this approach initially raised some concerns about its validity, Araya and Dabiri concluded that turbine wakes in the relevant operating range are independent from the driving mode [13]. They compared wake measurements of turbines in both motor-driven (ADM) and flow-driven (PDM) tests taken from several references and conducted their own study using PIV in a water channel. The limit of the application of this procedure was stablished at high TSRs where aerodynamic equilibrium between drag and lift is achieved. Recently, Dou et al. have also determined that unsteady flows and turbulence measured with hot-wire anemometry in a HAWT are identical using PDM or ADM [14]. So far, in the field of VAWT study, ADM has been employed mainly to run experiments at small scale for flow studies. Some examples can be found in the literature for the analysis of turbine flow using PIV techniques [15–17]. However, in those situations, the overall performance of the turbines is not provided, or, in best cases, it is obtained from additional tests with different experimental set-ups.

Both PDM and ADM provide an indirect measurement of the aerodynamic variables. In the case of PDM, the use of segregating routines to isolate the aerodynamic torque is already a common practice in the literature. However, up to the authors' knowledge, no formal method has been presented yet for ADM. Hence, the establishment of an accurate methodology to obtain the performance curves of lab-scale turbines under ADM would be really useful, allowing to finally circumvent all those previous limitations. It will also provide a more comprehensive way of analyzing flow visualization studies, relating them adequately with complementary performance measurements.

This paper presents the development of a novel methodology to characterize VAWT performance in active driving mode for wind tunnel testing at small scales. Although some references can be found regarding the employment of ADM for turbine characterization, a rigorous description on the application of this methodology is not available yet. A detailed process that may quantify the relevance of the different contributions is thus required. Some previous studies [18] briefly mention driving the turbine without flow to obtain a "tare" torque, but without subtracting parasitic drags. Other authors [13] are even disregarding the mechanical losses in the retrieval of the performance curves. This may lead to an excessive overestimation of the net aerodynamic power. Only using a well-posed method to decouple the different factors allows a correct estimation of the real values. This is the basic contribution of this research. In addition, it contributes to improve the practical study of low-solidity, high-efficiency turbines, which are essential for the above-mentioned applications. The methodology highlights for its moderate infrastructure, low instrumentation costs, easy-implementation, and reasonable degree of accuracy. This is particularly interesting for industrial-commercial application, where large-scale wind tunnels or high-cost instrumentation may not be accessible. This tool also allows a fast and simple utility to complement CFD studies and contribute to the ongoing growth of the VAWTs sector.

The methodology has been developed using an electric DC motor as the active element for the turbine control. The aerodynamic performance was obtained indirectly by the comparison of the supplied torque for different test conditions. Precisely, a remarkable effort has been made to isolate the aerodynamic torque from the mechanical losses and the parasitic drag of the struts. Note that this makes the methodology proposed here of special interest for the validation of analytical models or CFD simulations, in which the effect of the turbine structure or the blades struts is not usually considered. At the same time, a relevant part of the work was devoted to identifying the most problematic stages of the methodology, with special emphasis on those aspects requiring an in-depth study.

This work is structured as follows. First, the experimental set-up used is presented in Section 2, including the description of the measurement procedures. Then, Section 3 describes the development of the novel methodology, going from its theoretical basis to a practical approach. Critical aspects requiring special attention are also identified. The methodology is applied to the current set-up, and final results are shown. Section 4 is devoted to further exploring a key aspect of the methodology: the isolation of the aerodynamic drag from the mechanical losses. Afterwards, the influence on the methodology of the drag coming from the turbine struts is evaluated in Section 5. Greater detail is provided to improve the initial considerations given in Section 3. In Section 6 the results obtained are compared to numerical results from CFD simulations and a correction for blockage, based on previous works found in the literature, is proposed. Finally, relevant conclusions and future works are provided in Section 7.

2. Experimental SET-UP

A small-scale prototype of a 3-bladed VAWT, with a H-rotor based on the DU 06-W-200 profile, has been recently designed [19], developed [20] and constructed [21] by the authors. These actions are within the context of a National Research & Development Plan to promote the use and implementation of renewable energies for an ecological transition and a sustainable development.

Preliminary flow measurements have been conducted in a medium-size, 30 kW closed-loop wind tunnel, with a large blockage ratio in the test section. They were mainly devoted to quantifying tunnel-turbine interaction effects for the development of specific blockage corrections. Though maximum blockage ratios of a 5–10% are desirable, it is a common practice to employ higher values. This fact is due to the extremely wide test sections required by that limitation in case of typical VAWT prototypes [22]. Consequently, it is necessary to correct the blockage effect in order to extrapolate the measured output power for real-scale turbines operating under free-field conditions. Precisely, as a crucial part of this procedure, the existing facility and retrieved data have been used in the development of an ADM methodology to characterize the performance of the scaled prototype for different tip speed ratios.

The present experimental database corresponds to a high-blockage set-up, used to apply the proposed methodology for the performance characterization of VAWTs. Hence, the results must be considered only in the specific context of the research and may not be representative of the turbine design for expected characteristics in an actual wind environment. The reader is reminded to stay focused on the description and applicability of the methodology, of general use for wind tunnel testing. Hence the available data must be considered as a simple framework to exemplify its use.

The experimental set-up available for the present investigation includes:

Wind Tunnel. The experiments were conducted in the "XAWT" (*Xixón Aeroacustic Wind Tunnel*) located in the facilities of the Fluid Mechanics Area of the University of Oviedo. It is a closed-loop wind tunnel, driven by a 30 kW axial fan in an impulsion layout, with a total length of 24.6 m and 8.3 m high (arranged in a vertical position, see Fig. 1**, left**). It has an aerodynamic test section of 1.05 × 1.25 m^2, immersed in an anechoic chamber of 4.2 m long and cross-sectional area of 4.45 × 2.80 m^2. A 9.5:1 contraction nozzle with a logarithmic derivative profile accelerates the flow towards the test section. This wind tunnel can achieve velocities up to 22 m/s, for a maximum Reynolds number of $1.7{\cdot}10^6$ (based on the nozzle hydraulic diameter), with a mean turbulence intensity around 0.7% [23].

For the current research under high-blockage conditions, a hybrid modular enclosure has been used to fulfil a semi-confined environment with no wake blockage (shown disassembled in Fig. 1**, right**). More details can be found in [21].

Prototype. The turbine tested is a small-scale model of a 3-bladed "H"-type VAWT, specifically developed for urban environments (Kumar et al., 2018). "H"-VAWTs (Darrieus with straight blades) present lower manufacturing costs than other VAWT architectures and achieve good efficiencies. Nowadays, they are a trending choice for this kind of applications. The prototype has a diameter of 0.8 m and features 3 blades with the DU 06-W-200 airfoil. The blade chord is 0.067 m, and the blade length is 0.6 m, resulting in an aspect ratio H/D = 0.75 and a solidity σ = 0.5. The main geometrical characteristics are summarized in Table 1. This model has been built combining standard commercial elements, like aluminium profiles and joints, with custom-made parts manufactured by Fused Deposition Modelling (FDM). Special care was taken in the layer direction to avoid fatigue failure and abrupt fracture because of bending and centrifugal loads. The blades feature an epoxy coating to improve surface roughness and increase blade strength. To reduce the drag on the struts, a low-drag aerodynamic profile (EPPLER 863 Strut Airfoil) was introduced to cover the interior cylindrical rods. Fig. 2 shows the turbine inside the test chamber of the wind tunnel.

For this measurement campaign, the prototype was operated in motor-driven arrangement using a 1 kW, permanent magnet DC, electric motor. It has been powered by a 30 V/10 A laboratory power supply, which has a built-in measuring system. Previously, the motor was experimentally characterized in an independent test bench to determine its torque constant, k_t. This will allow to obtain the motor torque directly from the electric current in the different turbine tests, avoiding the need for an additional torquemeter and thus decreasing transmission mechanical losses.

Instrumentation. The flow velocity for the tests was controlled in the wind tunnel nozzle (inlet–outlet) using a Kimo CP210-R differential pressure transducer with an operative range of ± 1000 Pa and temperature compensation. The measurement of temperature allowed the correction of the air density inside the wind tunnel, as a function of the atmospheric pressure checked on an analogic barometer. The turbine rotational speed was measured instantaneously using a digital tachometer connected to a data acquisition card. In addition, the intensity of the power supply was also measured and registered in the computer by means of a specific software for its operation and recording. Ad-hoc acquisition software was also employed for the signal of the tachometer. Finally, a post-processing program was developed in MATLAB to obtain the test results. A simplified diagram of the instrumented experimental set-up is shown in Fig. 3. The measuring uncertainties of the different sensors are listed in Table 2.

Experimental routines. The objective is to measure the electric current supplied to the motor, for different rotating velocities of the turbine, when the wind tunnel is operated at a constant flow velocity.

Table 1
Main characteristics of the prototype.

Airfoil profile	DU 06-W-200
Blade number (N)	3
Chord (c) [m]	0.067
Diameter (D) [m]	0.8
Blade length (H) [m]	0.6
Solidity $\left(\sigma = \frac{N{\cdot}c}{D/2}\right)$	0.5
Aspect ratio (H/D)	0.75

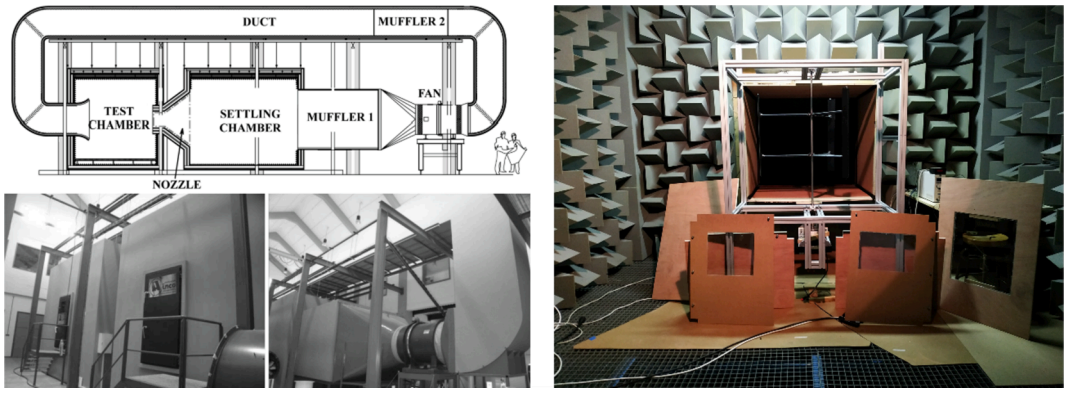

Fig. 1. XAWT wind tunnel (left). Aerodynamic test section with the turbine (right).

Fig. 2. Three-bladed H-VAWT installed inside an hybrid modular enclosure for the test chamber of the XAWT wind tunnel.

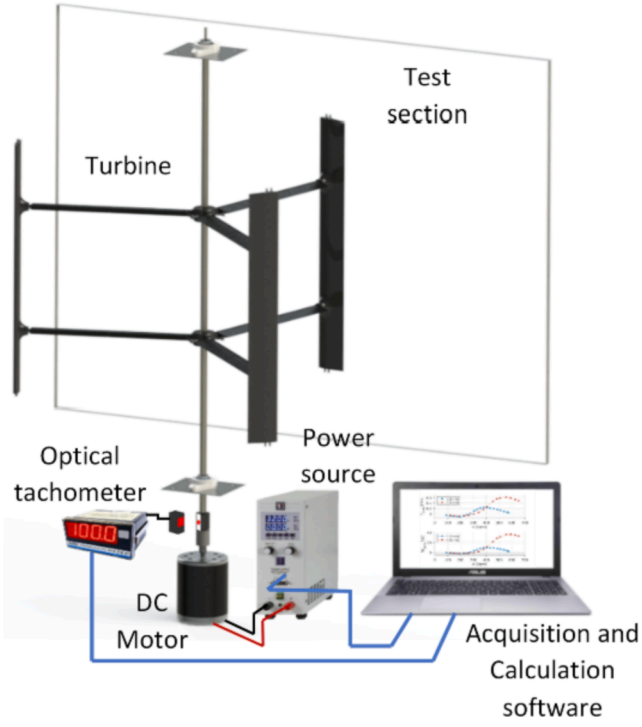

Fig. 3. Sketch with the experimental set-up and instrumentation used.

Table 2
Instrumentation uncertainties.

Sensor	Variable measured	Uncertainty
Differential pressure sensor Kimo CP210-R	Pressure difference	$u_{\Delta P} = \pm 0.005 \Delta P \pm 2[Pa]$
Optical tachometer	Rotational speed	$u_{\omega} = \pm 0.011 \left[\frac{rad}{s}\right]$
Laboratory power source Elektro Automatik PS 8360–10 T	Electric current	$u_I = \pm 0.01[A]$

The flow velocity in the wind tunnel is fixed regulating the flow rate delivered by the axial flow fan (opening/closing a set of louvers at the fan discharge). To modify the rotational speed of the motor-turbine assembly, the excitation of the DC motor is controlled by voltage regulation through the power supply, until the turbine reaches the desired rotational speed. The electric motor demands higher or lower current depending on the load, which varies with the rotational speed. Finally, the measurement is performed and stored after the prototype reaches a dynamic equilibrium.

The mechanical torque applied by the motor, T_{app}, is a function of the torque constant of the electric motor, k_t, the measured electric current, I, and a detrimental friction torque in the motor, T_f, according to:

$$T_{app} = k_t \cdot I - T_f \tag{1}$$

The friction torque depends on the speed of rotation and can be relevant at the wind tunnel scale, so it cannot be neglected. Nevertheless, the proposed methodology employs a sequence of different tests whose combined balance, in terms of torque, cancels out its influence for the final results. The complete procedure is detailed in the next section.

Note that for an accurate steady balance of the torques, the acquiring time of the measurements has to be maintained for a sufficiently extended period of time, so representative mean-time values can be obtained. Additionally, it is remarkable that the methodology described later is not dependent of the measuring instruments employed for the present work. In particular, the applied torque for equation (1) can be obtained directly from a torquemeter, thus suppressing the need for the experimental determination of the constant k_t. Alternatively, the electric current could have been measured using a high precision amperemeter/oscilloscope, instead of using the own utility of the power supply unit.

3. VAWT performance characterization in active driving mode (ADM)

The aerodynamic torque of a VAWT can be obtained indirectly from a motor-driven situation. To do so, similar fluid kinematic conditions to the wind-driven case must be satisfied and a precise subtraction of the system losses has to be performed. Precisely, a good estimation of the losses is the key point for the ADM to be really helpful for performance characterization. In the case of small-scale VAWTs in wind tunnels, this task can be quite challenging.

Two main sources of system losses can be identified in a conventional wind tunnel testing of a VAWT rotor. Firstly, mechanical losses arise due to bearing friction, transmission efficiencies in the couplings and even structural vibrations associated to slight misalignments and mass imbalances. Secondly, there are aerodynamic losses in the form of parasitic drag in the rotor struts. Additional aerodynamic losses can be accounted from blade-tip effects, although most authors consider them as a detrimental part of the aerodynamic efficiency of the rotor blades. Hence, they have been considered as a secondary flow of the blades for the present investigation, assuming that they are simply penalizing the rotor aerodynamics, instead of introducing further parasitic aerodynamic losses.

For the characterization of mechanical losses, two different approaches are suggested by the authors. The first approach is based on a turbine test that employs a rotor without blades, replicating similar conditions than a previous complete test with the blades mounted on the turbine. Under this condition, no aerodynamic power is generated. However, as the original bearing friction and mechanical resistance of the turbine is affected by the mass distribution of the rotor blades, the blade mass suppressed must be compensated with additional weights to maintain an equivalent structural behavior. This is difficult to implement in a realistic way without adding elements which produce new artificial aerodynamic losses. The second approach is based on a test where the turbine is driven without wind, thus avoiding additional disassembling operations. In this case, the main problem lays on how to isolate the mechanical losses from the aerodynamic drag torque due to the rotation of the blades. If that rotational drag is not discounted, it would result in an overestimation of the mechanical losses and of the aerodynamic torque. This second approach has been chosen by the authors for the present work, although the alternative option is also a

reliable possibility.

Regarding the second source for system losses, i.e. the parasitic losses drag in the struts, some recent works have employed analytical expressions to correct CFD results [24] for a better numerical estimation of VAWTs performance. For this work, an inverse insight is attempted through the isolation of the strut drag losses, leading to the retrieval of the aerodynamic power alone. This estimation can be later compared to CFD simulations. Note that due to the significant interaction of the blade wakes with the strut drag, an experimental approach may take into account this effect more easily. Therefore, two additional tests should be performed over the bladeless rotor comparing no wind conditions with respect to the inflow velocity situation. Its difference provides the estimation of the strut parasitic drag. However, this estimation is not considering the effect of the induction factor of the turbine when bladed, which may require an extra correction of the inflow velocity for the struts. Thus, the importance of this minor issue should be quantified.

Consequently, an effective procedure to evaluate the performance of a small-scale turbine under ADM on a wind tunnel experiment would require 2 main tests and 2 additional ones to account for strut parasitic drag. Note that the parasitic drag is rather relevant, especially in the case of typical prototype sizes. Hence, four tests were finally completed under different configuration and components, including:

Test 1. Whole turbine without wind.

Test 2. Whole turbine under constant wind velocity.

Test 3. Bladeless turbine without wind.

Test 4. Bladeless turbine under constant wind velocity.

As a result, Fig. 4 represents the evolution of the applied torque in the motor as a function of the rotational speed for all the tests performed. An inlet flow velocity of 7.5 m/s in the test section of the wind tunnel has been employed for tests 2 and 4. The solid lines account for tests with the complete turbine (1 and 2), while dashed lines correspond to the tests without turbine blades (3 and 4). Similarly, blue curves indicate tests with wind and black curves tests without wind. Tests 1, 3 and 4 (no aerodynamic power available) are fitted using a second-order polynomial (square markers) with a remarkable accuracy (RMSE less than 0.036, $R^2 > 0.9997$), as expected from the typical dependence of losses with rotational speed.

The different trend observed in the curve for test 2 evidences the effect of aerodynamic torque in the turbine performance. Firstly, with the turbine under stalled conditions, the set-up demands higher motor torque than in the no-wind situation. This corresponds to the velocity range between 100 and 250 rpm. Then, as the rotational speed is increased, the operating point of the turbine shifts to the positive torque

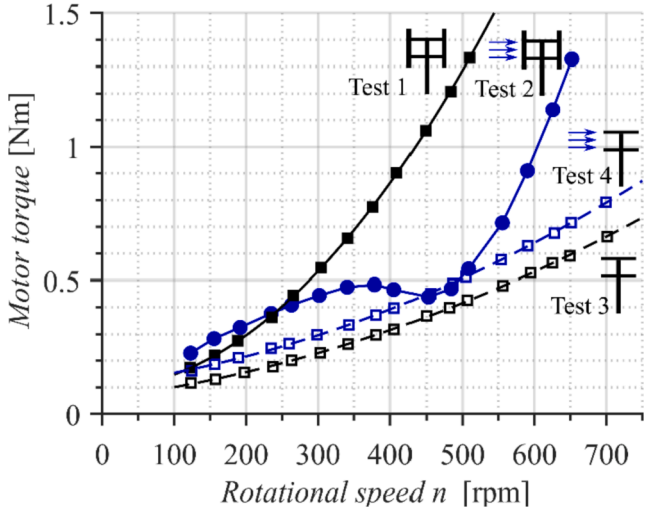

Fig. 4. Applied motor torque as a funtion of the rotational speed of the turbine for the different tests performed. Tests under wind conditions (2 and 4) were performed at 7.5 m/s inlet velocity.

generation zone, decreasing the demanded motor torque. In particular, the range between 350 (the local maximum) and 550 rpm (sudden increase of the slope) comprises that region. Finally, at high rotational velocities (higher than 550 rpm), the motor torque demand is significantly increased with a much stepper slope. At that final stage, the turbine is moving away from its optimal operating point and progressively declining its energy generation.

With that polynomial fits it is possible to evaluate the torques in the tests 1, 3 and 4 at the speeds corresponding to test 2. Following, the aerodynamic torque can be deduced with simple momentum equations in the shaft for the different cases. Firstly, the torque equilibrium for the complete turbine with no wind (test 1) yields:

$$T_{app_1} = T_{Db} + T_{Ds1} + T_{loss1} \tag{2}$$

where T_{app_1} is the applied torque by the electric motor, T_{Db} and T_{Ds1} are drag torques from the blades and struts respectively, and T_{loss1} is the friction torque associated to mechanical losses. Obviously, sub index 1 denotes the corresponding test. Similarly, for the second test the momentum equation leads to:

$$T_{app_2} + T_{aero} = T_{Ds2} + T_{loss1} \tag{3}$$

where T_{aero} represents the net aerodynamic torque provided by the blades. Note that, in this case, the mechanical losses, T_{loss1}, are identical to those found in the first test (both tests present the same machine configuration). On the contrary, the drag in the struts is not preserved because of its dependency to the incident relative velocity, which is function of the wind velocity and the rotational speed. Now, rearranging equation (2) to isolate the mechanical losses and substituting in equation (3), it is expressed as:

$$T_{aero} = \left(T_{app_1} - T_{app_2}\right) + \left(T_{Ds2} - T_{Ds1}\right) - T_{Db} \tag{4}$$

The term $(T_{Ds2} - T_{Ds1})$ in equation (4) can be easily obtained from the results given by tests 3 and 4. Since these tests correspond to the set-up with the bladeless turbine, the mechanical losses are different with respect to test 1 and 2, but equal between them. On the other hand, assuming that the struts drag is not modified between analogous tests of aerodynamic resistance (1–3 and 2–4), it can be easily expressed that:

$$T_{app_3} = T_{Ds1} + T_{loss3} \tag{5}$$

$$T_{app_4} = T_{Ds2} + T_{loss3} \tag{6}$$

After subtracting equations (5) and (6), it gives:

$$T_{Ds2} - T_{Ds1} = T_{app_4} - T_{app_3} \tag{7}$$

And finally, combining (4) and (7), it leads to this compact equation that includes all the torque data measured in the four tests:

$$T_{aero} = \left(T_{app_1} - T_{app_2} + T_{app_4} - T_{app_3}\right) - T_{Db} \tag{8}$$

In this expression, all the terms required to deduce the aerodynamic torque are known and represented in Fig. 4, expect for the last term, T_{Db}, which corresponds to the drag on the blades when the complete turbine is rotating under no wind conditions. Several possibilities can be employed to estimate this term. In particular, a 2D CFD simulation of a single rotating airfoil has been chosen as the best compromise between reliability and computational costs for the present application. More details and discussion are provided later in the next section.

The complete set of tests have been carried out for two different wind velocities, 5.5 and 7.5 m/s, in order to evaluate the reliability and functionality of this method. Higher velocities have not been employed to avoid possible mechanical failures in the prototype: an increment of the wind speed implies that the rotational speed must be increased linearly to fulfill dynamic similarity. This results in excessively high centrifugal forces compromising the structural integrity of the scaled turbine (for the lab materials and manufacturing methods employed).

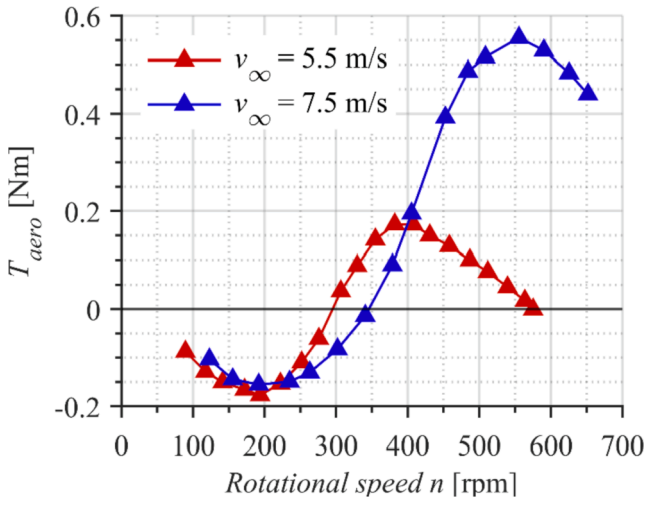

Fig. 5. Aerodynamic torque as a function of the rotational speed for two different wind velocities.

Fig. 5 shows the final results obtained of aerodynamic torque, as a function of the rotational speed of the turbine, for the two wind velocities tested.

Fig. 5 demonstrates that the developed methodology allows a thorough characterization of the performance, even at rotational velocities where the blades are stalled so the turbine does not produce positive torque. It is clearly revealed that the aerodynamic torque at these scales is not sufficient to exceed both mechanical losses and passive resistances. Hence, its measurement would be extremely difficult using conventional methods. Furthermore, it is manifested that the prototype is not able to surpass the cut-in threshold using only the wind force unless a motor-clutch driving system is provided. With the active driving mode these difficulties are overcome, and an accurate performance evaluation is obtained with a simple and cost-effective set-up. Moreover, the good control provided by the electric motor over the rotational speed of the turbine also allows to obtain a higher number of points than with conventional methodologies, even reducing the time required for the experimental tests.

To conclude this section, it is necessary to address the uncertainty of the instrumentation and its impact on the measuring procedures. Table 2 declares an uncertainty of $u_I = \pm 0.01[A]$ for the measurement of the electric current supplied by the power source. In addition, the torque constant has been determined with a relative uncertainty of $\frac{u_{k_t}}{k_t} = \pm 0.4[\%]$. The combined uncertainty of the resulting aerodynamic torque due to this instrumentation has been calculated following the procedure described in [25], which estimates a value of uncertainty transmitted through the measuring chain towards the desired variable. For the torque, it can be calculated according to:

$$u_{T_{aero}}(k_t, I) = \sqrt{\left(\frac{\partial T_{aero}}{\partial k_t}\right)^2 \cdot u_{kt}^2 + 4 \cdot \left(\frac{\partial T_{aero}}{\partial I}\right)^2 \cdot u_I^2} \tag{9}$$

For the test of 7.5 m/s reference velocity, it provides an uncertainty of ± 0.005 Nm for the maximum torque value, which in relative terms represents only a ± 0.9%. Note that it is a remarkable result, since the magnitude of the measured values is significantly small. Consequently, the accuracy verified, in combination with the affordable cost of these elements employed, dictates that the proposal is a rather interesting choice for the instrumentation of ADM tests.

Finally, further research efforts have been made over two key aspects of the methodology: a correct determination of the blades drag torque (the term T_{Db}); and a deep analysis of the influence of the wind velocity on the parasitic drag of the struts (on the term $T_{app_4} - T_{app_3}$). These topics are discussed in detail in Sections 4 and 5 respectively.

4. Isolating drag losses from mechanical ones

Under no wind situation, the drag on the airfoils is generated due to the circumferential velocity of the rotating blades. In the relative frame, it means that the inflow velocity can be assumed to be equal to the blade velocity with its direction tangential to the blade chord. Since the prototype tested corresponds to a rotor designed with zero-pitched blades, a 0 deg Angle-of-Attack (AoA) has to be considered. Note that this assumption is most accurate for low-solidity turbines, where the tangential distance between consecutive blades is large. In the case of high-solidities, the inflow velocity of every blade can be significantly affected by the wake deficit of the preceding blade, thus compromising the condition of uniform inlet flow.

In addition, if the radius of the turbine is at least one order of magnitude higher than the blade chord, it is also reasonable to consider that the aerodynamics of the blade are similar to that found in a linear cascade. Due to the absence of wind flow, the relative AoA is maintained during the whole turbine rotation, so drag coefficients can be taken directly from typical airfoil databases (like NREL reports, UIUC databases, etc.) or other published data for cascades. They can be also provided by low-order numerical programs like Xfoil, Javafoil or Rfoil among others. In the case that the required Re numbers are not available in the references, those programs allow easy extrapolation that can be attempted to obtain the values at the corresponding Re of the experiments.

However, in the case of small-scaled prototypes, the R/c ratio is usually reduced, compromising very seriously the assumption of equivalent flow to a linear cascade. Since the blades drag losses are very relevant for the correct computation of the aerodynamic torque, this is not a minor issue. In particular, for the present turbine with R/c = 6, it has been observed that the influence of rotational forces cannot be neglected, showing a severe impact on the evolution of the blade wakes and thus conditioning the final value of the drag loss. This has been observed through the simulation of the turbine airfoil, both in a linear cascade (LC) and a rotating cascade (RC). A 2D steady RANS simulation with a k-W SST turbulence modelling, recommended in the literature [26], has been employed for the purpose. Special attention has been paid to the spatial discretization of wall-adjacent mesh, with up to 450 nodes in the streamwise direction of the airfoil and further refinement in the normal direction to guarantee y+= 1 [27]. Since the flow at zero AoA is not suffering from detached conditions, unsteady computations or SRS turbulence modelling can be obviated. Conversely, additional options for curvature corrections and fully-swirl terms have been accounted in the resolution of the governing equations of the model with ANSYS Fluent v.17.2.

At this point, it is noted that it could be tempting to carry out the full 2D simulation of the whole turbine for its performance characterization. However, this implies extremely high computational costs, thus moving away from the initial objective of a low-cost, easy to implement methodology. A full simulation, even with a 2D model, of a typical VAWT requires high demanding unsteady simulations, with long-run executions and small time step sizes. This is mandatory to obtain a final fully-periodic simulation [26], as well as a high-order turbulence model to take into account all the vortical structures. Consequently, as a good compromise between economy and precision, a 2D simulation of a single rotating airfoil is finally proposed.

In Fig. 6, the vorticity normalized with the apparent wind velocity to chord ratio is shown in the vicinity of the airfoil for the two simulations. A typical Re number (based on the blade chord) equal to 100,000 has been selected for the analysis. In the upper map, the significant curvature of the blade wakes reveals the impact of the rotating effects. A comparison with the linear cascade map also shows how the turbulent wake is more pronounced in the internal side of the blades. These differences imply significant increments in the drag coefficients under rotation. This reveals that an accurate treatment of the drag losses is crucial for the estimation of the turbine performance.

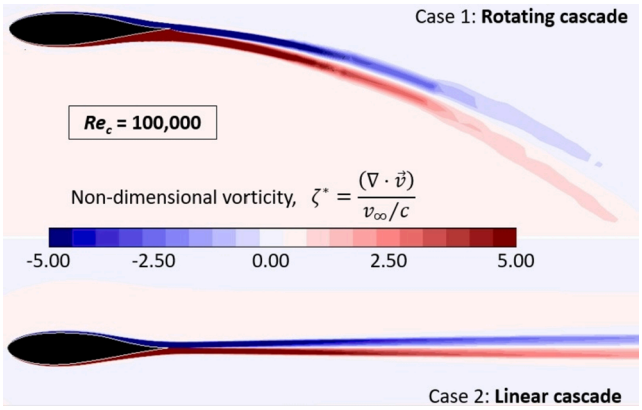

Fig. 6. Comparison of airfoil wakes obtained numerically with a rotating cascade (top) and a linear cascade (down).

Fig. 7 shows drag coefficients of the DU 06-W-200 airfoil for different Re numbers at 0 deg AoA, taken from various references in the literature (Rfoil, Xfoil and [28]). As expected, the available data is out-of-range for the small-scale experiments, so a power fit (black dashed line) was employed to extrapolate the coefficients at the required Reynolds numbers ($2.3{\cdot}10^4$ to $1.2{\cdot}10^5$, in the case of the 7.5 m/s test). In addition, drag coefficient values from both static 2D linear cascade (blue squares) and rotating cascade (red diamonds) simulations have been added to the representation. Note that at high Reynolds numbers ($Re > 3{\cdot}10^5$), the results from the bibliography are coincident with the values obtained from the LC simulation.

At Reynolds numbers lower than $5{\cdot}10^4$, the results from the different curves diverge significantly, although they are placed in a region with marginal impact in the estimation of the blades drag loss for the methodology (due to the low value of the rotational velocities). On the contrary, in the range from $5{\cdot}10^4$ to $1.2{\cdot}10^5$, the observed differences in Fig. 7 are lower, but their final relevance is more important. For example, at a tip-speed ratio of 2.6 (equivalent to $Re = 9{\cdot}10^4$) the power coefficient calculated from CFD-RC estimations differs around an 8% from those provided with the CFD-LC approach, and even a 12% using the extrapolated values from the references. Furthermore, at a tip-speed ratio of 3.5 (equivalent to $Re = 1.2{\cdot}10^5$), the differences increase up to 16% and 32% respectively.

Despite the significant disparities in the estimation of the drag coefficients, no alternative method with sufficient reliability has been found in the literature. On the contrary, the mechanical losses are frequently not considered or even grossly estimated. Therefore, depending on the desired level of accuracy, it is the user responsibility to decide the most convenient approximation to its particular set-up.

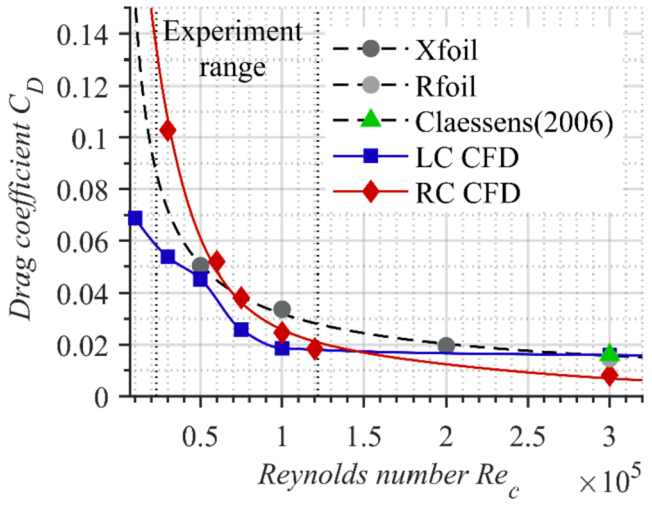

Fig. 7. Comparison of DU 06-W-200 drag coefficients for different approaches.

5. Parasitic strut drag

The parasitic drag of the turbine struts is the second key factor in the characterization of VAWTs performance in ADM. It is an important mechanism for resistant torque so it must be properly accounted to obtain reliable results.

In previous section 3, it was already discussed that strut parasitic drag can be easily isolated in ADM by performing the comparison between wind and no wind tests for the bladeless turbine (test 3 vs test 4). However, a concern was raised about the difference in the wind velocity perceived by the struts due to the induction factor when the turbine is bladed against when it is not. To analyze this question, the applied torque was measured for test 4 at three different wind velocities (v_∞ = 5.5, 7.5 and 10 m/s), and compared to the results for no wind velocity ($v_\infty = 0$) of test 3 (Fig. 8).

As a starting point, the figure demonstrates an evident quadratic dependence on the rotational velocity for the resistant torque of the struts in all the tests. Also, there is a linear evolution between the tests at 5.5, 7.5 and 10 m/s, showing the same vertical increment between the curves. It is noticeable, in the case of no wind velocity for test 3 (v_{inf} = 0), that the difference of this curve with respect to the others is progressively deviating from linearity as rotational velocity increases. However, this is a quite marginal effect, associated to the self-induced blockage of the turbine structure for high rotational speed on the cases with inflow velocity. More important is the difference in the struts drag between test 3 at zero velocity and any other curve of test 4, really significant at these small scales, even for the present prototype in which the struts are streamlined with low drag airfoils of thickness around 2% of the turbine span. Hence, this shows that accounting for parasitic strut drag is critical at wind tunnel scales, especially in case of prototypes with non-aerodynamic struts (although it is usually neglected, as reported in [22]).

Furthermore, there is an additional consideration for the estimation of this parasitic drag of the struts which needs further discussion. When the struts are rotating isolated from the blades (i.e., tests 4), the incoming velocity perceived by the struts is practically coincident to the inflow velocity from the wind tunnel section. However, when the full turbine is operated (test 2), the flow deceleration within the turbine (generated by the aerodynamics of blades and typically quantified as an induction factor) reduces the actual inlet velocity acting on the struts, thus modifying the net aerodynamic torque.

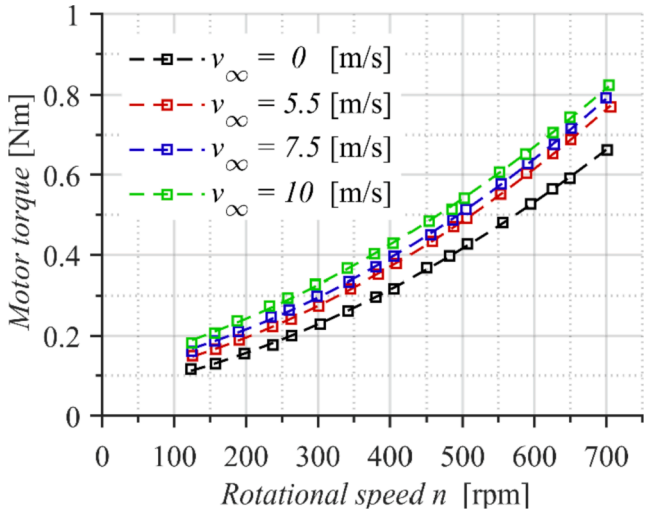

Fig. 8. Applied torque as a function of the rotating speed. Comparison between results for test 3 and test 4 at three different wind velocities.

In other words, to take into account the effect of the decelerated flow induced by the blades over the parasitic drag of the struts, it would be necessary to apply in equation (8) the torque of an equivalent test 4, T^{eq}_{app4}, operated with a reduced, "apparent" incoming velocity. Depending on the tip-speed ratio, this induction factor (relating the apparent and original inflow velocities) could represent a velocity reduction between 5 and 40% for a typical turbine design [19]. Unfortunately, this value cannot be easily known a priori, and it is also dependent on the particular characteristics of the turbine (geometry, struts design, solidity, airfoil family, etc.).

To estimate the importance of this effect, the final aerodynamic torque provided by this turbine (in the case of 7.5 m/s) is obtained introducing different parasitic torques – T^{eq}_{app4} in equation (8) –, retrieved from different apparent inflow velocities. The deviation from the result obtained without considering any correction is provided in Table 3 for nominal conditions (maximum available torque).

As expected, the higher the induction factor, the higher the difference in percentage. Significant discrepancies are observed for the highest flow deceleration, reaching up to 8.7% in the case of an induction factor equivalent to 0.4. However, the impact of this effect is sufficiently small (less than 3% at MTP and 5% at MVP) for low-to-moderate induction factors (below 0.2), indicating that it can be obviated maintaining a reasonable accuracy. Only in case of high-blocked turbines, with induction factors starting from 0.4, it is recommended to introduce this correction in the methodology to update the values of the resistant torque of the struts.

6. Comparison with CFD models

In this final section, the obtained performance results from the turbine are compared with complementary results from numerical simulations, as an example of real application and also for validation purposes. In particular, the results corresponding to a wind velocity of 7.5 m/s have been used for the comparison.

Firstly, a complete 2D URANS model of the VAWT turbine positioned on the extended casing of the wind tunnel nozzle (Fig. 9) has been developed with the objective of replicate the performance curve. A mesh density with the same requirements that the single-airfoil RC model was employed, resulting in a [450 × 40] O-mesh distribution over the blades and a total number of 350,000 cells for the whole domain. The sliding mesh technique was employed to resolve the rotational motion of the turbine, with a variable time-step size equivalent to 0.25 deg of angular displacement for every tip-speed ratio. At least, five complete rotations of the turbine were necessary to assure the periodic response of the aerodynamic torque. Similar k-ω SST turbulence modelling, discretization schemes and resolution algorithms to the RC simulation were employed.

In order to compare the results of this 2D CFD model with the real 3D experimental curves, it is necessary to introduce some scaling factors to take into account the vertical clearance of the turbine (H = 0.6 m) with respect to the casing height (L = 1.05 m). Calculating the ratio of the volumetric flow rates in both 2D and 3D situations (in 2D, the flow rate is per unit length; whereas in 3D it is considering the real transversal section), and assuming that it must be similar, a scaling factor for the tip-speed ratios between the 2D and 3D cases is obtained. On the other hand, considering the cubic dependence of the power coefficient with respect to the bulk velocities, a scaling factor for the power values can be also derived, yielding to:

$$\lambda_{3D} = \lambda_{2D}\frac{H}{L} \tag{10}$$

$$C_{p,3D} = C_{p,2D}\left(\frac{H}{L}\right)^3 \tag{11}$$

A complete range of equivalent tip-speed ratios, going from 1.5 to 3.9, have been simulated for an inlet velocity of 7.5 m/s in order to obtain the aerodynamic power curve of the turbine. As an illustration of the results, distributions of vorticity are represented in Fig. 10 for three different tip-speed ratios (2.1, 3.0 and 3.9) in a non-dimensional form (relative to the turbine rotating speed). Typical vortex shedding is identified in the development of the blade wakes, being more pronounced for lower tip-speed ratios. Thus, at 2.1, the turbine wake is more distorted, due to the downstream transport of the big vortices shed from the turbine blades, especially in the leeward region. Note also the relevant vortex shedding generated downstream of the turbine shaft. As the tip-speed ratio is increased, the boundary layers are more attached to the blades and the overall level of unsteadiness is reduced, including a weakened Von Kárman vortex street shed from the cylindrical shaft. The lateral casing prevents the widening of the turbine wake in all the cases. Moreover, an interaction between the vortices shed from the lateral shear layers of the turbine wake and the shear stress of the lateral walls is clearly established. As the turbine rotation is further increased (for TSR values of 3 and 3.9), a lateral high-jet region is progressively observed with a mitigation in the vortex shedding from the lateral casing but with a higher fluctuation for the overall wake.

With the factors defined in eq. (10) and (11), the performance results obtained from the 2D modelling (in terms of mean aerodynamic torque as a function of the TSR value) are transformed into the equivalent curve for a full 3D case. Hence, typical power coefficient, defined as $C_P = 2\dot{W}_{aero}/\rho v_\infty^3 HD$, are represented in Fig. 11 as a function of the tip-speed ratio, $\lambda = \omega D/2v_\infty$, for the present numerical simulations and compared to the experimental values of the set-up shown previously in Fig. 5. In particular, the corrected CFD results are shown as black squares in the figure, while experimental results are represented as blue triangles, with a remarkable level of agreement between them. Maximum aerodynamic power coefficients around 0.25 are predicted for a tip-speed ratio close to 3.0.

In addition, due to the high apparent blockage ratio of the experimental set-up, a correction has been introduced to approximate the non-dimensional performance of the turbine to real conditions (open-field). In particular, the correlations proposed in [29], have been modified to adapt some of their parameters for the studied VAWT turbine. Based on previous studies by Maskell [30], these authors presented a quadratic expression for the parameter m that it is typically used, in combination with the blockage ratio (B_R) of the wind tunnel, to "correct" the incoming flow velocity v_∞. These equations are given by:

$$\frac{v_c}{v_\infty} = \sqrt{\frac{1}{1 - mB_R}} \tag{12}$$

where.

$$m = 6.92B_R^2 - 6.76B_R + c_m \tag{13}$$

In equation (13), the independent term c_m is a function of the overall aerodynamics of the prototype, having proposed the values 3.5 for a square plate, 3.2 for a Savonius turbine and 2.8 for the straight-bladed (SB) Darrieus turbine studied in [29] (solidity $\sigma = 1.29$). Assuming an exponential-decay relationship between the parameter c_m and the

Table 3
Discrepancies in the turbine aerodynamic torque due to the overestimation of the resistant torque of the struts from uncorrected inflow velocities.

Flow deceleration (Induction factor)	0.05	0.10	0.15	0.20	0.30	0.40
Aerodynamic torque relative variation [%] (Maximum torque point-MTP)	−0.16	−1.03	−1.90	−2.78	−4.53	−6.27
Aerodynamic torque relative variation [%] (Maximum variation point-MVP)	−0.68	−1.82	−2.97	−4.11	−6.41	−8.70

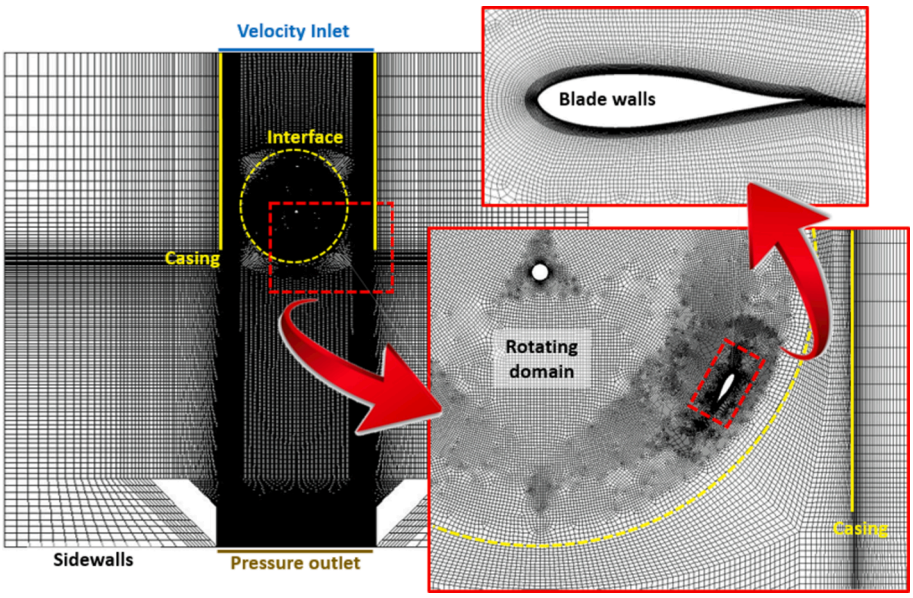

Fig. 9. Numerical 2D model of the rotating turbine: boundary conditions and mesh density.

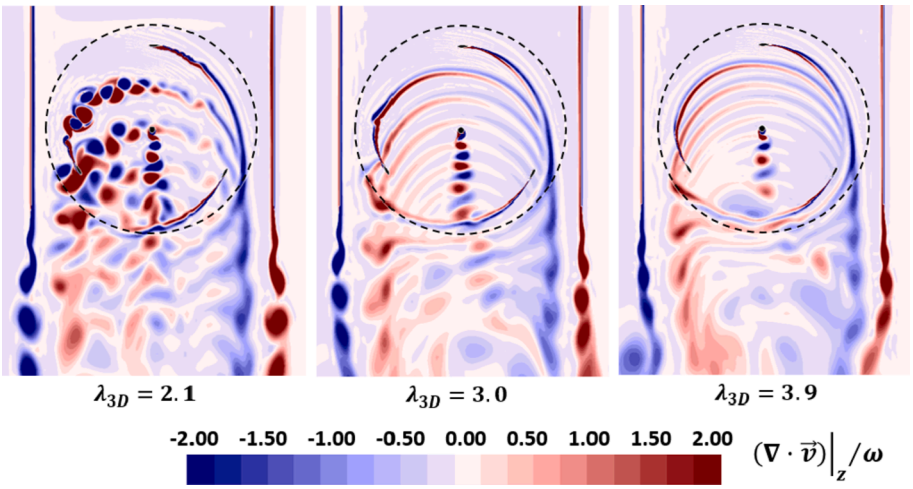

Fig. 10. Instantaneous vorticity distributions for different equivalent Tip-speed ratios.

apparent solidity of those bodies, a final value of $c_m = 1.72$ has been adopted for the VAWT of the present work (see Table 4).

Consequently, with the corrected value of the inlet velocity given by equation (12), the final performance outcome is transformed into the curve represented with the red markers in the Fig. 11. As a reference for the expected performance in open-field conditions, an analytical model of simple streamtube and actuator disc (SSTM), based on the work of Paraschivoiu [31], has been developed in MATLAB. This model has already been studied in [19] and good agreement was found with experimental data in the general trends, matching the tip-speed ratio of maximum power coefficient. The curve from this model has been included in Fig. 11, represented with a solid, doted grey line.

Note that, despite of the high blockage ratio of the experimental set-up, the correction introduced is really marginal due to the low solidity of the studied turbine with respect to the one studied in [29]. The maximum power coefficient is slightly reduced and displaced to a lower tip-speed ratio, closer to the TSR predicted by the analytical model. Although the SSTM model clearly overestimates the performance (typical of these analytical models), it is advising that the ratio v_c/v_∞ may be still higher than the optimal for the adequate blockage correction. Nevertheless, the available experimental data for the corrections used is very limited and further research is needed to evaluate the correlation between the parameter b and the turbine solidity. The methodology presented in this work can also contribute to this matter: Different turbine solidities could be achieved by modifying the airfoil chord, while only Test 2 (whole turbine with wind) would have to be performed for each new configuration.

7. Conclusions

In this work, the development and application of an innovative methodology for the performance characterization of small-scale VAWT prototypes using active driving mode in wind tunnels has been presented. The proposal circumvents the typical limitations found for prototypes of reduced size when conventional passive driving mode is employed, like those related to self-starting issues, cut-in thresholds, excessive frictional losses or narrow operative ranges. Furthermore, it has been found to provide superior control of the tests with simpler and cost-effective equipment, and with a better definition of the performance curves. The ADM methodology can be easily used with complementary tests for the experimental study of the flow patterns (PIV, hot-wire, visualization techniques, etc.).

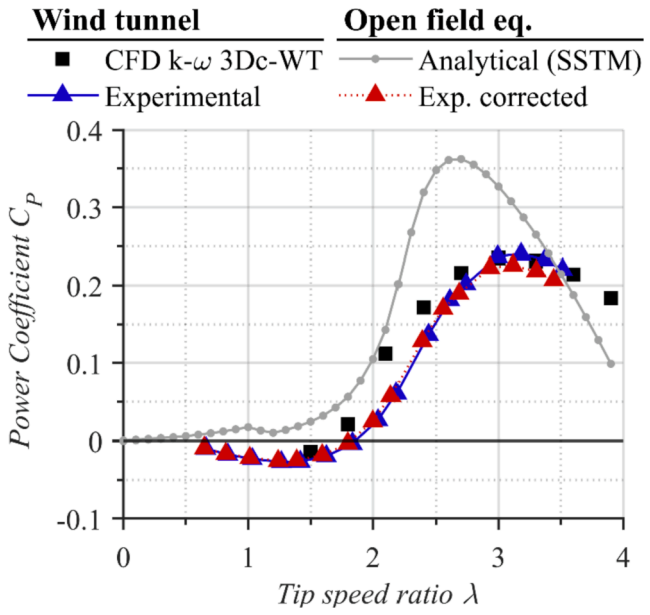

Fig. 11. Turbine performance in terms of power coefficient vs. tip-speed ratio. Comparison of 2D CFD results (open-field and confined) with respect to experimental values (original and blockage-corrected).

Table 4
Exponential fit of the parameter c_m for blockage correction.

Case	Square plate	Savonius	SB Darrieus [29]	SB Darrieus (Present work)
Solidity	∞	2	1.29	0.5
c_m	3.5	3.2	2.8	1.72

A typical experimental set-up with a DC-motor as the primary driver of a confined VAWT installed in a closed-loop wind tunnel has been employed for the application of the methodology. Detailed uncertainty analysis has been conducted to assure the validity of the results. Four different tests were finally carried out to obtain the aerodynamic per-formance of the turbine from the balance of the torque outputs. Ac-cording to the methodology, additional evaluation of the blades drag is required to complete the procedure.

The isolation of the blades drag from the overall mechanical losses has been identified as the most difficult challenge of the methodology. For that purpose, a 2D CFD simulation of one single rotating blade has been finally proposed as the most convenient method to estimate its contribution in terms of economy and reasonable accuracy. In addition, it has been confirmed that the influence of the strut parasitic drag must be accounted for in wind tunnel testing of small-scale prototypes for a precise determination of the aerodynamic torque. Although this para-sitic drag may be affected by the flow deceleration of the turbine, it has been demonstrated that the influence of a corrected strut drag with an apparent inflow velocity is minimal. In fact, it can be neglected in the case of low-to-moderate induction factors.

To conclude, final experimental results obtained with the proposed methodology have been presented for a typical H-type VAWT turbine with three DU 06-W-200 airfoil blades. To take into account blockage effects in the wind tunnel, specific correlations for VAWT turbines have been adopted and customized for the solidity of the present design. Complementarily, a 2D URANS simulation of a similar confined layout of the turbine has been developed for validation purposes. After scaling, the numerical performance curve has been compared to the full 3D experimental results, obtaining a remarkable agreement. The final aerodynamic power coefficient of the turbine predicted by the different methodologies indicates that the experimental procedure developed for this investigation is a reliable and valuable tool for other researchers in the field.

CRediT authorship contribution statement

Luis Santamaría: Methodology, Investigation, Data curation, Writing – original draft. **Jesús Manuel Fernández Oro:** Conceptualization, Methodology, Software, Writing – review & editing, Supervision, Project administration, Writing – review & editing. **Katia María Argüelles Díaz:** Supervision, Project administration, Writing – review & editing. **Andrés Meana-Fernández:** Investigation, Software. **Bruno Pereiras:** Methodology, Resources. **Sandra Velarde-Suárez:** Supervision, Funding acquisition.

Declaration of Competing Interest

The authors declare that they have no known competing financial interests or personal relationships that could have appeared to influence the work reported in this paper.

Acknowledgements

The authors wish to thank the financial support of the Spanish Ministry of Economy, Industry and Competitiveness for the R + D Project entitled “Development and Construction of Vertical Axis Wind Turbines for Urban Environments” (DEVTURB) – Ref. ENE2017-89965-P, under the National Plan for Scientific and Technical Research and Innovation.

The grant provided by the Principality of Asturias for the support of Research Activities, funded by the Institute for Economic Development (IDEPA) under reference GRUPIN IDI/2018/000205 is also gratefully acknowledged.

Additionally, the support given by the University Institute for Industrial Technology of Asturias (IUTA) and the City Hall of Gijón, through the financed project SV-18-GIJON-1-05, is also recognized.

Finally, the authors would like to acknowledge the contributions of Prof. José González and As. Prof. Mónica Galdo for their advice and support during the measurement campaign.

References

[1] IEA. World Energy Outlook 2021 - revised version October 2021 2021.
[2] Menéndez J, Loredo J, Galdo M, Fernández-Oro JM. Energy storage in underground coal mines in NW Spain: Assessment of an underground lower water reservoir and preliminary energy balance. Renewable Energy 2019;134:1381–91. https://doi.org/10.1016/j.renene.2018.09.042.
[3] de Prado LÁ, Menéndez J, Bernardo-Sánchez A, Galdo M, Loredo J, Fernández-Oro JM. Thermodynamic analysis of compressed air energy storage (Caes) reservoirs in abandoned mines using different sealing layers. Appl Sci (Switzerland) 2021;11. https://doi.org/10.3390/app11062573.
[4] Pinto ES, Serra LM, Lázaro A. Optimization of the design of polygeneration systems for the residential sector under different self-consumption regulations. Internat J Energy Res 2020;44:11248–73. https://doi.org/10.1002/er.5738.
[5] Balduzzi F, Bianchini A, Carnevale EA, Ferrari L, Magnani S. Feasibility analysis of a Darrieus vertical-axis wind turbine installation in the rooftop of a building. Appl Energy 2012;97:921–9. https://doi.org/10.1016/j.apenergy.2011.12.008.
[6] Borg M, Collu M. A comparison between the dynamics of horizontal and vertical axis offshore floating wind turbines. Phil Trans R Soc A 2015;373(2035): 20140076.
[7] Zhao Z, Wang D, Wang T, Shen W, Liu H, Chen M. A review: Approaches for aerodynamic performance improvement of lift-type vertical axis wind turbine. Sustainable Energy Technol Assess 2022;49:101789. https://doi.org/10.1016/j.seta.2021.101789.
[8] Du L, Ingram G, Dominy RG. A review of H-Darrieus wind turbine aerodynamic research. Proc Instit Mech Eng, Part C: J Mechan Eng Sci 2019;233(23-24): 7590–616.
[9] Castelli MR, Ardizzon G, Battisti L, Benini E, Pavesi G. Modeling strategy and numerical validation for a Darrieus vertical axis micro-wind turbine. ASME International mechanical engineering congress and exposition, Proceedings (IMECE) 2010;7:409–18. https://doi.org/10.1115/IMECE2010-39548.
[10] Mertens S, Van Kuik G, Van Bussel G. Performance of an H-Darrieus in the skewed flow on a roof. J Solar Energy Eng Trans ASME 2003;125:433–40. https://doi.org/10.1115/1.1629309.
[11] Du L, Ingram G, Dominy RG. Experimental study of the effects of turbine solidity, blade profile, pitch angle, surface roughness, and aspect ratio on the H-Darrieus wind turbine self-starting and overall performance. Energy Sci Eng 2019;7: 2421–36. https://doi.org/10.1002/ese3.430.

[12] Edwards JM, Angelo Danao L, Howell RJ. Novel experimental power curve determination and computational methods for the performance analysis of vertical axis wind turbines. J Solar Energy Eng Trans ASME 2012;134:1–11. https://doi.org/10.1115/1.4006196.
[13] Araya DB, Dabiri JO. A comparison of wake measurements in motor-driven and flow-driven turbine experiments. Exp Fluids 2015;56:1–15. https://doi.org/10.1007/s00348-015-2022-7.
[14] Dou B, Yang Z, Guala M, Qu T, Lei L, Zeng P. Comparison of Different Driving Modes for the Wind Turbine Wake in Wind Tunnels n.d. https://doi.org/10.3390/en13081915.
[15] Fujisawa N, Shibuya S. Observations of dynamic stall on turbine blades. J Wind Eng Ind Aerodyn 2001;89:201–14. https://doi.org/10.1016/S0167-6105(00)00062-3.
[16] Simão Ferreira C, Van Kuik G, Van Bussel G, Scarano F. Visualization by PIV of dynamic stall on a vertical axis wind turbine. Exp Fluids 2009;46:97–108. https://doi.org/10.1007/s00348-008-0543-z.
[17] Edwards JM, Angelo Danao L, Howell RJ. Novel experimental power curve determination and computational methods for the performance analysis of vertical axis wind turbines. J Sol Energy Eng 2012;134:031008. https://doi.org/10.1115/1.4006196.
[18] Bachant P, Wosnik M. Reynolds number dependence of cross-flow turbine performance and near-wake characteristics. In: Proc of the 2nd marine energy technology symposium; 2014. p. 1–9.
[19] Meana-Fernández A, Solís-Gallego I, Fernández Oro JM, Argüelles Díaz KM, Velarde-Suárez S. Parametrical evaluation of the aerodynamic performance of vertical axis wind turbines for the proposal of optimized designs. Energy 2018;147:504–17. https://doi.org/10.1016/j.energy.2018.01.062.
[20] Santamaría L, Vega MG. Training Program for Researchers in Design and Manufacturing of Experimental Prototypes for Fluids Engineering using Additive Technologies 2021:1–8. https://doi.org/10.1088/1757-899X/1193/1/012096.
[21] Santamaría L, María K, Díaz A, Pereiras B, Vega MG, Pérez JG, et al. Preliminary flow measurements of a small-scale , vertical axis wind turbine for the analysis of blockage influence in wind tunnels. vol. AICFM16. 2022.
[22] Battisti L, Persico G, Dossena V, Paradiso B, Raciti Castelli M, Brighenti A, et al. Experimental benchmark data for H-shaped and troposkien VAWT architectures. Renewable Energy 2018;125:425–44.
[23] Rodríguez Lastra M, Fernández Oro JM, Galdo Vega M, Blanco Marigorta E, Santolaria MC. Novel design and experimental validation of a contraction nozzle for aerodynamic measurements in a subsonic wind tunnel. J Wind Eng Ind Aerodyn 2013;118:35–43. https://doi.org/10.1016/j.jweia.2013.04.008.
[24] Bianchini A, Balduzzi F, Bachant P, Ferrara G, Ferrari L. Effectiveness of two-dimensional CFD simulations for Darrieus VAWTs: a combined numerical and experimental assessment. Energy Convers Manage 2017;136:318–28. https://doi.org/10.1016/j.enconman.2017.01.026.
[25] Kline SJ. The purposes of uncertainty analysis. J Fluids Eng Trans ASME 1985;107:153–60. https://doi.org/10.1115/1.3242449.
[26] Rezaeiha A, Montazeri H, Blocken B. Towards accurate CFD simulations of vertical axis wind turbines at different tip speed ratios and solidities: Guidelines for azimuthal increment, domain size and convergence. Energy Convers Manage 2018;156:301–16. https://doi.org/10.1016/j.enconman.2017.11.026.
[27] Castelli MR, Masi M, Battisti L, Benini E, Brighenti A, Dossena V, et al. Reliability of numerical wind tunnels for VAWT simulation. J Phys Conf Ser 2016;753:082025.
[28] Claessens MC. The design and testing of airfoils for application in small vertical axis wind turbines. Masters Thesis 2006:1–137.
[29] Jeong H, Lee S, Kwon SD. Blockage corrections for wind tunnel tests conducted on a Darrieus wind turbine. J Wind Eng Ind Aerodyn 2018;179:229–39. https://doi.org/10.1016/j.jweia.2018.06.002.
[30] Maskell EC. A theory of blockage effects on bulff bodies and stalled wings in a closed wind tunnel. Her Majesty's Stat Off 1965:1–27.
[31] Paraschivoiu I. Wind Turbine Design: With Emphasis on Darrieus Concept. 2002.

3.3. Métricas de la revista

Clarivate Analytics
Journal Citation Reports

Clarivate Web of Science™

ENERGY CONVERSION AND MANAGEMENT

ISSN
0196-8904

EISSN
1879-2227

JCR ABBREVIATION
ENERG CONVERS MANAGE

ISO ABBREVIATION
Energy Conv. Manag.

Journal information

EDITION
Science Citation Index Expanded (SCIE)

CATEGORY
ENERGY & FUELS - SCIE
THERMODYNAMICS - SCIE
MECHANICS - SCIE

LANGUAGES	REGION	1ST ELECTRONIC JCR YEAR
English	ENGLAND	1997

Publisher information

PUBLISHER	ADDRESS	PUBLICATION FREQUENCY
PERGAMON-ELSEVIER SCIENCE LTD	THE BOULEVARD, LANGFORD LANE, KIDLINGTON, OXFORD OX5 1GB, ENGLAND	24 issues/year

2021 JOURNAL IMPACT FACTOR
11.533
View calculation

JOURNAL IMPACT FACTOR WITHOUT SELF CITATIONS
9.932
View calculation

Journal Impact Factor Trend 2021 Export

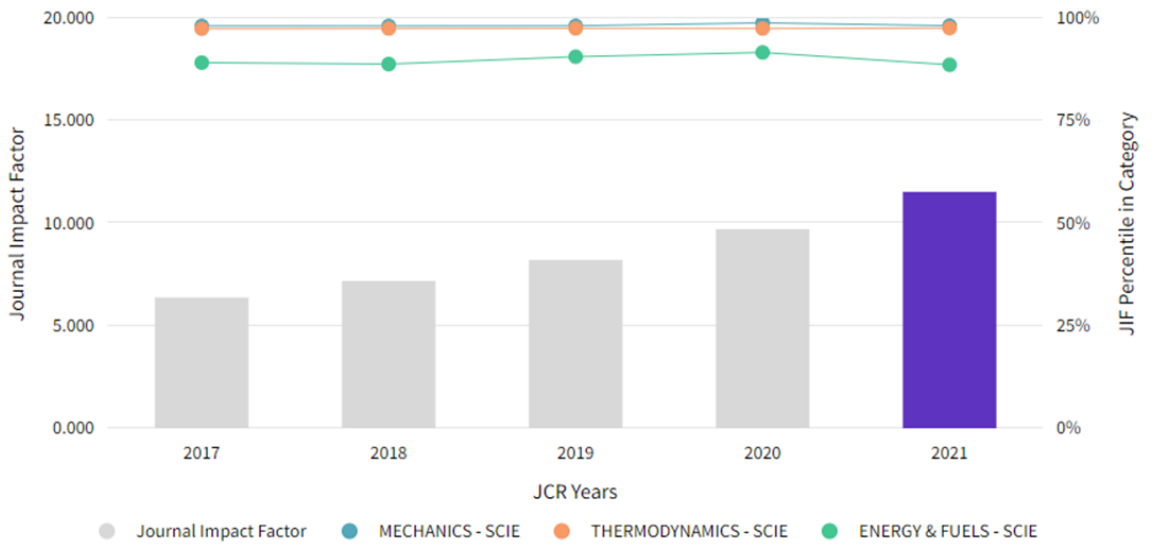

SJR
Scimago Journal & Country Rank

Scopus
ELSEVIER

Energy Conversion and Management

Formerly known as: Energy Conversion

Scopus coverage years: from 1979 to 2023

Publisher: Elsevier

ISSN: 0196-8904

CiteScore 2021	SJR 2021	SNIP 2021	H-INDEX
18.0	2.829	2.369	210

Subject area: Energy: Nuclear Energy and Engineering | Energy: Energy Engineering and Power Technology | Energy: Fuel Technology | Energy: Renewable Energy, Sustainability and the Environment

CiteScore 2021

18.0 = 83.487 Citations 2018 - 2021 / 4629 Documents 2018 - 2021

Calculated on 05 May, 2022

CiteScore rank 2021

Category	Rank	Percentile
Energy — Nuclear Energy and Engineering	#2/64	97th
Energy — Energy Engineering and Power Technology	#7/235	97th

CiteScore trend

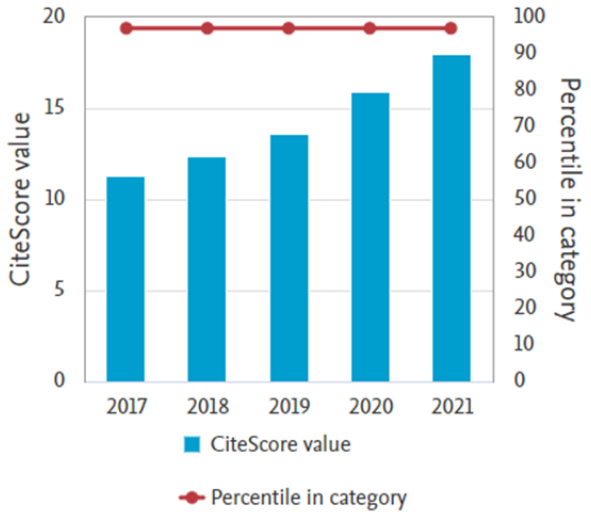

CAPÍTULO 4

CARACTERIZACIÓN DE PRESTACIONES A PARTIR DE MEDIDAS AERODINÁMICAS

4.1. Resumen

Como se ha mencionado anteriormente, los ensayos en túnel aerodinámico son una de las herramientas más importantes para el estudio de VAWT, pero presentan una complicada problemática difícil de superar. Este trabajo presenta el desarrollo formal y la aplicación de una metodología alternativa para la caracterización sin contacto de las fuerzas de empuje y el rendimiento de la turbina, utilizando datos procedentes de mediciones de flujo. Realizando un número muy asequible de mediciones experimentales del flujo, se obtienen datos suficientes que permiten la aplicación de la teoría de Volúmenes de Control (VC), superando los típicos problemas mecánicos derivados de los prototipos a pequeña escala. Esta metodología alternativa es de especial interés en montajes que presentan configuración confinada o dispositivos de aceleración de flujo (FADs), así como para estudios centrados en técnicas de visualización del flujo como PIV o ensayos sobre varias máquinas a la vez.

En este trabajo se han realizado medidas completas de la presión de entrada y el perfil de velocidades de la estela, para varios TSR distintos. Además, se ha medido también el perfil de velocidades en el centro del hueco inferior entre la turbina y el túnel. Estas medidas por si solas proporcionan información interesante sobre la naturaleza del flujo. No obstante, lo más relevante es que a partir de estas mediciones, se han estimado el empuje, el par y el rendimiento de la turbina estudiada mediante la teoría de VC, obteniendo una buena concordancia con los datos experimentales anteriores. La metodología descrita revela cómo un número moderado de medidas experimentales es suficiente para obtener la curva de rendimiento con una precisión razonable. Además, se ha realizado un análisis detallado sobre la incertidumbre, para comprobar la validez del método y prever variables críticas que requieren una precisión especial.

Sustainable Energy Technologies and Assessments 54 (2022) 102811

Contents lists available at ScienceDirect

Sustainable Energy Technologies and Assessments

journal homepage: www.elsevier.com/locate/seta

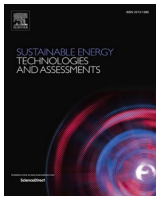

Performance assessment of vertical axis wind turbines (VAWT) through control volume theory

Luis Santamaría *, Katia María Argüelles Díaz, Mónica Galdo Vega, José González Pérez, Sandra Velarde-Suárez, Jesús Manuel Fernández Oro

Fluid Mechanics Area, Department of Energy, University of Oviedo, C/Wifredo Ricart s/n, Gijon, Asturias 33204, Spain

ARTICLE INFO

Keywords:
Vertical axis wind turbine
VAWT
Wind tunnel
Performance characterization
Control volume theory

ABSTRACT

Renewable technologies are the focus of today's energetic scenario. In this context, vertical axis wind turbines (VAWT) have been attracting interest in the last decade as they emerge as good candidates for urban applications and deep-water, multi-megawatt, offshore projects. Nevertheless, their current development state is still limited. Wind tunnel testing is one of the most important tools for their study, but involves high infrastructure costs, which lead to an important downscaling of the prototypes and the consequent problems associated. This work presents the formal development and use of an alternative methodology for characterization of turbine thrust, torque and performance without contact, using data from flow measurements. This is achieved by applying Control Volume (CV) theory which overcomes the typical mechanical issues derived from small-scale prototypes. Complete inlet pressure and wake velocity measurements have been performed and are presented here. From these measurements, turbine thrust, torque and performance have been obtained through CV theory, revealing good agreement with previous experimental data.

Introduction

The global awareness for the 17 Sustainable Development Goals (SDG), where climate action and demographic sustainability are basic pillars, is driving international governments to strongly support renewable energies, economically, legislatively, and politically. However, to meet the ambitious objectives being raised, as achieving net zero emissions by 2050, a massive effort is still needed. Conventional wind power and solar photovoltaic are the technologies currently leading the renewable scenario, with the focus on upscaling. However, with the incoming addition of hydrogen and other grid stabilization and/or energy storage technologies, alternative power generation technologies may still have a role in decarbonization. Furthermore, poly-generation and integrated technology approaches are becoming more common every day, not only in the industrial sector [1] but also in the residential one [2]. Therefore, in this framework, these alternative power generation technologies can find synergies and provide interesting and cost-effective solutions.

In this context vertical axis wind turbines (VAWT) have been receiving increased attention in the last decade, with deep water offshore and urban environments as their main applications. However, their aerodynamics are far complicated and there is still a lack of agreement in a best reference rotor design [3]. Hence, despite their interesting advantages, there is an important lack of real-scale projects, especially in the offshore setting [4]. In the urban application, were there is a small, but stablished, market for these turbines, the biggest setback is the low quality of the wind resource [5]. Thus, one of the latest trends in this field is flow augmentation, achieved either with devices as deflectors or wind lens, or taking advantage of architectural features [6]. Nevertheless, these devices, as well as the turbines are still in development and more research is needed to obtain competitive products.

Wind tunnel testing is vital for the study of this technology, both for the validation of models and simulations and for enhancing the understanding of the flow interactions, which ultimately produce the power output. However, there are some intrinsic problems derived from downscaling that conventional testing methodologies strive to overcome. Mainly, the torque measurement with torquemeters [7] or passive/resistant devices (Prony or electromagnetic brakes [8,9]) increases the mechanical resistance, thus compromising the testable operative ranges. Though sophisticated control systems have been proposed to measure positive torque gradients for the torque-speed ratio curve [10], important restrictions still arise at low power regimes. Therefore, the

* Corresponding author.
E-mail address: santamarialuis@uniovi.es (L. Santamaría).

https://doi.org/10.1016/j.seta.2022.102811
Received 20 May 2022; Received in revised form 22 September 2022; Accepted 28 September 2022
Available online 7 October 2022

Nomenclature

ADM	Active driving mode
b	Wind tunnel test section width
c	Turbine blade airfoil cord
C_P	Power coefficient $\left(\frac{2\omega T_{aero}}{\rho D H v_\infty^3}\right)$
CV	Control Volume
D	Turbine diameter
$\vec{F}$	Acting forces on the fluid
F_w	Frictional shear forces on the tunnel sidewalls (wall)
F_x	Thrust force
h	Wind tunnel test section height
H	Turbine blade Span
I_{x_i}	Turbulent intensity for the streamwise component, in position i
k	Turbulent kinetic energy
$\dot{m}$	Mass flow rate
$\vec{n}$	Normal vector of control surface
N	Number of blades
p_i	Static pressure in position i
p_i'	Fluctuating term of the static pressure in position i
P_i	Averaged term of static pressure in position i
PDM	Passive driving mode
Q_i	Volumetric flow rate in position i
R	Turbine radius
S	Control surface
t	Instant of time
$\vec{t}_i$	Time vector associated to a variable in position i
T	Time period
T_{aero}	Aerodynamic torque
u_i	Streamwise component of total (averaged plus fluctuating) velocity in position i
u_i'	Fluctuating term of the streamwise component of the velocity
U_i	Streamwise component of averaged velocity in position i
v_i	Transversal component of total (averaged plus fluctuating) velocity in position i
v_i'	Fluctuating term of the transversal component of the velocity
$\vec{v}_i$	Averaged wind velocity measured in position i
v_∞	Reference wind velocity ($\vec{v}_1$)
V_i	Transversal component of averaged velocity in position i
$\dot{W}_{vis}$	Viscous drag energy losses in the walls
$\dot{W}_{shear}$	Shear losses in the walls
$\dot{W}_T$	Mechanical energy of the turbine
x	Streamwise direction
y	Transversal direction
Z	Vertical coordinate of measurement positions
α_2	Averaged wind velocity angle in a point of the turbine section outlet (near wake)
ΔP_{i-i}	Pressure difference between different i positions
λ	Tip-speed ratio $\left(\frac{\omega R}{v_\infty}\right)$
ρ	Air density
σ	Turbine solidity $\left(\frac{2Nc}{D}\right)$
τ_i	Shear stress in position i
ω	Turbine rotational speed
0	Position 0, wind tunnel settling chamber
1	Position 1, wind tunnel nozzle outlet
1′	Position 1′, turbine section inlet
2	Position 2, turbine section outlet
$-mid$	Referred to a variable measured in the midplane (Z = 0)
$-gap$	Referred to a variable measured in the center of the gap between the turbine and the floor of the test section (Z = −0.75H)

development of alternative methodologies which are able to avoid these difficulties is inherently interesting.

This work presents an alternative methodology based on performance assessment without contact, obtained from the study of the flow. This alternative methodology is of special interest in set-ups which have a confined configuration or the previously mentioned flow augmentation devices, as well as for studies which are centered in flow visualization techniques as PIV [11]. In both cases, active driving mode (ADM) tests can be applied, producing an equivalent flow behavior to the conventional passive driving mode (PDM) [12,13]. This has the advantage of avoiding cut-in problems and other issues derived from the low available torque with respect to the set-up mechanical losses. Then, carrying out a very affordable number of experimental flow measurements, sufficient data is obtained allowing the application of Control Volume (CV) theory.

Although specifically developed for research environments at the laboratory, the methodology can be applied for real-scale turbines. However, significant difficulties, like the proper definition of control volume or the cost-effective extension of the measurement rakes, discourages its application in favor of a direct mechanical characterization of the turbine performance.

Up to the authors' knowledge on open literature, this is the first time that CV theory is used to provide valuable results for the experimental characterization of VAWTs performance at lab scale. When small-scale prototypes have to be tested in research facilities, the direct determination of mechanical variables for performance measurement can be an issue. Alternatively, aerodynamic variables can be better measured and CV theory employed as a feasible option to complete the mechanical and power balance of the turbine at a convenient cost. In this paper, the methodology described reveals how a moderate number of experimental measurements is sufficient to obtain the performance curve with a reasonable precision. Moreover, a detailed analysis is performed on uncertainty control to check the validity of the method and foresee critical variables requiring especial accuracy.

This work presents a successful application of this methodology to a VAWT wind tunnel set-up described in section 2 and includes the formal development of the control volume theory analysis (section 3). The results from the experimental flow measurements, which serve as basis for its application, are shown in section 4, whereas results from the application of CV theory are exposed and discussed in section 5. Finally, conclusions are drawn, and future works are proposed in section 6.

Experimental set-up and measurements

For this investigation, a specific set-up was designed and arranged in the facilities of the Fluid Mechanics Area of the University of Oviedo. The experiments were performed in the "XAWT" (Xixón Aeroacustic Wind Tunnel), which is a medium size, closed-loop wind tunnel powered by a 30 kW axial fan. The test chamber is anechoic with a cross-section area of 4.45x2.80 m^2 and 4.2 m in length. Fig. 1a), displays a general view of the facility. Velocities up to 22 m/s can be achieved for a mean turbulence intensity around 0.7 % in the test section of 1.15x1 m^2; additional data can be found in [14]. A semi-confined environment is used to enclose the vertical axis turbine, so the dimensions of the test section are preserved towards the exit (extension of 1.7 m). A detailed diagram of the layout of the test chamber with the turbine enclosure is

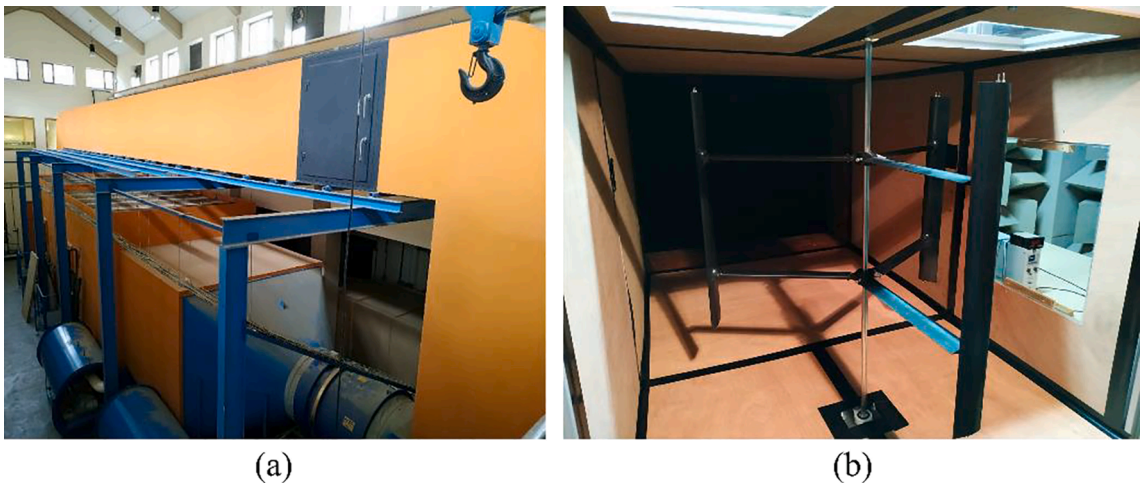

Fig. 1. a) Picture of general overview of the wind tunnel. b) Turbine prototype inside the test section of the wind tunnel.

found later in Fig. 2.

For this research, preliminary aerodynamic measurements of an H-rotor VAWT, performed for a previous work [15], are used in combination with some additional data. To evaluate the performance of the turbine, the authors have recently developed and presented a novel methodology based on active driving mode tests (ADM). This methodology is able to overcome the intrinsic problems from downscaling in a lab environment, assuring good results with remarkable agreement to equivalent CFD simulations. More details can be found in [16]. Precisely, those results are used now as a reference to analyze the outcome of the present work.

The studied turbine was designed for urban environments [17] and it is composed of 3 straight blades (N) with airfoil profile DU 06-W-200, each of them supported by two airfoil-shaped struts with the EPPLER 863 profile (for minimum drag). The dimensions of the scaled prototype are: 0.8 m of diameter (D), 0.6 m of span (H) and 0.067 m of airfoil cord (c), corresponding to a solidity ($\sigma = 2Nc/D$) of 0.5 and aspect ratio (H/D) of 0.75. Fig. 1b), shows the turbine prototype inside the test section of the wind tunnel.

Regarding instrumentation, several pressure transducers were used in combination with pressure tabs to measure static pressures and/or with probes to measure wind velocity. In particular, a digital, differential pressure manometer has been used to measure the inlet velocity, from the pressure difference between the settling chamber and the nozzle outlet. Due to the contraction ratio of 16:1 in the nozzle, the wind velocity in the settling chamber is assumed negligible. For all the experimental dataset, a nominal test velocity of 7.5 m/s has been fixed. Two additional digital manometers were used to measure mean static pressure differences between position 1 and 1′ and between position 1 and 2 (see Fig. 2). A pitot tube was used in the center of the test section at position 1′ to obtain the streamwise velocity upstream of the turbine. Finally, a tailor-made 3-hole pressure probe ("Cobra" type) was used in position 2 to measure in-plane velocity components of the horizontal wake. This pressure probe has been previously developed and tested by members of the research team in precedent works [18,19] and provides a wide angular range of ± 80 deg. This significant feature, and the inherent characteristics of the probe, make it an exceptional tool for this kind of measurements. The Cobra probe is mounted in a positioning system which allows an easy and precise transversal displacement to measure accurately the wake velocity profile. A figure featuring the positioning system and the Cobra probe can be found in the supplementary material accompanying this article.

The measurements were performed in 3 stages. Firstly, the upstream velocity was measured with the pitot tube for 5 different tip-speed ratios ($\lambda = \frac{\omega R}{v_\infty}$, where λ is the tip-speed ratio, ω is the rotational speed of the turbine, R is the radius and v_∞ is the reference wind velocity v_1). To

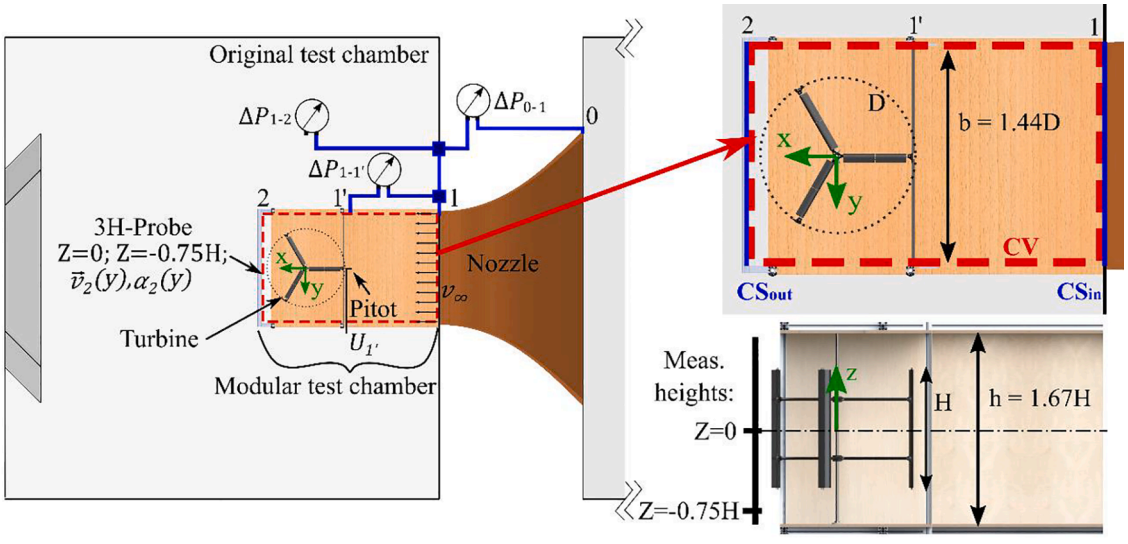

Fig. 2. Three-bladed H-VAWT installed inside an hybrid modular enclosure for the test chamber of the XAWT wind tunnel.

avoid any downstream interferences, these single measurements were completed independently, removing the pitot afterwards. Secondly, in order to obtain a detailed insight on the performance and aerodynamic behavior of the turbine, intensive measurements were performed for 9 different tip-speed ratios at both inlet and outlet midspan sections of the enclosure. The inlet wind velocity (v_1) was kept constant, while the rotational velocity was modified using active driving mode by means of a DC motor. For each tip-speed ratio, meantime wake velocities and incidence angles were measured transversally in the mid-plane at 39 positions (3 cm resolution approximately). While these measurements were obtained, both pressure differences $\Delta P_{1-1'}$ and ΔP_{1-2}, as well as the inlet velocity, have been also recorded, and time-averaged later. Finally, the procedure is repeated placing the cobra probe in the middle of the lower gap between the turbine tip and the enclosure end-wall, which corresponds to a height of Z = − 0.75H below the mid-plane. A complete diagram of the set-up layout and the measurement positions is included in Fig. 2. The uncertainties of the instrumentation used in this work have been detailed in a table included in the supplementary material accompanying this article.

The complete set-up used allows the application of Control Volume (CV) theory in the dashed-red volume defined in Fig. 2. The next section presents in detail the formal development and analysis of this procedure.

Control volume theory

Integral relations obtained from control volume theory can be applied over a turbomachine to evaluate its performance in terms of torque, power consumption and exerting forces. Using the Reynolds transport theorem, balances of mass flow, linear and angular momentum, and energy can be established in multirow environments over integral flow quantities for that purpose. Alternatively, the direct integration of differential balances within the rotor domain provides equivalent formulations for the estimation of the machine performance [20].

Despite it is usually considered as a preliminary approach for the analysis of the internal flow in turbomachinery, CV has been used successfully by several authors to obtain valuable results for both axial and centrifugal geometries [21–24]. Note that a precise analysis requires the inclusion of centrifugal, Coriolis, viscous and blade forces acting in an unsteady fashion, though unsteady components are usually not included in the framework. This has been quite controversial since the demonstration of the necessity of unsteady flow in turbomachines [25], but generally circumvented using CV surfaces outside the blades' vicinity. Time-averaging can also be employed to retrieve the mean-time performance of the turbomachinery, thus introducing additional terms that must be addressed conveniently.

Mass conservation

In the case of the VAWT under study, the control volume depicted in Fig. 2 has been defined for further consideration. Inlet and outlet sections are denoted as (1) and (2) in the figure, with the CV encapsulating all the adjacent blade walls and other solid boundaries. Note that the vertical axis responsible for the turbine rotation corresponds to the axial direction (z-coordinate).

Despite of the cylindrical geometry of the turbine, Cartesian coordinates have been preserved in the following analysis. This is more convenient because the velocity distributions at both inlet and outlet sections are expressed according to the streamwise (u) and transversal (v) directions more easily. After some algebra, the mass conservation equation can be rearranged and expressed as follows:

$$\frac{\partial}{\partial t}\int_{CV}\rho dV + \int_1 -\rho u_1 dS + \int_2 \rho u_2 dS = 0 \tag{1}$$

All the flow variables can be split into average and fluctuating terms due to total unsteadiness (turbulence and periodic wake shedding). In a 2D fashion at the midspan section of the turbine, it is expressed as:

$$u = U + u', v = V + v' \tag{2}$$

where the mean quantities are defined as time averaged variables over a sufficient amount of time.

$$U = \frac{1}{T}\int_t^{t+T} u(t)dt; V = \frac{1}{T}\int_t^{t+T} v(t)dt \tag{3}$$

The time-averaged value of the axial torque can be obtained applying the averaging operator over equation (1). The temporal term is cancelled and taking advantage of the averaging properties, this final expression for incompressible flow is easily found:

$$\int_1 U_1 dS = \int_2 U_2 dS = \int_2 U_{2,gap}\, dS + \int_2 U_{2,mid}\, dS \tag{4}$$

where the outlet section (2) has been split in two different zones (see Fig. 2): the inner region corresponding to midspan locations of the turbine (mid) and the outer region for the vertical clearance with the ducted tunnel (gap).

Linear momentum

In general, the temporal variation of the linear momentum is a consequence of the momentum exchange in the inlet and outlet sections of the control volume, as well as the contribution of both static pressure and shear stress acting on the surfaces of the control volume. A particular form can be retrieved to isolate the force acting on the surfaces of the turbomachinery, resulting in the following classical expression (a nice derivation can be found in [20]):

$$\begin{aligned}\sum \vec{F} = &-\frac{\partial}{\partial t}\int_{CV}\rho\vec{v}\, dV + \int_1 d\dot{m}\, \vec{v}_1 - \int_2 d\dot{m}\, \vec{v}_2 + \int_1\left(-\vec{n}_1 p_1 dS\right)\\ &+\int_2\left(-\vec{n}_2 p_2 dS\right) + \int_1\left(-\vec{t}_1\tau_1 dS\right) + \int_2\left(-\vec{t}_2\tau_2 dS\right)\end{aligned} \tag{5}$$

where $d\dot{m} = \rho\, dS\, \vec{n}\cdot\vec{v}$ represents the differential mass flow rate and 1, 2 are identified as inlet and outlet sections respectively. All the terms in the equation are fully unsteady and stand for the accumulated (integral) contributions of the momentum of static pressures and shear stresses at flow boundaries, as well as the impulse of both incoming and outgoing momentum flow rates. The temporal variation of enclosed kinetic impulse in the CV is also considered. The left-hand side term, $\vec{F}$, includes volumetric forces (i.e. gravitational forces), frictional shear forces on the tunnel sidewalls (wall) and the overall force exerted by the VAWT. Of particular interest is the streamwise component, F_x, acting on the turbomachine since it provides the expression to obtain the axial thrust:

$$F_x + F_w = -\frac{\partial}{\partial t}\int_{CV}\rho u\, dV + \int_1 \left(p_1 + \rho u_1^2\right) dS - \int_2 \left(p_2 + \rho u_2^2\right) dS \tag{6}$$

where the shear stresses on both inlet and outlet sections are vanished. Finally, the time-averaged expression for the linear momentum equation can be obtained considering second-order statistics for the x-velocity component ($\overline{u^2} = \overline{u'^2} + U^2$) and first-order decomposition for the static pressure ($p = P + p'$), resulting:

$$\overline{F_x} = -\overline{F_w} + \int_1 \left[P_1 + \rho\left(U_1^2 + \overline{u_1^2}\right)\right] dS - \int_2 \left[P_2 + \rho\left(U_2^2 + \overline{u_2^2}\right)\right] dS \tag{7}$$

In the present analysis, the inlet section (1) is located far upstream (at × = − 1.85D) to avoid interference effects of the turbine blockage, thus being relevant the longitudinal wall friction in the tunnel. Simple considerations, based on the D'Arcy-Weisbach equation, can be employed to express the tangential force as a function of the pressure

loss in the duct, giving to: $\overline{F_w} = \overline{\Delta P}_{1-1'} hb$, where h and b represent the height and width of the enclosure respectively.

Finally, equation (7) requires the evaluation of the turbulent quantities. It is a common practice to define the turbulent intensity for the streamwise component, I_x, as the ratio between the fluctuating velocities and its mean value according to: $I_x = \sqrt{\overline{u'2}}/U$. Consequently, the final equation to retrieve the time-averaged thrust on the turbine yields:

$$\overline{F_x} = -\overline{P}_{1-1'} hb + \int_1 \left[P_1 + \rho U_1^2\left(1 + I_{x,1}^2\right)\right] dS - \int_2 \left[P_2 + \rho U_2^2\left(1 + I_{x,2}^2\right)\right] dS \tag{8}$$

Though not expressed in eq. (8) for compactness, the outlet integral (2) is also split into the midspan (mid) section and the outer region of vertical clearance (gap) for further evaluation.

Energy equation

The general expression for the exchange of mechanical energy with the turbine (neglecting heat transfer and variations of internal energy and elevation) is expressed as:

$$\begin{aligned} -\dot{W}_T - \dot{W}_{vis} = &-\frac{\partial}{\partial t}\int_{CV}\left(\frac{1}{2}\vec{v}\cdot\vec{v}\right)dV - \int_1\left[\frac{P_1}{\rho} + \frac{1}{2}\vec{v}_1\cdot\vec{v}_1\right]\rho dS\vec{n}_1\vec{v}_1 \\ &+ \int_2\left[\frac{P_2}{\rho} + \frac{1}{2}\vec{v}_2\cdot\vec{v}_2\right]\rho dS\vec{n}_2\vec{v}_2 + \int_1\left(-\vec{t}_1\tau_1 dS\vec{v}_1\right) \\ &+ \int_2\left(-\vec{t}_2\tau_2 dS\vec{v}_2\right) \end{aligned} \tag{9}$$

The triadic tensor terms derived from the time-averaged transport of kinetic energy in the inlet and outlet sections complicates the evaluation of eq. (9). After some manipulation, this contribution (in vectorial form) can be arranged as follows [26]:

$$\left(\frac{1}{2}\vec{v}\cdot\vec{v}\right)\vec{v} = \frac{1}{2}\begin{bmatrix}\left(U^2+V^2\right)U + \left(\overline{u^2}+\overline{v^2}\right)U + \overline{\left(u^2+v^2\right)u'} + 2\left(U\overline{u^2} + V\overline{u'v'}\right) \\ \left(U^2+V^2\right)V + \left(\overline{u^2}+\overline{v^2}\right)V + \overline{\left(u^2+v^2\right)v'} + 2\left(+U\overline{u'v'} + V\overline{v^2}\right)\end{bmatrix}, \tag{10}$$

Following, with the time-averaging operator applied over eq. (9), a reordering of all the terms leads to:

$$\begin{aligned} \overline{\dot{W}_T} = &\underbrace{\int_1\left[P_1 + \frac{1}{2}\rho\left(U_1^2+V_1^2\right)U_1 dS - \int_2\left[P_2 + \frac{1}{2}\rho\left(U_2^2+V_2^2\right)U_2 dS\right]\right]}_{[I]} + \\ &\underbrace{\int_1\frac{1}{2}\left[\left(\overline{u_1^2}+\overline{v_1^2}\right)U_1 + 2\left(U_1\overline{u_1^2} + V_1\overline{u_1'v_1'}\right)\rho dS - \int_2\frac{1}{2}\left[\left(\overline{u_2^2}+\overline{v_2^2}\right)U_2 + 2\left(U_2\overline{u_2^2} + V_2\overline{u_2'v_2'}\right)\right]\rho dS\right]}_{II} + \\ &\underbrace{\int_1\left[\overline{p_1'u_1'} + \frac{1}{2}\rho\overline{\left(u_1^2+v_1^2\right)u_1'}\right]ds - \int_2\left[\overline{p_2'u_2'} + \frac{1}{2}\rho\overline{\left(u_2^2+v_2^2\right)u_2'}\right]dS}_{III} - \underbrace{\overline{\dot{W}}_{shear} - \overline{\dot{W}}_{vis}}_{IV} \end{aligned} \tag{11}$$

In eq. (11), the first term [I] stands for the energy transport of the mean-time mechanical energy of the flow. The second term [II] is associated with the transport of turbulent fluctuations, while the third term [III] is a pure fluctuating term. The final contribution in [IV] accounts for the shear stresses at the flow boundaries and the frictional force at the inlet duct.

Further considerations can be made for the second term in order to reduce the number of variables concerned. In particular, introducing the experimental observation that the stress-intensity ratio $\overline{u'v'}/k$ can be approximated to 0.3 in the log layer of thin shear layer flows [27], being k the turbulent kinetic energy, and assuming isotropic turbulence so $\overline{u^2} = 2k/3$, the turbulent quantities involved in [II] can be expressed as a function of the mean values. Thus, also using the definition of turbulent intensity, it is straightforward to obtain:

$$\begin{aligned} \overline{\dot{W}_T} = &\int_1\left[P_1 + \frac{1}{2}\rho\left(U_1^2+V_1^2\right)\right]U_1 dS - \int_2\left[P_2 + \frac{1}{2}\rho\left(U_2^2+V_2^2\right)\right]U_2 dS \\ &+ \int_1\left[2\,U_1 + a^2V_1\right]\rho U_1^2 I_{x,1}^2 dS - \int_2\left[2\,U_2 + a^2V_2\right]\rho U_2^2 I_{x,2}^2 dS - \overline{P}_{1-1'}Q \end{aligned} \tag{12}$$

where $a^2 = 0.45$ and the third term [III] has been assumed to be negligible [26]. In addition, the energy loss due to the shear stresses at the entrance and exit cross sections of the flow channel in [IV] must usually be ignored in practical applications.

This final equation (12) allows to compute the aerodynamic power of the VAWT as a function of the mean time values of the flow field measured at both inlet and outlet sections. A rough estimation of the turbulent intensity for the streamwise component must also be provided in order to analyze the averaged impact of the flow fluctuations in the aerodynamic power. Moreover, assuming uniform pressure distributions at both sections (at the inlet it is fulfill due to symmetric kinematic conditions at the nozzle discharge, whereas there are atmospheric conditions at the flow discharge), the pressure work can be easily evaluated. Note that only in-plane components have been considered relevant: local variations of out-plane components related to departure from 2D flow in the axial direction (at midspan) and streamwise mixing-out within the turbine enclosure are considered marginal for the evaluation of the turbine power. As before, the integral in section (2) has been divided in the inner (mid) and outer (gap) zones for the evaluation of the velocity distributions measured experimentally.

Measurement results

Upstream velocity and inlet pressure drop

The evolution of the upstream velocity at the turbine inlet, normalized by the incoming velocity, is shown in Fig. 3a). At low tip-speed ratios (from 0.0 to 1.6), streamwise velocity in position 1′ is practically identical to the inlet velocity. Between tip-speed ratios from 1.6 to 2.5 there is a remarkable decrease of roughly 10 % in the velocity value. Note that this result is coherent with previous experimental data evidencing that positive net torque generation starts around a tip-speed ratio of 2 for this rotor design [16]. From 2.5 to 3.5, the velocity drop is slowed down, although a total reduction of almost a 15 % is perceived. This evidence justifies the extension of the inlet section for the control volume and the need for considering the influence of section 1-1′ in the analysis.

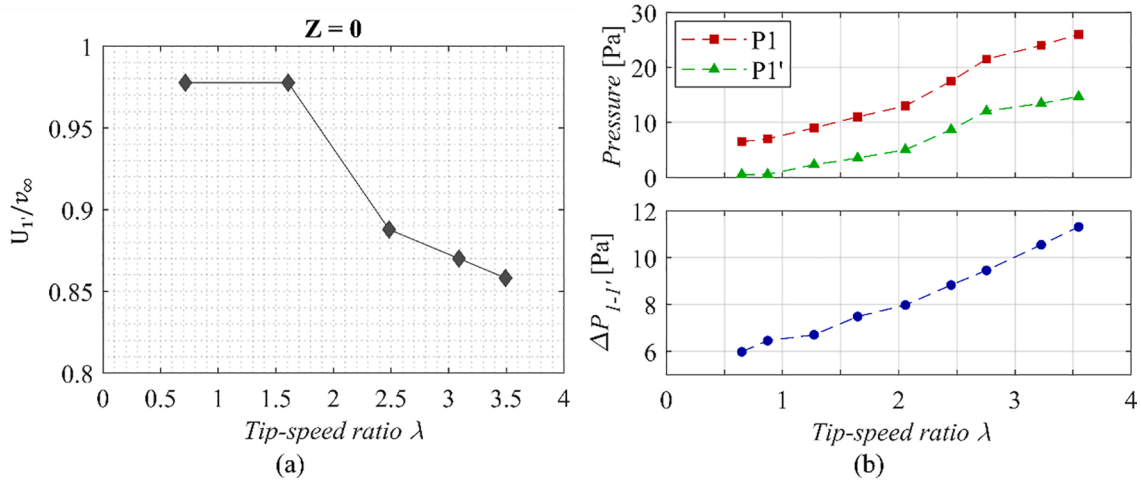

Fig. 3. a) Dimensionless mean velocity in the upstream section (mid-plane height) for 5 different tip speed ratios. b) Manometric pressure at 1 and 1′ and pressure difference for 9 different tip-speed ratios.

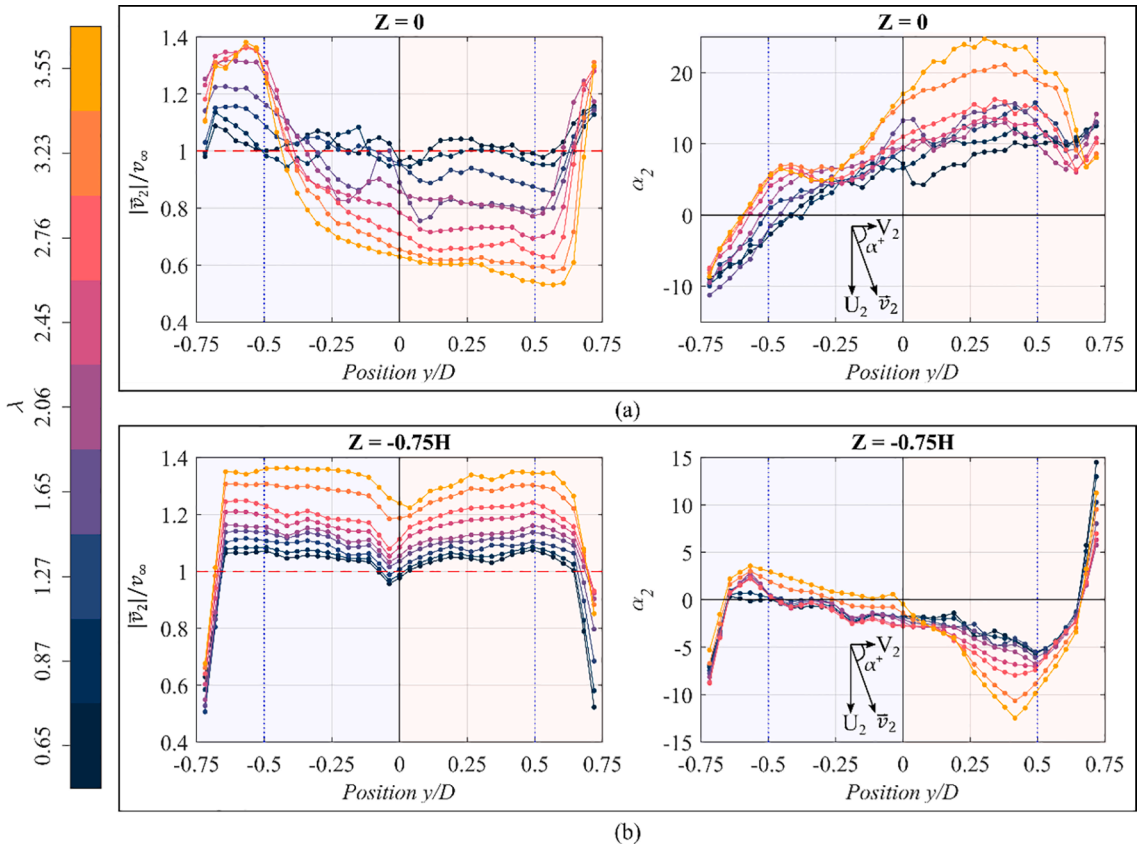

Fig. 4. Transversal distributions of velocity magnitude and flow angle as a function of the tip-speed ratio *a)* measured in the mid-plane of the near wake area. b) measured in the axial gap of the near wake area.

Figure 3b), shows the evolution of the static pressure measured at the turbine inlet for the whole range of tip-speed ratios tested. It is expressed in relative terms (gauge) since the manometric pressure in position 2 (*P2*) is atmospheric (0 Pa). The pressure loss between sections 1 and 1′ increases almost linearly with the tip speed ratio, exhibiting a quite small difference that ranges from 6 to 12 Pa (blue dashed line). The pressure drop across the turbine is quite similar, ranging from 0 to 15 Pa (green dashed line), although its increasing trend somewhat resembles the behavior of the turbine performance curve. Note that the total pressure difference between the inlet and outlet sections of the CV is significant, ranging from 8 to 28 Pa (red dashed line).

Wake velocity profiles

A complete characterization of the wake velocities and in-plane flow angles has been performed transversally in position 2 for the whole range of tip-speed ratios. Fig. 4a) shows the results of the measurements conducted in the mid-plane (Z = 0). The velocity magnitude $\left|\vec{v}_2\right|$, made dimensionless with the inlet velocity, is plotted along the transversal

position over the turbine diameter, in the left graph. Vertical dashed lines indicate the turbine width. The light blue area of the graph corresponds to the zone in which the turbine blade is moving leeward, while the light red area corresponds the windward zone. The velocity distribution for each tip-speed ratio has been colored according to the color-bar scale. There is a progressive increase in the velocity magnitude at the lateral sides, especially in the leeward area. Likewise, in the wake of the turbine there is a remarkable decrease in the velocity magnitude, particularly in the windward area in which a 50 % reduction with respect to the inlet velocity is observed at the highest tip-speed ratio. Regarding the flow angle (right plot), there is a significant increment across the whole range of tip-speed ratios, indicating a progressive enlargement of the transversal component of the velocity that matches the direction of rotation of the turbine. This angle increase is mostly appreciated in the windward area.

In Fig. 4b), similar velocity and angle profiles are presented, but now corresponding to the central line of the gap (axial clearance, $Z = -0.75$) between the turbine and the wind tunnel.

The overall magnitude of the velocity in this section is quite constant, except for the central part, which is probably affected by the shaft shadow. On the sides, the shear layer produced by the wind tunnel walls is easily identifiable. As it can be noted, there is a remarkable increase of the gap velocity, achieving almost 140 % of the inlet velocity. Also, there is a noticeable increase in the magnitude of the angle, especially in the windward area, indicating a widening of the stream.

Control volume theory results

Steady measurements shown in previous section have been employed to evaluate the integral relationships derived from CV theory for the present set-up (equations (4), (8) and (12)). Unsteady contributions due to turbulence have been introduced assuming characteristic turbulent intensity levels for both mid-span and gap zones. These values were roughly estimated based on auxiliary hot-wire measurements and results from CFD simulations. In particular, an averaged turbulence level of 0.7 % has been assumed at the control volume inlet, while an increased turbulent intensity of a 12 % was employed at the turbine exit, and a 2 % in the gap section. Although unsteady effects can be relevant and should not be omitted, it is demonstrated that a precise quantification of the turbulence level is marginal for a correct application of the method. In following section 5.4, other factors are shown to have a critical impact for a sufficient characterization of the turbine performance.

Mass conservation

Two approaches have been compared to assess the minimum number of measurements required for a representative application of the control volume theory. Firstly, applying mass conservation (eq. (4)), the flow rate in the gap region of the outlet section can be derived from the measurements at the mid-plane. Following, this result is compared with the flow rate computed directly from the measurements in the center of the gap clearance (considered representative for the hole gap). Table 1a) shows the flow rates for the different tip-speed ratios measured and the flow rate obtained indirectly from mass balance for the gap area. Likewise, Table 1b) shows the resultant flow rate in section 2 obtained from the use of the gap measurements. Also, the absolute and relative differences in the computed flow rate at the outlet are provided. Note that the maximum flow rate difference is only a 3 %, in the case of the highest tip-speed ratio. Moreover, characteristic discrepancy can be established around 1 % which it is remarkably low to validate the assumption of planar flow.

Linear momentum

Linear momentum equation has been applied to obtain the axial thrust of the turbine. Typically, the direct measurement of aerodynamic forces is a complex task, involving elaborate set-ups where the turbine is installed on a multiple component balance. Moreover, at a lab scale these forces are significantly small, which usually compromises the obtention of a reliable value. Complementary methods for an indirect estimation of the forces in VAWTs prototypes are thus interesting and demanded.

Consequently, both approaches (applying continuity or measuring the gap flow) have been compared for the estimation of the axial thrust using equation (8). The obtained results are shown in Table 2. Thrust forces range from almost 0 to 11 or 14 N (depending on the approach) which are coherent values for this kind of turbine rotor. In addition, the greatest difference in the estimation of the reaction force at the outlet gap is only a 10 % at the highest tip-speed ratio, which it is a quite remarkable result considering the small values of those forces. In this worst case, maximum differences between approaches represent only a couple of N for the overall thrust of the turbine.

Energy equation

Finally, the measured data is employed to evaluate the integral terms of the energy equation to obtain the performance curve of the turbine. Equation (12) provides the aerodynamic power directly, which can be further divided by the rotational velocity to retrieve the aerodynamic torque. The results are compared with the experimental measurements obtained from the application of the ADM methodology in the same set-up [16].

Fig. 5 shows the power coefficient ($C_P = 2\omega T_{aero}/\rho DHv_\infty^3$) versus tip-speed ratio in a non-dimensional form. The same figure in terms of aerodynamic torque versus rotational velocity can be found in the supplementary material accompanying this article. Results derived from the application of mass conservation are plotted with red circles and dotted lines. Likewise, results using the gap measurements are plotted with green squares and dotted lines. The experimental results are represented

Table 1
a) Computed volume flow rates using mid-plane measurements and continuity equation. b) Computed volume flow rates using mid-plane measurements and gap measurements. Absolute and relative differences in computed flow rate at the outlet (position 2).

(a)				(b)			
λ	$Q_1 = Q_2$	Q_{2mid}	Q_{2gap} (Continuity)	Q_{2gap} (meas.)	Q_2	E_{abs}	E_r
[-]	[m^3/s]	[m^3/s]	[m^3/s]	[m^3/s]	[m^3/s]	[m^3/s]	[%]
0.65	8.77	5.33	3.44	3.56	8.89	−0.12	−1.33
0.87	8.76	5.19	3.57	3.60	8.80	−0.03	−0.39
1.27	8.75	5.13	3.62	3.68	8.82	−0.06	−0.71
1.65	8.74	4.89	3.85	3.78	8.68	0.07	0.75
2.06	8.85	5.09	3.76	3.90	8.99	−0.14	−1.57
2.45	8.84	4.81	4.03	4.03	8.84	0.00	−0.02
2.76	8.82	4.53	4.29	4.14	8.67	0.15	1.74
3.23	8.81	4.24	4.57	4.37	8.61	0.19	2.18
3.55	8.79	3.99	4.80	4.53	8.52	0.27	3.03

Table 2
a) Computed thrust forces using mid-plane measurements and continuity equation. b) Computed thrust forces using mid-plane measurements and gap measurements. Absolute and relative differences in computed flow rate at the outlet (position 2).

(a)						(b)			
λ [-]	F_{x1} [N]	$F_{x\ wall}$ [N]	$F_{x2\text{-}mid}$ [N]	$F_{x2\text{-}gap}$ (Continuity) [N]	F_x (Continuity) [N]	$F_{x2\text{-}gap}$ (Measured) [N]	F_x (Measured) [N]	E_{abs} (F_{x2}) [N]	E_{rel} (F_{x2}) [%]
0.65	47.07	−6.86	−24.74	−15.59	−0.12	−16.80	−1.33	−1.21	7.76
0.87	47.65	−7.41	−23.58	−16.74	−0.08	−17.21	−0.55	−0.47	2.81
1.27	49.94	−7.69	−23.25	−17.22	1.78	−17.97	1.02	−0.76	4.36
1.65	52.35	−8.59	−21.58	−19.46	2.72	−18.94	3.24	0.52	−2.67
2.06	56.26	−9.15	−23.70	−18.61	4.79	−20.14	3.27	−1.53	8.22
2.45	60.85	−10.14	−21.79	−21.33	7.59	−21.49	7.44	−0.15	0.75
2.76	65.15	−10.86	−19.81	−24.22	10.27	−22.65	11.84	1.57	−6.48
3.23	68.31	−12.11	−17.91	−27.38	10.91	−25.29	13.00	2.08	−7.63
3.55	70.61	−12.99	−16.29	−30.23	11.10	−27.18	14.15	3.05	−10.09

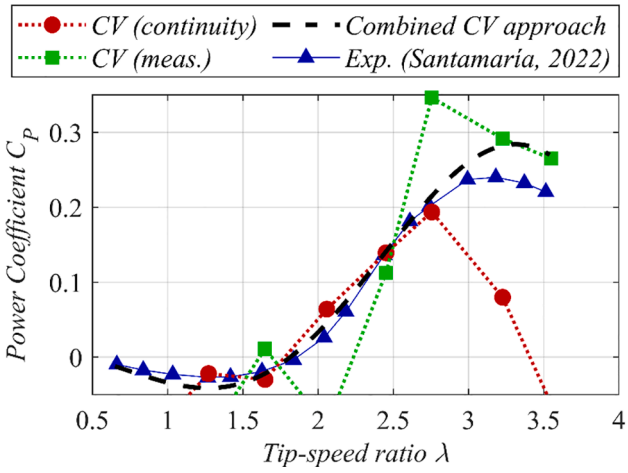

Fig. 5. Computed aerodynamic performance as a function of the tip-speed ratio. Comparison of results from the application of CV theory with experimental measurements.

with blue triangles and continuous lines in the figure.

For low tip-speed ratios (below 1.27, corresponding to 230 rpm), the results obtained with the CV theory are not consistent with the experimental values. Power coefficient and torque values drop severely to high negative values ([-0.1, −0.23] and [-1, −2.2] Nm for the continuity and the gap measurement approaches respectively), revealing that the measured values are excessively small to obtain reliable estimations from the integral relationships. For moderate tip-speed ratios, between 1.27 and 2.76 (505 rpm), the results of the CV theory with the continuity approach perfectly reproduce the experimental curve for both torque and performance coefficient. Alternatively, the CV results using gap measurements present important discrepancies, exhibiting significant oscillations. Finally, in the case of high tip-speed ratios (above 2.76), the results of CV theory using the gap measurements predict the experimental curve beyond the maximum point with high accuracy, while CV results using continuity suffer from a sudden, overestimated drop.

The deviation of the continuity-based CV theory at high tip-speed ratios is produced by the blockage effect of the turbine, which intensifies the relative importance of the gap flow. The moderate-to-low solidity of the turbine prevents this effect to be relevant at low tip-speed ratios. However, when the rotational speed is progressively increased, the apparent flow area in the turbine zone is reduced and a remarkable enlargement in the gap velocity is produced. Because of the limited gap, the increased velocity reduces the flow homogeneity in the spanwise direction. Thus, the mid-plane measurements are not sufficient to describe the outlet flow of the whole turbine span and, hence, the application of the continuity balance is no longer valid.

The fact that the results of the CV approach using gap measurements approximate better the experimental curve at high-tip speed ratios evidences the considerable influence of the gap over the turbine performance. However, this approach is also susceptible of introducing errors, especially at moderate tip-speed ratios, as observed in the points of tip-speed ratio 2.06 and 2.76, clearly out of range. This feature indicates the need for a concise assessment of the relevant variables introducing major uncertainties in the estimation of the turbine performance. A thorough analysis is presented in section 5.4.

To conclude, a performance curve based on CV theory is finally provided using the combined results of both approaches (plotted in Fig. 5 as a dashed, black line). A sum of sine waveforms has been used to blend the different datasets. In general, flow velocities at the gap can be derived from mass conservation to determine the torque and power coefficient curves when positive torque gradients are guaranteed (corresponding to low-to-moderate tip-speed ratios). On the contrary, the gap velocity and flow angle should be measured in case of high tip-speed ratios. The coherence of the results corresponding to very low tip-speed ratios requires further evaluation and ultimately it could be replaced by placing a first point in the origin.

Error transmission and influence

This paper is concluded presenting a detailed assessment of the most critical variables showing a major impact on the CV results. In particular, a thorough empirical analysis has been performed on error transmission and influence over the final performance figures. For that purpose, 1 % and 5 % deviations were applied to the measured variables independently, to evaluate the effect of these deviations in the final results. Special attention is devoted to the pressure and velocity components at both inlet and outlet sections of the control volume. Negative deviations were also applied, obtaining an almost fully symmetrical response, so they are not shown here for simplicity. The errors of the performance coefficients have been reduced to a single value by applying the Euclidean norm, in the following way:

$$\epsilon_r(C_P) = \frac{\|C_P - C_P^{'}\|}{\|C_P\|} = \frac{\sqrt{\sum \left(C_{P_i} - C_{P_i}^{'}\right)^2}}{\sqrt{\sum C_{P_i}^2}} \tag{13}$$

where C_P contains the values of the power coefficient for every tip-speed ratio in the original curve and $C_P^{'}$ are the deviated curves for each deviated variable. This is performed both for the continuity equation approach and the approach using gap measurements. The results for both approaches have been included in Fig. 6.

As expected, small errors in the measurements of the pressure and in the streamwise component of the velocity can cause large errors in the final performance coefficient, thus indicating that these variables are the most critical to the procedure. In the case of the continuity approach, it is shown that errors in the power coefficient estimation can be as high as a 60 % if pressure and velocity measurements are deviated roughly a 5 %

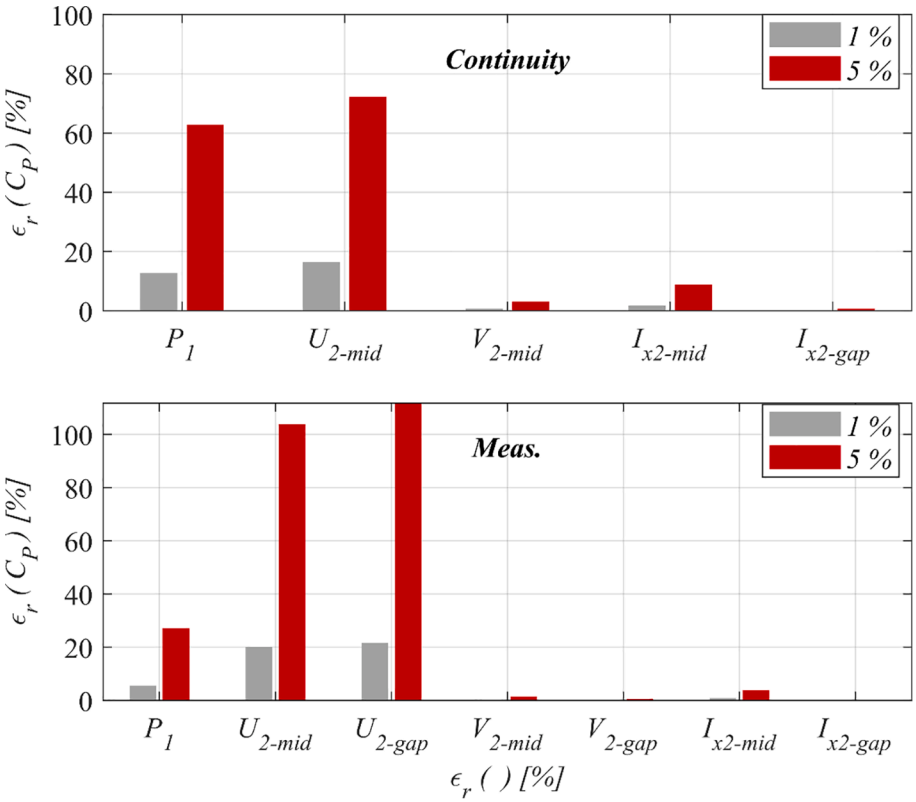

Fig. 6. Relative errors in the estimation of the turbine performance as a function of 1% and 5% errors in the input variables. Comparison between continuity equation and gap measurement approaches.

from its true value. Moreover, the worst situations are observed when the gap velocity is taken from the measurements, though the influence of the pressure is less important in that case. On the other hand, the transversal component of the velocity and the turbulence intensity in the gap have very small relevance, with deviations smaller than 3.1 % and 0.7 % respectively, for the 5 % input deviation and continuity equation approach and even lower in the approach based on gap measurements (1.3 % and 0.03 %). Turbulence intensity in the turbine region has a slightly higher relevance, with lower output than input deviations in the gap-measurements approach, being duplicated in the case of the continuity equation approach. In general, a maximum uncertainty below 1 % in the measured variables is recommended to preserve inaccuracies in the range of a 10 % in the estimation of the performance curve.

Conclusions

In this work, control volume theory has been presented as a useful tool for performance and thrust assessment of vertical axis wind turbines using flow measurements. The methodology has been formally developed from the theory and applied to a real set-up.

This methodology is of particular interest for the characterization of lab-scale prototypes, where the direct measurement of mechanical variables can be problematic at low power regimes. With a detailed measurement and analysis of the evolution of inlet pressures and outlet wake velocities, quality data has been provided and shown valid for the application of control volume theory.

The range of application of this methodology is found to be limited to the positive torque generation region, i.e. from $\lambda = 2.06$ on in the present turbine set-up, due to the quite low magnitude of the measured values at very low tip-speed ratios. From low to moderate tip-speed ratios an approach based on the continuity equation provides the best results. From moderate to high tip-speed ratios, the assumption of planar flow decays due to the increased blockage. Hence, additional measurements are needed to obtain a more representative characterization of the outlet flow, which allows a more precise evaluation of the torque and performance in this range.

To conclude, remarkable agreement has been found between the control volume theory results and experimental torque and performance measurements, validating the procedure. Likewise, thrust results are found coherent and in range. Nevertheless, high precision is needed in the measurement of the velocities, as they have been identified as the most critical variables to the application of the methodology. In particular, deviations of a 5 % in the velocity measurements may lead to a 60 % error in the correct estimation of the power coefficient. Thus, overall measurement uncertainty should be kept below 1 % to preserve maximum inaccuracies in the range of a 10 % for the performance curve.

Finally, as future works, the use of control volume theory in set-ups different to the one studied here is proposed, being particularly interesting the application of the procedure to wind turbine array testing.

CRediT authorship contribution statement

Luis Santamaría: Conceptualization, Investigation, Data curation, Writing – original draft. **Katia María Argüelles Díaz:** Investigation, Project administration, Writing – review & editing. **Mónica Galdo Vega:** Investigation. **José González Pérez:** Visualization. **Sandra Velarde Suárez:** Supervision, Funding acquisition. **Jesús Manuel Fernández Oro:** Formal analysis, Methodology, Writing – review & editing, Supervision.

Declaration of Competing Interest

The authors declare that they have no known competing financial interests or personal relationships that could have appeared to influence the work reported in this paper.

Data availability

Data will be made available on request.

Acknowledgements

The authors wish to thank the financial support of the Spanish Ministry of Economy, Industry and Competitiveness for the R + D Project entitled "Development and Construction of Vertical Axis Wind Turbines for Urban Environments" (DEVTURB) – Ref. ENE2017-89965-P, under the National Plan for Scientific and Technical Research and Innovation.

The grant provided by the Principality of Asturias for the support of Research Activities, funded by the Institute for Economic Development (IDEPA) under reference GRUPIN IDI/2018/000205 is also gratefully acknowledged.

Additionally, the support given by the University Institute for Industrial Technology of Asturias (IUTA) and the City Hall of Gijón, through the financed project SV-18-GIJON-1-05, is also recognized.

Finally, the authors would like to acknowledge the contribution of Prof. Bruno Pereiras for his advice and support during the measurement campaign.

Appendix A. Supplementary data

Supplementary data to this article can be found online at https://doi.org/10.1016/j.seta.2022.102811.

References

[1] Costa M, Buono A, Caputo C, Carotenuto A, Cirillo D, Costagliola MA, et al. The "INNOVARE" project: Innovative plants for distributed poly-generation by residual biomass. Energies 2020;13. https://doi.org/10.3390/en13154020.
[2] Pinto ES, Serra LM, Lázaro A. Optimization of the design of polygeneration systems for the residential sector under different self-consumption regulations. Int J Energy Res 2020;44:11248–73. https://doi.org/10.1002/er.5738.
[3] Barnes A, Marshall-Cross D, Hughes BR. Towards a standard approach for future Vertical Axis Wind Turbine aerodynamics research and development. Renew Sustain Energy Rev 2021;148:111221. https://doi.org/10.1016/j.rser.2021.111221.
[4] Hand B, Cashman A. A review on the historical development of the lift-type vertical axis wind turbine: From onshore to offshore floating application. Sustainable Energy Technol Assess 2020;38. https://doi.org/10.1016/j.seta.2020.100646.
[5] Kumar R, Raahemifar K, Fung AS. A critical review of vertical axis wind turbines for urban applications. Renew Sustain Energy Rev 2018;89:281–91. https://doi.org/10.1016/j.rser.2018.03.033.
[6] Zhao Z, Wang D, Wang T, Shen W, Liu H, Chen M. A review: Approaches for aerodynamic performance improvement of lift-type vertical axis wind turbine. Sustainable Energy Technol Assess 2022;49:101789. https://doi.org/10.1016/j.seta.2021.101789.
[7] Castelli MR, Ardizzon G, Battisti L, Benini E, Pavesi G. Modeling Strategy and Numerical Validation. In: Proceedings of the ASME 2010 International Mechanical Engineering Congress & Exposition; 2010. p. 1–10.
[8] Mertens S, Van Kuik G, Van Bussel G. Performance of an H-Darrieus in the skewed flow on a roof. J Solar Energy Eng, Trans ASME 2003;125:433–40. https://doi.org/10.1115/1.1629309.
[9] Du L, Ingram G, Dominy RG. Experimental study of the effects of turbine solidity, blade profile, pitch angle, surface roughness, and aspect ratio on the H-Darrieus wind turbine self-starting and overall performance. Energy Sci Eng 2019;7:2421–36. https://doi.org/10.1002/ese3.430.
[10] Edwards JM, Angelo Danao L, Howell RJ. Novel experimental power curve determination and computational methods for the performance analysis of vertical axis wind turbines. J Solar Energy Eng, Trans ASME 2012;134:1–11. https://doi.org/10.1115/1.4006196.
[11] Arpino F, Cortellessa G, Scungio M, Fresilli G, Facci A, Frattolillo A. PIV measurements over a double bladed Darrieus-type vertical axis wind turbine: A validation benchmark. Flow Measurement and Instrumentation 2021;82. 10.1016/j.flowmeasinst.2021.102064.
[12] Dou B, Yang Z, Guala M, Qu T, Lei L, Zeng P. Comparison of different driving modes for the wind turbine wake in wind tunnels. Energies 2020;13. https://doi.org/10.3390/en13081915.
[13] Araya DB, Dabiri JO. A comparison of wake measurements in motor-driven and flow-driven turbine experiments. Exp Fluids 2015;56:1–15. https://doi.org/10.1007/s00348-015-2022-7.
[14] Rodríguez Lastra M, Fernández Oro JM, Galdo Vega M, Blanco Marigorta E, Santolaria MC. Novel design and experimental validation of a contraction nozzle for aerodynamic measurements in a subsonic wind tunnel. J Wind Eng Ind Aerodyn 2013;118:35–43. https://doi.org/10.1016/j.jweia.2013.04.008.
[15] Santamaría L, María K, Díaz A, Pereiras B, Vega MG, Pérez JG, et al. Preliminary flow measurements of a small-scale, vertical axis wind turbine for the analysis of blockage influence in wind tunnels. AICFM16 J Phys Conf Ser 2022. https://doi.org/10.1088/1742-6596/2217/1/012039.
[16] Santamaría L, Fernández Oro JM, Argüelles Díaz KM, Meana-Fernández A, Pereiras B, Velarde-Suárez S. Novel methodology for performance characterization of vertical axis wind turbines (VAWT) prototypes through active driving mode. Energy Convers Manage 2022;258:115530. https://doi.org/10.1016/j.enconman.2022.115530.
[17] Meana-Fernández A, Solís-Gallego I, Fernández Oro JM, Argüelles Díaz KM, Velarde-Suárez S. Parametrical evaluation of the aerodynamic performance of vertical axis wind turbines for the proposal of optimized designs. Energy 2018;147:504–17. https://doi.org/10.1016/j.energy.2018.01.062.
[18] Díaz KMA, Oro JMF, Marigorta EB. Extended angular range of a three-hole cobra pressure probe for incompressible flow. J Fluids Eng, Trans ASME 2008;130:1014011–6. https://doi.org/10.1115/1.2969457.
[19] Argüelles Díaz KM, Fernández Oro JM, Blanco Marigorta E, Barrio PR. Head geometry effects on pneumatic three-hole pressure probes for wide angular range. Flow Meas Instrum 2010;21:330–9. https://doi.org/10.1016/j.flowmeasinst.2010.04.004.
[20] Vavra MH. Aero-thermodynamics and flow in turbomachines. New York: John Wiley & Sons, Inc.; 1960.
[21] Selig MS, McGranahan BD. Wind tunnel aerodynamic tests of six airfoils for use on small wind turbines. 2004. 10.2514/6.2004-1188.
[22] Yan P, Chu N, Wu D, Cao L, Yang S, Wu P. Computational fluid dynamics- based pump redesign to improve efficiency and decrease unsteady radial forces. J Fluids Eng, Trans ASME 2017;139. https://doi.org/10.1115/1.4034365.
[23] Olasek K, Karczewski M. Velocity data-based determination of airfoil characteristics with circulation and fluid momentum change methods, including a control surface size independence test. Exp Fluids 2021;62:1–21. https://doi.org/10.1007/s00348-021-03193-9.
[24] Kaupert KA. An evaluation of impeller blade torque during an impeller-diffuser interaction. J Fluids Eng, Trans ASME 2004;126:960–5. https://doi.org/10.1115/1.1839929.
[25] Dean RC. On the necessity of unsteady flow in fluid machines. J Basic Eng 1959;81. https://doi.org/10.1115/1.4008350.
[26] Young J, Tian F-B, Liu Z, Lai JCS, Nadim N, Lucey AD. Analysis of unsteady flow effects on the Betz limit for flapping foil power generation. J Fluid Mech 2020;902. https://doi.org/10.1017/jfm.2020.612.
[27] Durbin PA, Petterson Reif BA. Statistical theory and modelling for turbulent flows. Chinchester: John Wiley & Sons, Inc.; 2011.

Appendix A. Supplementary data

The following are the Supplementary data to this article:

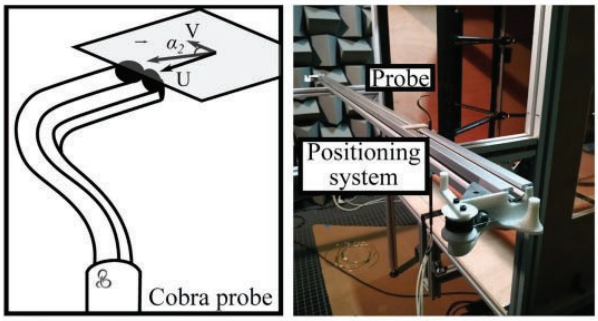

Figure. Cobra probe diagram and probe positioning system.

Download : Download high-res image (161KB) Download : Download full-size image

Supplementary figure 1.

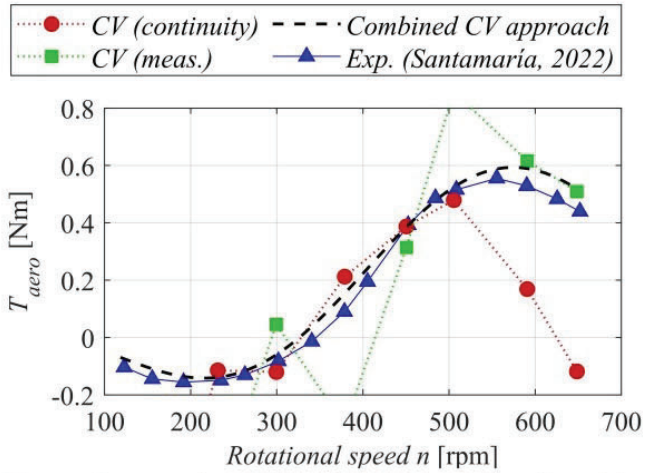

Figure. Computed aerodynamic torque as a function of the rotational speed. Comparison of results from the application of CV theory with experimental measurements.

Download : Download high-res image (472KB) Download : Download full-size image

Supplementary figure 2.

Table. Instrumentation uncertainties.

Sensor	Variable measured	Uncertainty
Differential pressure sensors 1in H_20	ΔP_{0-1} , $\Delta P_{1-1'}$, ΔP_{1-2} v_∞ , $U_{1'}$	$u_{\Delta P} = \pm 0.63\ [Pa]$ $u_v = \pm 0.15\ [m/s]$
Cobra probe (calibrated before measurement)	$\vec{v}_2$, α_2	$u_{\vec{v}_2} = \pm 0.3\ [m/s]$ $u_{\alpha_2} = 0.6\ [°]$
Optical tachometer	ω	$u_\omega = \pm 0.011 \left[\frac{rad}{s}\right]$

Download : Download high-res image (157KB) Download : Download full-size image

Supplementary figure 3.

4.3. Métricas de la revista

Clarivate Analytics
Journal Citation Reports

Clarivate Web of Science™

Sustainable Energy Technologies and Assessments

ISSN
2213-1388

EISSN
2213-1396

JCR ABBREVIATION
SUSTAIN ENERGY TECHN

ISO ABBREVIATION
Sustain. Energy Technol. Assess.

Journal information

EDITION
Science Citation Index Expanded (SCIE)

CATEGORY
GREEN & SUSTAINABLE SCIENCE & TECHNOLOGY - SCIE

ENERGY & FUELS - SCIE

LANGUAGES	REGION	1ST ELECTRONIC JCR YEAR
English	USA	2018

Publisher information

PUBLISHER	ADDRESS	PUBLICATION FREQUENCY
ELSEVIER	RADARWEG 29, 1043 NX AMSTERDAM, NETHERLANDS	6 issues/year

2021 JOURNAL IMPACT FACTOR

7.632

View calculation

JOURNAL IMPACT FACTOR WITHOUT SELF CITATIONS

6.184

View calculation

Journal Impact Factor Trend 2021

Export

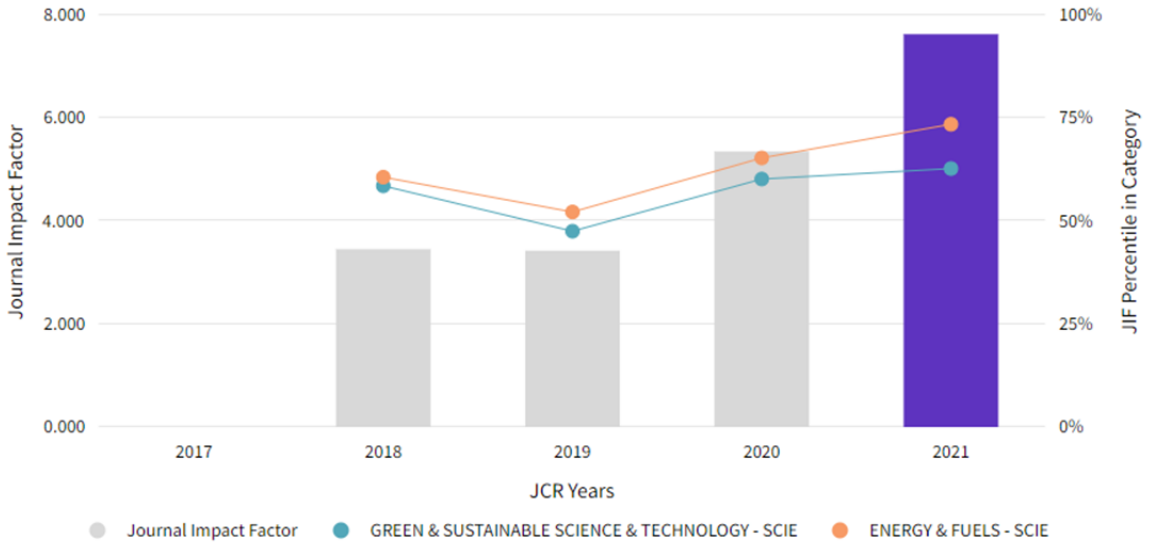

SJR
Scimago Journal & Country Rank

Scopus
ELSEVIER

Sustainable Energy Technologies and Assessments

Scopus coverage years: from 2013 to 2023
Publisher: Elsevier
ISSN: 2213-1388

CiteScore 2021	SJR 2021	SNIP 2021	H-INDEX
6.5	1.356	1.703	48

Subject area: Energy: Energy Engineering and Power Technology | Energy: Renewable Energy, Sustainability and the Environment

CiteScore 2021

$$6.5 = \frac{7925 \text{ Citations } 2018 - 2021}{1218 \text{ Documents } 2018 - 2021}$$

Calculated on 05 May, 2022

CiteScore rank 2021 ⓘ

Category	Rank	Percentile
Energy └ Energy Engineering and Power Technology	#49/235	79th
Energy └ Renewable Energy, Sustainability and the Environment	#62/215	71st

CiteScore trend

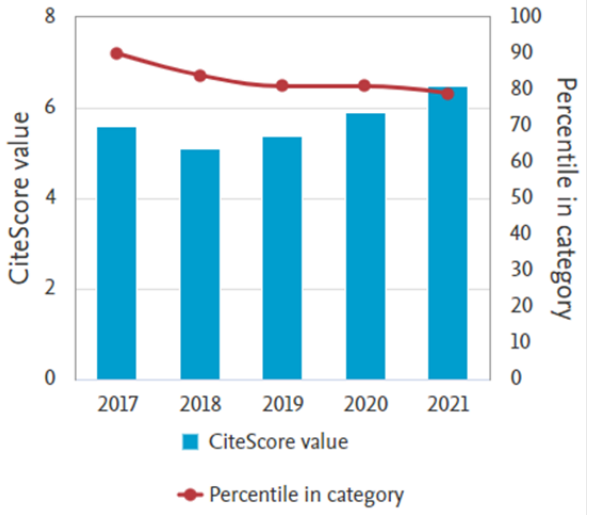

CAPÍTULO 5

DISCUSIÓN GENERAL Y CONCLUSIONES

5.1. Discusión de los resultados y principales descubrimientos

El foco de este trabajo han sido los ensayos experimentales en el ámbito del estudio de VAWT a escala de laboratorio.

En el apartado relacionado con el ensayo de perfiles en túnel de viento, se estudiaron las fuerzas aerodinámicas y momentos de cabeceo en prototipos de placa plana y del perfil aerodinámico DU06-W-200 con un nuevo diseño de balanza aerodinámica. Los resultados sobre placa plana demuestran que prototipos de longitud 0.44 veces el ancho del túnel con un factor de aspecto de 3.2 reproducen perfectamente los resultados de flujo 3D, mientras que con longitud igual al ancho del túnel y factor de aspecto de 7.2 se consiguen resultados 2D con mínimo efecto de las paredes. Asimismo, los resultados del perfil aerodinámico demuestran que el factor de aspecto puede ser aún menor en formas aerodinámicas. Adicionalmente, la buena correspondencia encontrada en todo el rango angular (incluso en las zonas de flujo desprendido) entre los resultados experimentales y los datos de la bibliografía, indica que el nuevo diseño de balanza probado y la metodología desarrollada son apropiados para este tipo de medidas. Los trabajos en curso relacionados con la implementación de un sistema de orientación robotizado y la ampliación del rango efectivo de calibración de la balanza ayudarán a conseguir una mejor caracterización, particularmente en las zonas de histéresis. También se han obtenido resultados del flujo sobre el perfil aerodinámico obtenidos gracias a simulaciones no estacionarias utilizando el modelo de turbulencia GEKO. En estos resultados se ha encontrado correspondencia entre la fluctuación de las fuerzas aerodinámicas y la generación de vórtices alternativos derivados del desprendimiento, tanto en frecuencia como en magnitud, fenómenos relacionados con la variación del punto de desprendimiento respecto al ángulo de ataque.

En el trabajo relacionado con la caracterización de prestaciones mediante el enfoque mecánico, se desarrolló una metodología innovadora para ensayar prototipos a escala en túnel de viento basada en el método de conducción activa (ADM). Se aplicó la metodología a un prototipo real y se compararon los resultados con simulaciones CFD obteniendo una notable concordancia. La metodología desarrollada demostró ser capaz de superar los problemas típicos de los ensayos de estas turbinas a pequeña escala, proporcionando un control superior de los ensayos, con un equipamiento más sencillo y económico que las metodologías convencionales basadas en conducción pasiva (PDM), y obteniendo una completa definición de la curva de rendimiento en todo el rango. Dentro de la problemática propia de la metodología propuesta, la diferenciación entre las pérdidas mecánicas y el arrastre de las palas en ensayos sin viento resulta el mayor desafío. A partir de los resultados, y como solución de compromiso en términos económicos y de precisión, se ha propuesto el uso complementario de una simulación CFD de un perfil en rotación. Además, en este trabajo se ha demostrado la alta relevancia de las pérdidas parásitas de los soportes de las palas y la inherente necesidad de tenerlas en cuenta a la hora de obtener la curva de prestaciones. Asimismo, se propuso una corrección para el bloqueo de este tipo de turbinas, basado en una adaptación de una corrección de la bibliografía, obteniendo resultados razonables. Dicha adaptación relaciona el nivel de bloqueo con la solidez de la máquina, permitiendo su aplicación a cualquier diseño de rotor. Adicionalmente, también se propuso una corrección para simulaciones CFD 2D, que permite corregir los efectos de la diferencia de bloqueo al flujo en dirección vertical y horizontal, ajustando perfectamente los resultados a entornos 3D como el ensayado.

Finalmente, en el trabajo que aborda la caracterización de prestaciones a partir de medidas aerodinámicas, se realizó una completa caracterización de las presiones a la entrada y el perfil de velocidades de la salida para múltiples TSR obteniendo resultados de las fuerzas de empuje y el rendimiento de la turbina mediante la aplicación del método de volúmenes de control. Se ha demostrado que esta metodología es de especial interés para la caracterización de prototipos a escala de laboratorio, donde la medición directa de variables mecánicas puede ser problemática. Asimismo, se ha determinado que el rango de aplicación de esta metodología se

encuentra limitado a la región de generación de par positivo, debido a la pequeña magnitud de los valores medidos a muy bajos TSR. Con TSR de bajos a moderados, un enfoque basado en la ecuación de continuidad proporciona los mejores resultados. Por el contrario, con TSR de moderados a altos la hipótesis de flujo plano se deteriora, debido al aumento del bloqueo (similarmente a lo que sucedía con la corrección de flujo 3D para modelos CFD 2D). Por lo tanto, se necesitan mediciones adicionales para obtener una caracterización más representativa del flujo de salida. Al comparar los resultados con los obtenidos utilizando el enfoque mecánico se ha encontrado una notable concordancia, validando el procedimiento. Asimismo, los resultados de empuje son coherentes y dentro de un rango razonable. Adicionalmente, mediante el análisis de la incertidumbre se ha demostrado que es necesaria una gran precisión en la medida de las velocidades, ya que se han identificado como las variables más críticas para la aplicación de la metodología. En particular, desviaciones de un 5% en las medidas de velocidad pueden conducir a un 60% de error en la estimación del coeficiente de potencia. De esta manera, la incertidumbre global de las mediciones debe mantenerse por debajo del 1% para preservar imprecisiones máximas en el rango de un 10% para la curva de rendimiento.

El resultado general de la investigación se puede resumir en que se han generado las metodologías necesarias para el estudio de VAWT a escala de laboratorio y que permiten superar la problemática típica de este ámbito. Esto, sumado al desarrollo de equipamiento realizado, proporciona las herramientas necesarias para realizar ambiciosas investigaciones en este campo. Adicionalmente, la base de conocimiento generada y la calidad de los resultados pueden servir de referencia para otros trabajos y contribuir también al propio desarrollo de estas máquinas.

5.2. Cumplimiento de los objetivos de la investigación

El objetivo principal de esta tesis es el desarrollo y aplicación de metodologías efectivas para el ensayo experimental de turbinas VAWT en túneles de viento. Tras una extensa revisión bibliográfica y un completo trabajo de laboratorio, se ha identificado la problemática concreta de esta disciplina y se han desarrollado las herramientas necesarias para abordarla dando respuesta a los objetivos específicos planteados.

En primer lugar, atendiendo al objetivo específico número 1, en el marco de esta tesis se ha diseñado y construido un montaje experimental para el ensayo de un modelo a escala de VAWT en túnel de viento. Para reducir los costes de infraestructura se han utilizado técnicas de prototipado rápido y específicamente fabricación aditiva. Para el ensayo del prototipo y la caracterización de sus prestaciones se han desarrollaron dos metodologías diferentes que permiten superar las dificultades de los ensayos a escala. La primera metodología (Capítulo 3) utiliza un enfoque mecánico y está basada en la realización de varios ensayos con diferentes configuraciones de máquina, utilizando el principio de conducción activa (ADM). Adicionalmente, para reducir los costes de instrumentación y simplificar el montaje, se elaboró un procedimiento que permitía obtener el par con fiabilidad a partir de la corriente suministrada a un motor DC, medida con una fuente de alimentación de laboratorio. De esta manera se elimina la necesidad de añadir un torquímetro al montaje. La segunda metodología (Capítulo 4) utiliza medidas aerodinámicas de la estela de la turbina para proporcionar una estimación de las prestaciones sin necesidad de contacto con la máquina, aplicando el método de volúmenes de control. Para validar esta metodología se han utilizado medidas de una sonda de presión desarrollada en el propio grupo de investigación, confirmando la utilidad de esta herramienta para su aplicación en este tipo de estudios.

En cuanto al objetivo específico 2, relacionado con la corrección por bloqueo, en el Capítulo 3 se ha propuesto una mejora sobre una de las correcciones disponibles en la bibliografía que permite tener en cuenta las características de la máquina para establecer la intensidad del

bloqueo que genera. Además, a partir de las medidas aerodinámicas se ha estudiado la relevancia de la desigualdad de bloqueo producida en las zonas superior e inferior y en los laterales de la turbina. Sobre esta base, se identificó la necesidad de corregir las ecuaciones de la segunda metodología desarrollada utilizando medidas del flujo en un hueco (superior o inferior) cuando el bloqueo es alto, obteniendo mejores resultados que con la metodología de base (Capítulo 4). Asimismo, a partir de este conocimiento se ha propuesto una corrección del flujo 3D para modelos CFD 2D relacionada con el bloqueo (Capítulo 3 y Sección 6.3 del Anexo I).

Respecto al objetivo específico 3, mediante el trabajo presentado en el Capítulo 2 se han sentado las bases necesarias para el estudio de perfiles típicos de VAWT en túnel de viento. Se han fabricado prototipos tanto de perfiles aerodinámicos como de otras secciones aerodinámicas utilizando fabricación aditiva. Se ha identificado equipamiento adecuado y especialmente interesante para este tipo de ensayos, y se ha validado su uso mediante contrastación de medidas con la bibliografía. Asimismo, se han identificado los diferentes factores físicos que influyen en este tipo de ensayos y determinadas áreas de mejora. Estas áreas de mejora ya están siendo abordadas con trabajos en curso, brevemente recogidos en el Anexo II, Sección 7.2.

El objetivo específico 4 ha sido parcialmente abordado mediante las simulaciones CFD no estacionarias cuyos resultados se han descrito en el Capítulo 3. Además, a partir de la base del montaje utilizado en las medidas aerodinámicas estacionarias (Capítulo 4 y Sección 6.2 del Anexo I), se ha concebido un sistema modular automatizado de posicionamiento de sondas (MAPPS), dirigido a la utilización de sondas de hilo caliente para la caracterización del flujo no estacionario. Aunque el grueso de este trabajo queda fuera del alcance de esta investigación y por ello se ha subcontratado, se ha participado activamente en la elaboración del diseño y el sistema de control. Este trabajo en curso se encuentra brevemente recogido en el Anexo II, Sección 7.1.

Finalmente, como se muestra en los resultados presentados en el Capítulo 3, se ha podido evaluar la fiabilidad de modelos analíticos y CFD desarrollados por el equipo investigador, cumpliendo el objetivo específico 5.

Por tanto, basándose en lo anterior se consideran ampliamente cumplidos los objetivos de esta tesis. Además, durante y a través de la compleción de estos objetivos se han producido descubrimientos y conclusiones relevantes que han dado lugar a las publicaciones presentadas en este trabajo.

5.3. Impacto e implicaciones

En primer lugar, los conocimientos y experiencia adquiridos durante el proceso de desarrollo de los montajes experimentales permitieron la elaboración de un programa de formación sobre fabricación de prototipos experimentales, que fue presentado en el congreso internacional MESIC9 y fue publicado en una revista indexada en SJR (Sección 6.1 del Anexo II). Además, en el plano laboral estas competencias han permitido al autor de esta tesis emprender su actividad por cuenta propia en torno al campo de la impresión 3D, suministrando equipos y proveyendo servicios de formación, mantenimiento y reparación. Esta actividad permitió paliar parcialmente la falta de financiación en el último año de realización de esta tesis.

Asimismo, en el contexto de la investigación sobre VAWT, tanto el equipamiento como las metodologías desarrolladas han dotado al Área de Mecánica de Fluidos de la Universidad de Oviedo con la capacidad para realizar ambiciosas investigaciones experimentales en este campo. De esta manera se ha afianzado la línea de investigación en la que se enmarca esta tesis, completando los objetivos del Proyecto de Plan Nacional: “Desarrollo y construcción de turbinas eólicas de eje vertical para entornos urbanos (DEVTURB)” (ref. ENE2017-89965-P).

Así como se ha facilitado la obtención de financiación para su continuación, asegurada mediante la concesión de otro proyecto de Plan Nacional: "Optimización mediante técnicas de control de flujo de una turbina eólica de eje vertical para entornos urbanos" (ref. TED2021-131307B-I00).

Este trabajo ha obtenido reconocimiento internacional mediante la aceptación de las publicaciones presentadas en los Capítulos 2, 3 y 4, y las comunicaciones en congresos del Anexo I. Destaca sobre todo la publicación del Capítulo 3, en una revista con un altísimo factor de impacto (11.5) y posición 3 de 138 en la categoría "Mechanics" del JCR. Además, esta publicación cuenta ya (nótese que se publicó este mismo año) con 2 citas de trabajos ajenos en revistas indexadas. Asimismo, destaca también la publicación del capítulo 4, en una revista con un alto factor de impacto (7.6) y claramente creciente, encontrándose en 2019 en el percentil 52 y en 2021 en el 74 de la categoría "Energy and Fuels" del JCR.

Tabla 5.1. Publicaciones JCR.

Publicación	Capítulo Tesis	Revista	Fecha publicación	Cuartil JCR	Cuartil SJR	Citas (31/12/2022)
[1]	2	Energies	10/12/2022	Q3	Q1	0
[2]	3	Energy Convers. Manag.	31/03/2022	Q1	Q1	3
[3]	4	Sustain. Energy Technol. Assess.	07/10/2022	Q2	Q1	0

Tabla 5.2. Comunicaciones en congresos internacionales.

Publicación	Anexo Tesis	Congreso internacional	Lugar	Fechas	Revista
[4]	I.I	MESIC9	Gijón, España	Jun. 23-25 2021	IOP Conf. Ser.: Mater. Sci. Eng.
[5]	I.II	AICFM16	Yokohama, Japón	Sept. 13-15 2021	J. Phys.: Conf. Ser.
[6]	I.III	SFMC1	Cádiz, España	Jun. 19-22 2022	SFMC1-Book of Abstracts

Finalmente, en lo que se refiere a transferencia de conocimiento, los trabajos realizados por el equipo investigador en el marco de esta tesis han sido difundidos en Webinarios internacionales. Además, se espera que trabajos en curso como el de la Sección 7.3 del Anexo II capten la atención de empresas regionales o nacionales, promoviendo el desarrollo comercial de esta tecnología.

Tabla 5.3. Webinarios internacionales.

Webinario	Organizador	Fechas	Portada
"Tecnologías disruptivas del sector eólico"	Plataforma Tecnológica del Sector Eólico (REOLTEC)	Feb. 23 2022	
Jornadas REGEDIS-CIATEQ	Red de Energía Eólica para la Generación Distribuida en el Entorno Urbano (REGEDIS)	Oct. 24-28 2022	

5.4. Posibles líneas de investigación futuras

La mejora de la eficiencia de las turbinas VAWT desde el punto de vista aerodinámico es una línea de investigación bastante madura actualmente debido al gran interés que han recibido estas turbinas en los últimos años. Como se explicó en la introducción, los parámetros óptimos de la máquina están mayormente acotados, así como los mejores perfiles aerodinámicos disponibles. El desarrollo de dispositivos de control de flujo está alcanzando también un alto grado de conocimiento generado y aunque continuamente aparecen nuevos diseños, su complejidad difícilmente justifica la sutil mejora que supone su implementación. Lo mismo sucede con los mecanismos de aceleración de flujo.

No obstante, hasta ahora el enfoque empleado en el estudio de las turbinas ha estado principalmente centrado en las palas, analizándolas además como un elemento homogéneo en toda su envergadura. Sin embargo, apenas existen estudios sobre elementos intrínsecamente necesarios en estas máquinas, como son los soportes de las palas y que tienen una notable relevancia en las prestaciones reales. Además, tanto la unión de los soportes con las palas como los propios extremos de las palas causan que el flujo real no sea homogéneo en toda la envergadura. Por ello, una posible línea de investigación futura podría ser la caracterización del flujo 3D en las zonas de pala cercanas a los extremos y a los soportes y el desarrollo de soluciones específicas para el control del flujo.

Adicionalmente, al igual que sucede actualmente con las turbinas HAWT, si se quieren alcanzar las grandes escalas a las que las VAWT pueden ser competitivas, es necesario plantear su estudio mediante modelos acoplados mecánicos y aerodinámicos (FEM-CFD) y estudios de aeroelasticidad. Dado que las turbinas VAWT han sido principalmente desarrolladas en la pequeña escala, este tipo de estudios no ha sido todavía abordado. Aunque es un campo complejo y exigente, el desarrollo de estudios de este tipo puede suponer un paso notable en la implementación de estas turbinas a escala comercial.

Por último, en el camino para conseguir el desarrollo comercial de esta tecnología, resulta necesario superar el enfoque parcial centrado solo en la parte aerodinámica de control del flujo y las prestaciones, y pasar a analizar qué tipo de soluciones pueden beneficiar tanto a la parte eléctrica y de control como a la parte mecánica, o incluso a la fabricación o al mantenimiento. Es decir, tener en cuenta todo el proceso para generar desarrollos aerodinámicos que tengan un impacto relevante en el coste de la energía (LCOE).

ANEXO I

COMUNICACIONES EN CONGRESOS INTERNACIONALES

IOP Conf. Series: Materials Science and Engineering 1193 (2021) 012096 doi:10.1088/1757-899X/1193/1/012096

Training program for researchers in design and manufacturing of experimental prototypes for fluids engineering using additive technologies

L Santamaría[1*], M García[1], A Gharib[1,2], M Galdo[1], E Blanco[1], J M Fernández[1] and S Velarde[1]

[1] Fluid Mechanics Area, Department of Energy, University of Oviedo, C/Wifredo Ricart s/n, Gijon, Asturias, 33204, Spain.
[2] Mechanical Power Department, Faculty of Engineering, Port Said University, Egypt.

*Corresponding author: santamarialuis@uniovi.es

Abstract: Experimental testing is one of the pillars in Fluids Engineering research. The arrival of rapid prototyping, and especially, Additive Manufacturing (AM), has revolutionized this field, allowing fast and flexible prototype manufacturing. Among these technologies, Fused Deposition Modelling (FDM) allows to fabricate complex parts using light, resistant, composite materials at a very affordable cost. To harness the full potential of this technology, the fluid dynamics engineering research group (GIFD) of the University of Oviedo started a training program for researchers in this area. This rich and complete program is presented herein, emphasizing its elaborate methodology and highlighting the successful case-studies derived from its application. Knowledge and integration of this technology has granted the capability of self-manufacturing customizable, low-cost experimental prototypes with adequate mechanical properties and accuracy, which produce high-quality results. Additionally, it has widened remarkably the possibilities of experimental research, resulting in a significant increase of experimental publications.

Keywords: Experimental prototypes, Additive manufacturing, Fused deposition modelling, Training techniques, Design for manufacturing and assembly.

1. Introduction

Experimental tests are considered one of the most important study methods in Fluids Engineering research as they provide valuable, reliable data, which is often used for the validation of analytical and computational models. Within the experimental testing phase, dimensional analysis is one of the most common methodologies, which allows testing scaled prototypes at conditions equivalent to those of the real-scale prototype and extrapolate the results. In this context, prototype manufacturing entails a tremendous challenge, as they are on-demand single parts, subjected to design changes and usually feature complex geometries. These characteristics make conventional prototype manufacturing an extremely expensive and time-consuming process.

In the past, experimental prototypes in fluids engineering were frequently handmade by skilled craftsman in materials as balsa wood, with its limitations in manufacturable geometries, shape accuracy and material properties (the last often improved adding composites as fiber glass) [1]. On the other hand, when metal parts were required, they were manufactured by means of conventional processes as forging,

casting, welding, and folding, usually demanding customized tooling equipment. These are methods which require machining and post-processing after fabrication through different operations (drilling, turning, milling and grinding) to achieve the desired geometries with an adequate surface finish. Furthermore, these processes involve high initial cost and require professional operators; frequently being profitable only for mass production, not for a limited number of parts. Additionally, they do not allow easy implementation of design changes, which is a key aspect at prototype stage.

Nevertheless, with the arrival of rapid prototyping, and especially Additive Manufacturing (AM), the scenario has changed radically, allowing quick physical model production directly from Computer Aided Design (CAD) data files. These extremely flexible technologies can adapt to design changes without need of customized tooling or cost increase, and have a wide range of materials [2].

Within AM, Fused Deposition Modelling (FDM) has become an extraordinarily useful tool for experimental testing, allowing affordable fabrication of complex parts with light, resistant, composite materials [2]. Furthermore, there is Computer Aided Manufacturing (CAM) software available which reduces the need of technical knowledge needed to use the technology.

With the aim of harnessing the full potential of this technology, the fluid dynamics engineering research group (GIFD) of the University of Oviedo started in 2018 a training program for their researchers in this field. The main objective of this work is to show the benefits and applications of incorporating AM and more specifically FDM, as a resource for experimental research in Fluids Engineering, sharing the methodology used to address this task, as well as the results and experience obtained.

2. Methodology

After the expiration of Stratasys' patent describing the basics of FDM in 2009, there was a massive and continuous price drop in commercial 3D printers. Hence, in 2015, with 3D printing at user reach, a PhD student at the University of Oviedo, acquired a BQ WitBox to try the technology in the field of OWC turbines. In his thesis and subsequent papers, he reported very good agreement between experimental and numerical tests, validating the technology for its use in this field [3]. Based on these works the GIFD decided to incorporate its first 3D printer in 2016.The first machine purchased was "The Beast v1.2" from Cultivate3D, a large DIY kit printer (figure 1(a)) whose main specifications, and those from the following machines, are detailed in table 1. Given the good preliminary results with this technology, the GIFD decided to set up a 3D printing cluster in 2017, starting with the purchase of a BCN3D SIGMAX dual extruder printer (figure 1 (b)).

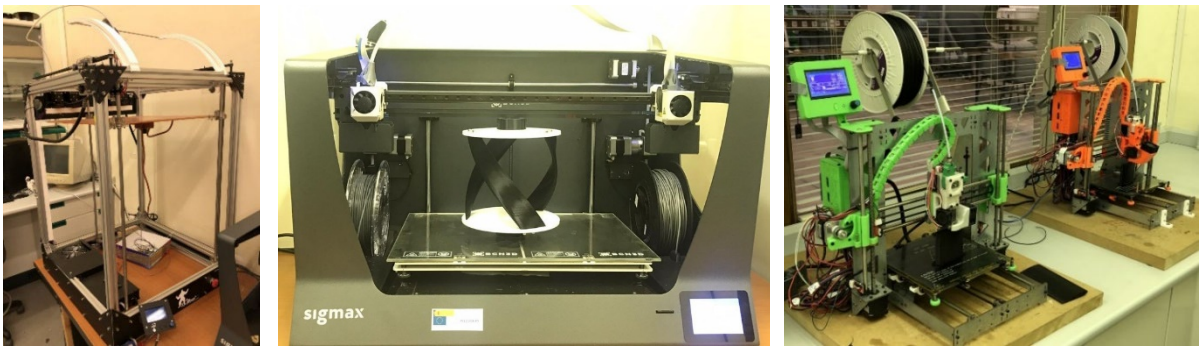

(a) (b) (c)

Figure 1. (a) The Beast v1.2 from Cultivate3D. **(b)** BCN3D SIGMAX. **(c)** HTA3D P3Steel.

Once the technology was established, the next step was to open it up for all GIFD researchers to use in their fields. For this purpose, two intensive courses of 30 and 14 hours respectively were taught. A summary diagram of the contents and methodology used in the training program is shown in figure 2.

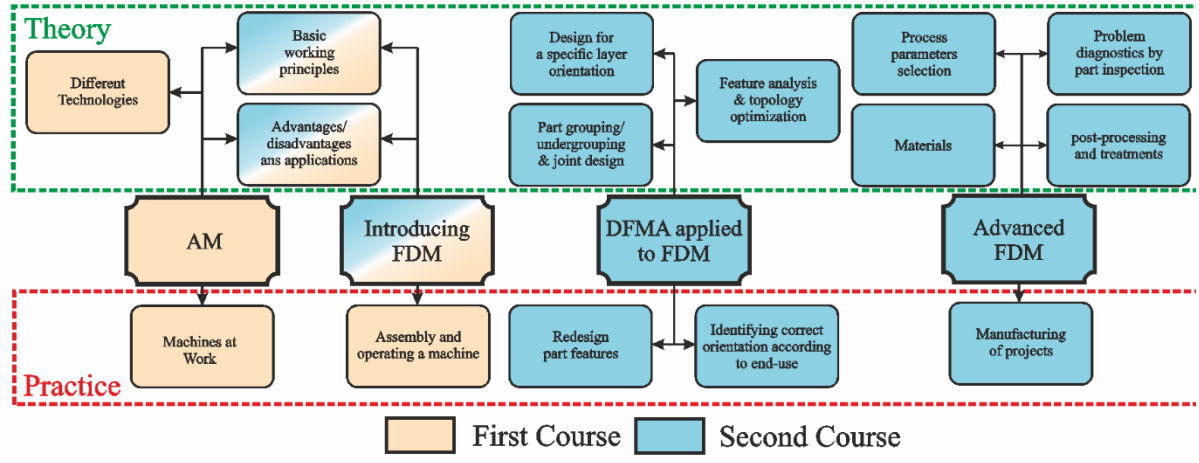

Figure 2. Summary diagram of the contents and methodology used in the training program.

First one was a one-week 3D printing course, which was given in collaboration with Prodintec foundation (now part of Idonial) and MediaLab. Prodintec technicians were in charge of providing the theoretical part of the course. They gave a seminar in their facilities and a guided tour, showing the students the different existing technologies, their practical applications, and their industrial machines at work. The rest of the course took place in the university, with an introduction to FDM by MediaLab covering: the fundamentals and working principles, available materials, 3D model databases and different machine types and components. Finally, researchers were tasked with assembling and operating a series of DIY kits of Prusa i3-type printers from the brand HTA3D (figure 1 (c)), to achieve first-hand knowledge of the technology. In addition, after the course, they were added to the GIFD 3D printing cluster.

Table 1. Equipment specifications and characteristics.

3D printer	Build Volume (mm)	Hot End	# hot ends	Extrusion type	Architecture
The Beast v1.2	470×435×690	E3D v6	1-4	bowden	cartesian
BCN3D SIGMAX	420×297×210	BCN3D	2	bowden	cartesian
HTA3D P3Steel	200×200×210	E3D v6	1	direct	cartesian

The second course was intended to deepen in FDM, but it also kept a brief introduction to additive manufacturing for researchers who did not take the first course. This course focused on teaching a systematic proceeding to the researchers and building a solid base from which they could grow by themselves. The course was divided in three modules:

The first module covered a brief summary of what was taught in the first course. After, researchers were assigned projects to work in during the course.

The second module faced in depth the topic of design for manufacturing and assembly (DFMA), which is one of the keys to exploiting the full potential of FDM technology [4]. First, some general rules DFMA applied to FDM technology were given, as for example: rounding edges when possible in the XY plane, to avoid mechanical and thermal stress concentrators [4]. Then, a strong emphasis was laid in designing 3D parts for a specific part orientation, taking into consideration surface finish requirements or mechanical properties [5]. DFMA of problematic part features was also revised, as how to make overhangs or “bridges” printable or designing strong durable joints [6]. A strong effort was put in exemplifying every theoretical principle with its practical application to a technical part. Furthermore, as a practical exercise, attendants were tasked with redesigning some of their project part features to improve manufacturing and assembly.

The third module started covering the operation, calibration, and basic maintenance of the machines. Then, the topic shifted to material properties and appropriate material selection for each application, focusing specially on experimental prototypes for fluid engineering. Next, process parameter selection was addressed from a systematic approach, identifying part features which drive certain process parameters, as for example: details in the Z direction which require lower layer height [7]. To minimize process parameter setting adjustments, a series of predefined profiles were created for part families based on those characteristics. Additionally, a complete, methodical guide on problem diagnostics and solving based on part inspection was taught, including several practical exercises in which possible causes for the defects found in real parts had to be identified. Finally, the basic post-processing techniques and treatments were explained, and the course ended with the researchers fabricating their projects. As a tool for continuous improvement and targeting future courses, a feedback loop was implemented by means of an anonymous quality survey, whose results indicated a high level of satisfaction with the course (9.8/10).

3. Successful case-studies

After taking the courses, researchers were able to apply the new resource to their investigations. This section shows a diverse selection of successful case-studies in which FDM was applied by the researchers not only for manufacturing experimental prototypes, as airfoils or even complete turbines, but also for a great number of auxiliary systems.

3.1. Auxiliary systems

3.1.1. Aerodynamic balance orientation system. Experimental characterization of airfoil profiles is one of the active research lines of the GIFD research group. For this purpose, lift and drag coefficients are measured with an aerodynamic balance for a range of attack angles and at different Reynolds numbers. Achieving the correct positioning of the airfoil at different attack angles is a difficult and tedious task, which researchers of the group were able to overcome with the design and FDM manufacturing of a worm drive orientation system (figure 3(a)).

3.1.2. Probe positioning system. One of the most common aerodynamic measurements are wake velocity profiles, which usually require a high number of measurement positions. The probes must keep the same calibration angle and measurements are usually performed in two or three dimensions. The acquired knowledge allowed the design and FDM fabricating of a simple, yet efficient, mechanical probe positioning system (figure 3(b)). By means of a crank-pulley-wire-slider system, the desired linear displacement is achieved by a revolution of the pulley, which has the adequate diameter. This system allows correct probe positioning and quick and comfortable displacement, with the implicit precision enhancement and test time optimization.

3.1.3. Epicyclic gear train. A planetary gearing system with gear ratio of 10:1 was designed and FDM fabricated (figure 3(c)) to be used in wind tunnel experiments. It is coupled with a small vertical axis turbine (shown further on) to reduce the starting torque required and make the turbine model rotate easily. In fact, fabricating this gear train system using FDM added more flexibility, allowing the use of the same arrangement to multiply the velocity in another application (gear ratio of 1:10) by only printing one additional part, which was able to change the positions of both the drive and driven gears.

3.1.4. Venturi tube. The Venturi tube is one of the most widely used devices for measuring the flow rate through a pipe and is present in most experimental tests involving this kind of flow. For this reason, a Venturi has been built (figure 3(d)), measuring 1200mm in length and 350mm in diameter at its widest part and consisting of 17 glued parts. For it to perform accurately, it has been designed in accordance with the UNE-EN ISO 5167-4 standard and calibrated based on the velocity profile at the outlet to calculate the real flow rate, giving a discharge coefficient of 0.99.

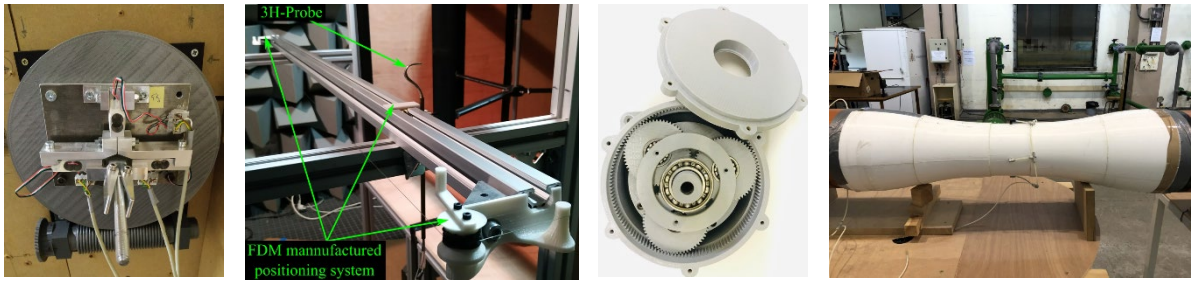

(a) (b) (c) (d)

Figure 3. (a) Worm drive orientation system. **(b)** Probe positioning system. **(c)** Planetary gear box. **(d)** Standardized venturi tube.

3.2. Airfoil profile fabrication

3.2.1. Aerodynamic studies. As it was previously mentioned in sub-subsection 3.1.1. experimental airfoil characterization is an active research line. The new knowledge and availability of FDM technology has allowed an important cost reduction in airfoil profile prototype fabrication. For example, a methacrylate airfoil prototype which was bought some years before, cost 20 times more than an equivalent in-house FDM fabricated airfoil (figure 4(a)). Also, it has increased the research possibilities since, more complex geometries can be fabricated, and design changes can be easily and quickly implemented because the researchers control the whole process. Furthermore, results show that the technology is valid for this application, as obtained data matches the bibliography one. An example is shown in figure 4(b) comparing experimental data from an experimental FDM flat plate prototype and the theoretical results obtained by analytical methods available in [8].

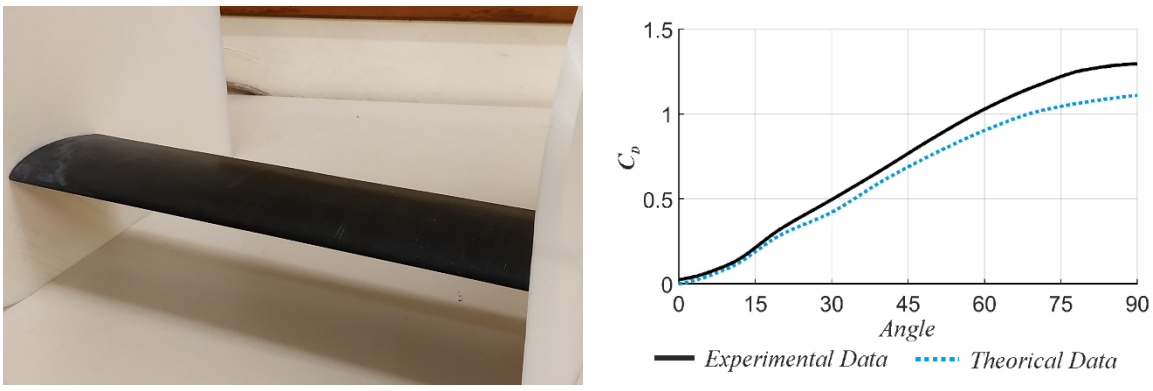

(a) (b)

Figure 4. (a) FDM Airfoil prototype. **(b)** Comparison between experimental obtained in a FDM prototype and theoretical data of a flat plate (Drag coefficient vs. Attack angle).

3.2.2. Vertical Axis Turbine prototypes. FDM fabricated airfoils have also been applied to the manufacturing of vertical axis turbine prototypes, for wind energy (VAWTs), as well as for tidal currents (VATTs).

In the first field, an existing scaled VAWT prototype for wind tunnel testing, which had broken due to extreme centrifugal forces, was redesigned and FDM technology was used for the airfoils and several of its components. Knowledge from part orientation was applied in the manufacturing of the blades, achieving an increase of 43.4% in bending resistance and a 61.5% in strain and shifting fragile behaviour to ductile at fracture. The results were obtained from the 3-point bending test of 2 blade section specimens, manufactured with the same process parameters, but different layer orientation (figure 5 (a)).

Also, a well optimized topology of the critical features such as joints allowed the new prototype to be tested at the required rotational velocities. Furthermore, the cost of the new blades was astonishingly lower, only 2% of the original ones. After 2 years of being used in demanding experiments with high rotational velocities the prototype (figure 5 (b)) has proven to be a great application of this technology. The results and experience gained by its testing have led to start the manufacturing a real-scale prototype for field experiments.

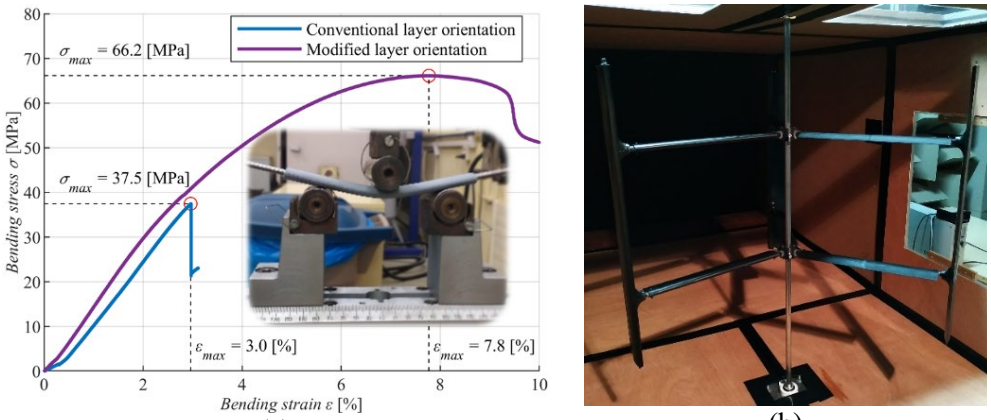

Figure 5. **(a)** 3-point bending test of 2 blade section specimens with same manufacturing parameters but different layer orientation. **(b)** FDM turbine prototype.

In the other field, several prototypes of Vertical Axis Tidal Turbine (VATT) have been manufactured and tested successfully inside a water channel [9] (figure 6 (a), (b)).

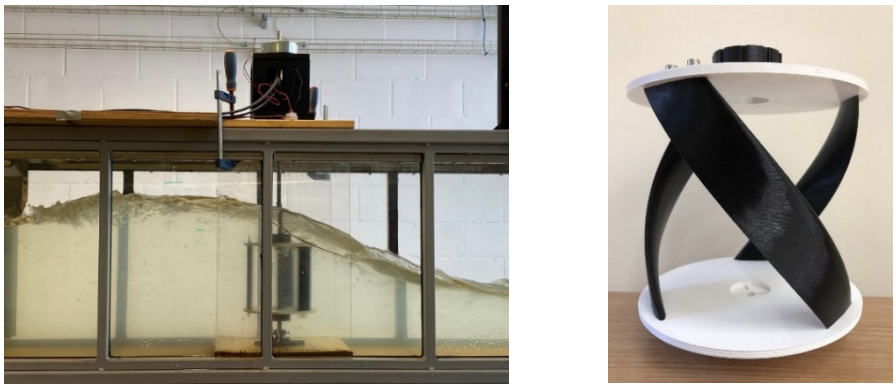

Figure 6. (a) VATT prototype tested in water channel. **(b)** Close-up of other of the designs manufactured.

The proposed models worked properly under the continuous hydrodynamic loading, without any change in the design nor the properties during months of experiments. In addition, one of the experimental requirements was to change the turbine position along a vertical axis, thanks to the FDM, a slotted collet (collet chuck) mechanism was fabricated and equipped with the VATT to achieve more than one vertical position. Also, other accessories were fabricated to complete the turbine support system, including bearing beds and shaft holders. In fact, testing these kinds of turbines inside channel was not limited only for straight blade type, but also it was extended to helical blade models. The flexibility and ability of generating complex shapes of FDM allowed the fabrication of helical turbine

models with different helix angles (30 º, 45 º, 60 º, 90 º and 120º) to be tested and evaluated inside the water channel.

3.3. OWC turbine prototypes

One of the GIFD's lines of research focuses on turbines for harnessing wave energy. Within this line, an axial turbine has been designed and built, completely inside the laboratory and without external help. Constructive design copies real gas turbines and was based in a previous work found in the bibliography [10]. Figure 7(a), (b) shows the exploded view, as well as the real turbine.

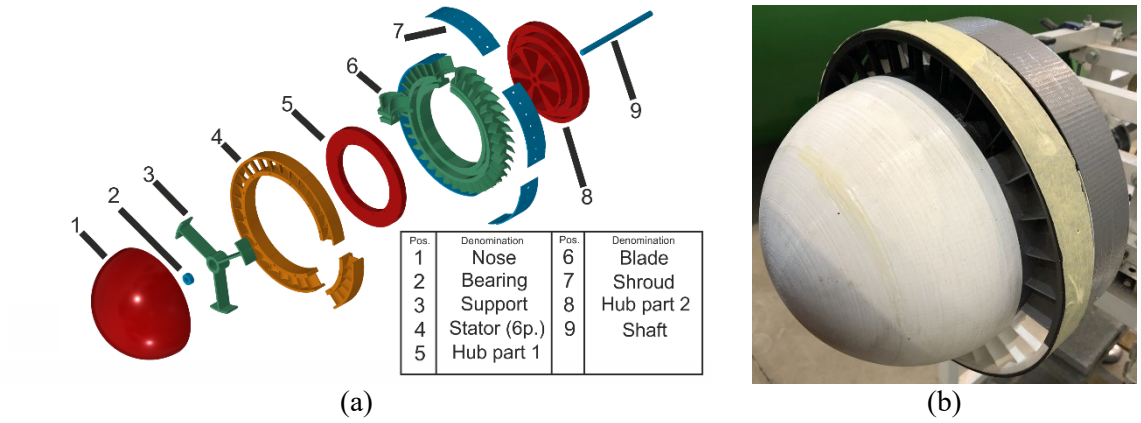

Figure 7. (a) Exploded view of the turbine. **(b)** FDM axial turbine prototype.

A research work has been published on this turbine [11] in which the experimental-numerical validation can be seen, a sample of this data is shown in figure 8. As it can be seen, FDM technology gives great results in the field of fluid mechanics.

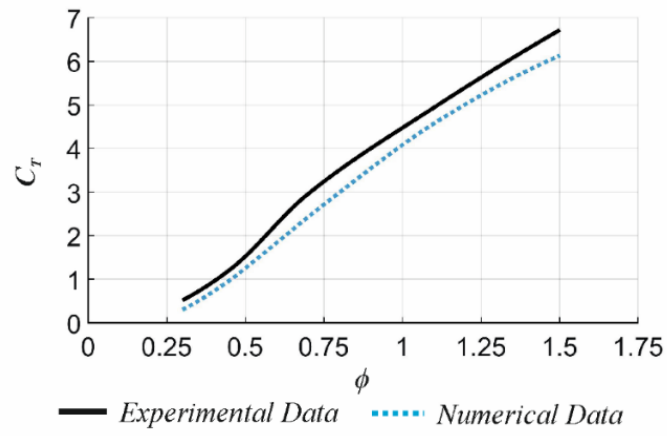

Figure 8. Numerical model validation through experimental testing of FDM prototype (Torque coefficient vs. Flow coefficient).

4. Conclusions and Future Works

A rich and complete training program in AM, and more specifically FDM for researchers in the field of fluids engineering, has been shared in this work, emphasizing its elaborate methodology and highlighting the successful case-studies derived from its application. Researchers which were new to this technology have now become experienced users with great skill.

Integrating this technology and knowledge in this research area has granted the capability of self-manufacturing customizable, low-cost experimental prototypes with adequate mechanical properties and accuracy, and which produce high-quality results. Additionally, FDM is being used to improve the experimental procedures and even to produce ad hoc equipment. The possibilities of experimental research have been widened remarkably and it is expected that this will result in a significant increase in number and quality of the experimental publications in the near future.

Given the success of integrating FDM and the expected academic outcome, betting on this technology can be taken as an investment for the future. This opens the door for investing in other AM technologies, as Stereolithography (SLA) or Selective Laser Sintering (SLS), whose interest for this application has yet to be analyzed.

Additionally, the evaluation system implemented in the courses indicated that the training methods were adequate, and it will enable the continuous improvement of the training program, which given its success will continue in the following years.

Acknowledgements
The authors wish to thank the support of: MINECO, Spain [ENE 2017-89965], MECD, Spain [FPU15/04375], Ministry of Higher Education and Scientific Research, Egypt, GRUPIN [IDI/2018/000205], University Institute of Industrial Technology of Asturias (IUTA) and Ayto. Gijón [SV-18-GIJON-1-05], and the collaboration of Prodintec (Idonial) and MediaLab (Univ. Oviedo).

References

[1] Walters S 1974 Power from Wind. *Mechanical Engineering* **96** 55–65
[2] Ngo T D, Kashani A, Imbalzano G, Nguyen K T Q and Hui D 2018 Additive manufacturing (3D printing): A review of materials, methods, applications and challenges *Composites Part B: Engineering* **143** pp 172–96
[3] Rodríguez L, Pereiras B, Fernández-Oro J and Castro F 2018 Viability of unidirectional radial turbines for twin-turbine configuration of OWC wave energy converters *Ocean Engineering* **154** pp 288–97
[4] Medellin-Castillo H I and Zaragoza-Siqueiros J 2019 Design and Manufacturing Strategies for Fused Deposition Modelling in Additive Manufacturing: A Review *Chinese Journal of Mechanical Engineering (English Edition)* **32** p 53
[5] Chacón J M, Caminero M A, García-Plaza E and Núñez P J 2017 Additive manufacturing of PLA structures using fused deposition modelling: Effect of process parameters on mechanical properties and their optimal selection *Materials and Design* **124** pp 143–57
[6] Laliberté T, Gosselin C M and Côté G 2000 Rapid Prototyping of Lower-Pair, Geared-Pair and Cam Mechanisms (*ASME International)* pp 1353–61
[7] Górski F, Kuczko W and Wichniarek R 2013 Influence of Process Parameters on Dimensional Accuracy of Parts Manufactured Using Fused Deposition Modelling Technology *Advances in Science and Technology – Research Journal* **7** pp 27–35
[8] Blevins R D 1984 *Applied fluid dynamics handbook*
[9] Gharib Yosry A, Fernández-Jiménez A, Álvarez-Álvarez E and Blanco Marigorta E 2021 Design and characterization of a vertical-axis micro tidal turbine for low velocity scenarios *Energy Conversion and Management* **237** p 114144
[10] Thakker A, Jarvis J, Buggy M and Sahed A 2009 3DCAD conceptual design of the next-generation impulse turbine using the Pugh decision-matrix *Materials and Design* **30** pp 2676–84
[11] García-Díaz M, Pereiras B, Miguel-González C, Rodríguez L and Fernández-Oro J 2020 Design of a new turbine for OWC Wave Energy Converters: the DDT concept *Renewable Energy* **169** pp 404–13

Preliminary flow measurements of a small-scale, vertical axis wind turbine for the analysis of blockage influence in wind tunnels

Luis Santamaría[1], Katia María Argüelles Díaz[1], Bruno Pereiras[1], Mónica Galdo Vega[1], José González Pérez[1], Sandra Velarde-Suárez[1] and Jesús Manuel Fernández Oro[1]

[1]Department of Energy, University of Oviedo. C/Wifredo Ricart s/n, Gijón, Asturias, 33204, Spain.

santamarialuis@uniovi.es

Abstract. The development of competitive lift vertical axis wind turbines (VAWTs) is yet a challenge in wind power research. New designs typically require wind tunnel testing before in site implementation. One of the major problems at the laboratory stage is the appearance of a significant flow blockage for small scale models, which affects the performance of the tested wind turbines and prevents the direct extrapolation of results to open field conditions without previous correction. Unfortunately, a suitable blockage correction for lift VAWTs has not been achieved yet, so more studies are needed in this research field to fill the gap. As part of preliminary work with this aim, a small scale VAWT prototype has been designed, constructed, and tested in a 1.15x1 m^2 test section wind tunnel with a semi-closed chamber, featuring a blockage ratio of 0.37. Preliminary aerodynamic measurements were performed for different tip speed ratios on the downstream near wake using a special 3-hole pressure probe. Results show that the wake velocity profiles present a velocity increase around the prototype with a low velocity region in the windward quadrant of the turbine, indicating an important influence of the tunnel boundaries. These preliminary measurements have given an initial insight on the aerodynamic relationships between turbine performance and flow patterns. Additionally, they will help to devise an appropriate strategy for the following experiments, with the final objective of developing a blockage correction for small scaled VAWTs.

1. Introduction

Nowadays, renewable energy projects are experimenting an exponential growth, with wind energy and solar photovoltaic in the lead. As wind energy projects increase worldwide, interest is rising in challenging fields, such as urban environments and deep-water, offshore sites. After receiving an important research effort in the last two decades, especially by the academic community, lift-type, vertical axis wind turbines (VAWT) are presented as good candidates for this kind of applications [1,2]. However, these turbines are still in a developing phase, and there is still a great research gap to fill and technical barriers to study and overcome.

Wind tunnel testing provides a necessary starting point in the experimental research of this kind of turbines. However, one of the main problems in wind tunnel testing is the prototype-tunnel interaction, which affects the characteristic turbine performance and flow, and is usually addressed as blockage. To

avoid this kind of interactions, prototypes are usually forced to be scaled down, hindering reliable torque measurements, and enhancing mechanical losses and self-starting issues. Furthermore, with the down-scaling, test conditions get harder, as small prototypes must withstand high rotational velocities. Consequently, most of the wind tunnel campaigns conducted on VAWTs feature a relevant level of blockage [3]. Hence, understanding turbine-tunnel flow relations is crucial to perform an objective analysis of experimental results, especially if their aim is to predict real-scale prototype behaviors.

2. Previous works in VAWT blockage

A first approach for wind tunnel testing of bluff objects, airfoils, propellers and airscrews was developed by Glauert [4] and later by Maskell [5] and Pope and Harper [6], laying the basis of blockage research. Savonius turbines blockage correction was addressed by Alexander and Holownia [7] first, and later by Ross and Altman [8]. Mikkelsen and Sørensen [9] developed a wall correction model for HAWT wind tunnel testing, based on the work by Glauert. Battisti et al. Dossena et al., studied Darrieus turbine blockage, basing their corrections on experimental thrust measurements [10,11]. Finally, the most recent contributions to Darrieus VAWT blockage was provided by Jeong et al. [12] and [13].

Nevertheless, despite the works mentioned, there is still limited knowledge about the fluid behavior and its effects in tests with relevant blockage levels.

With the aim of obtaining more information about wind tunnel-turbine interactions and improving the existing correction methods, the authors have started an experimental research campaign in this topic. As part of this campaign preliminary aerodynamic measurements have been performed and are presented in this work.

3. Experimental Set-up

3.1. Turbine.

The turbine used in this research is small-scale prototype of a straight bladed or H-Type VAWT, with 3 fixed blades with no pitch, featuring the airfoil “DU06-W-200” developed by Delft University [14]. It has a diameter (D) of 0.8 m, an effective blade span (H) of 0.52 m and a blade chord (c) of 0.065 m. These dimensions provide a solidity (σ) of 0.5 and an aspect ratio (H/D) of 0.65. The turbine was manufactured combining conventional materials such as: aluminum profiles, bearings, a steel shaft; with Fused Deposition Modeling (FDM) PLA parts where complex geometries were needed, as in the blades and the struts. The assembly of the turbine includes a 1kW DC motor, which allows great rotational speed control and a digital optical tachometer to measure axis rotational speed. A realistic sketch of the turbine assembly is shown in figure 1 a.).

3.2. Wind-Tunnel.

The turbine was tested in the Xixón Aero-acoustic Wind Tunnel (XAWT) which is a closed-circuit wind tunnel. This wind tunnel can achieve velocities up to 22 m/s featuring a mean turbulence intensity around 0.7%; additional data can be found in [15]. The original test chamber is 4.2 m long and has a cross-section of 4.45x2.80 m^2, while the test section is 1.15x1 m^2. This combination of turbine and test section dimensions gives a blockage ratio (projected turbine area over test section area) of 37%, which is a high-blockage condition, chosen so that blockage effects are noticeable. Usually, to avoid blockage effects in measurements, blockage ratio is kept under 10%.

To research blockage effects in a confined environment, a special modular test chamber was built with the same dimensions of the test section, formed by an empty duct module of 1 m (1.25D) and a module of 0.77 m (0.96D) in which the turbine is placed. The first module is devised to avoid disturbances in the inlet velocity, which is a known effect of solid blockage. As it is shown in [12] as the blockage ratio increases, the perturbation of inlet velocity is also greater, but occurs closer to the turbine. Thus, it is expected that the chosen duct length will be suitable, given the test wind velocity, blockage ratio, turbine dimensions and solidity. A characterization of the velocity distribution in the outlet of modular test chamber without the turbine was carried out to verify its suitability and make sure

that the boundary layer thickness was not relevant to the overall dimensions. The outlet of the modular test chamber is open to the original chamber, so the wake can expand freely and only wall and inlet section blockage is studied. In figure 1 b.) a realistic sketch of the modular test chamber is shown.

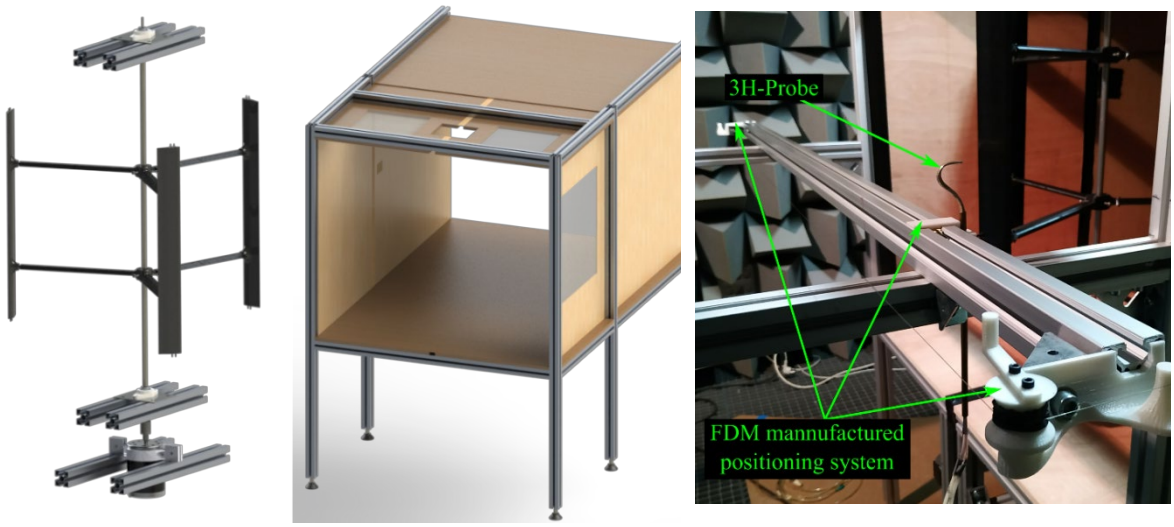

a) b) c)

Figure 1. a) VAWT model assembly, b) special test chamber, c) 3-hole probe and positioning system.

3.3. Instrumentation.

Regarding the instrumentation, inlet velocity is measured with a differential pressure sensor (CP210-R) with pressure tabs at the inlet and outlet of the nozzle. Additional pressure sensors were used to evaluate the pressure at several positions along the test chamber, but these are not relevant to the aerodynamic measurements presented in this work. At the outlet, the velocity profiles were measured using a special 3-Hole pressure probe called "Cobra-probe" designed and manufactured in earlier works by some of the authors. This type of probe is used to measure mean wind velocity and mean incidence angle, since its frequency response is too low to perform instantaneous measurements. More information can be found in [16,17]. The new calibration method devised and presented in [16] extends the angular range of this probe up to ± 80 ° which makes it suitable for its use in the vicinity of the turbine. Each probe tube is connected to a Validyne DP15-26 pressure transducer, each transducer to a voltage amplifier and finally each amplifier to a data acquisition card. The data acquisition card also receives the signals from the other pressure sensors and the tachometer. Equipment uncertainties are detailed in table 1.

Differential pressure sensor	Pressure transducers & amplifiers	Cobra probe	Positioning system	Tachometer
Inlet pressure difference: $\frac{u\Delta P_{0-1}}{\Delta P_{0-1}} = \pm 5.98\%$	Hole pressure measurement: $\frac{uP_i}{P_i} = \pm 0.25\%$	Angle: $\frac{u\alpha}{uP_i/P_i} \cdot 100 = = 0.6[°]*$	Probe displacement step $\frac{u\Delta x}{\Delta x} = \pm 6.6\%**$	Rotational speed: $\frac{un}{n} = \pm[0.09 - 0.16]\%$
Temperature for density correction: $\frac{uT}{T} = \pm 3.18\%$		Dynamic pressure: $\frac{uP_d}{uP_i} = \pm 0.95[\%]*$		

*(relative to the sensor uncertainty)
**(increased to account for possible random wire slip)

Table 1. Equipment uncertainties.

In order to measure several velocity profiles with precision and optimizing test times, a positioning system was designed and manufactured using FDM (figure 1 c.)). The system transforms the circular motion of a manual crank joined to a pulley, to linear displacement of a slider which carries the probe, by means of a non-elastic wire. The pulley has been designed so the that its perimeter is multiple of the test section width. In this way, different steps-sizes can be chosen as a function of the pulley's rotation. A general view of the wind tunnel and a diagram of the experimental set-up is shown in figure 2.

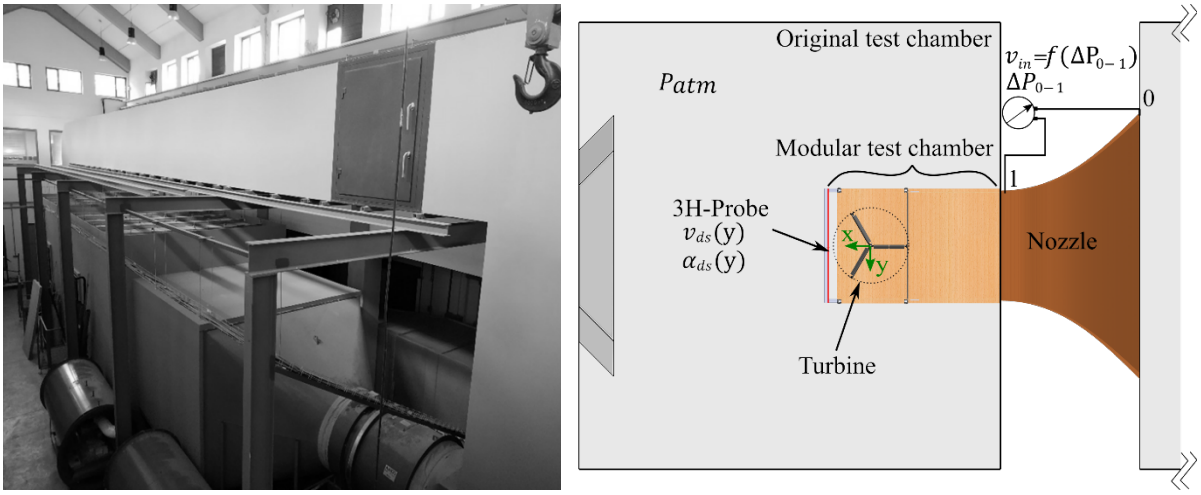

Figure 2. XAWT wind tunnel general view and experimental set-up diagram.

4. Measurements

Using the 3-hole cobra probe, downstream velocity profiles in a near wake position (0.59D) have been measured for 9 different tip-speed ratios (blade velocity over reference wind velocity) ranging from $\lambda = 0.87$ to $\lambda = 3.55$. The reference wind velocity was kept constant at approximately 7.5 m/s which is the velocity at the nozzle outlet. The different tip-speed ratios are achieved by spinning the turbine at different rotational speeds. The turbine is continuously driven by the DC motor which is controlled through voltage regulation. This procedure allows great rotational speed control. A lateral displacement step of approximately 3 cm (half crank turn) was chosen for the cobra probe, producing a total of 39 measurement positions. For each measurement, the chosen acquisition frequency and time were 1000 Hz and 5 s respectively, which was found to be sufficient to produce accurate averages. Figure 3, shows a picture taken during a measurement.

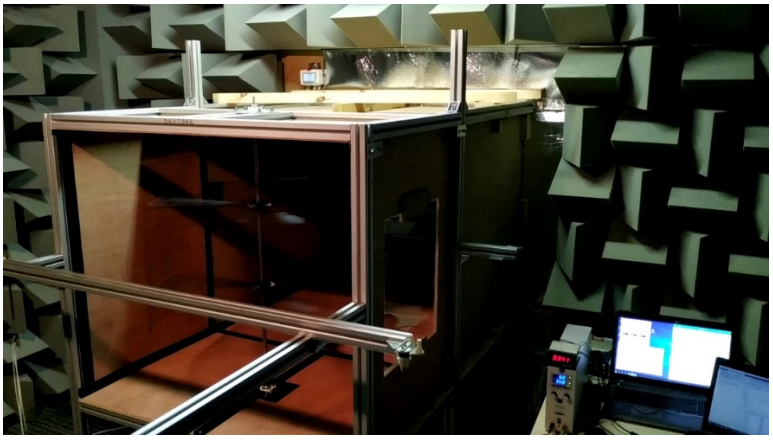

Figure 3. Picture taken during a measurement.

5. Results and discussion

A selection of 4 velocity profiles corresponding to tip-speed ratios: $\lambda = (0.87, 2.06, 2.76, 3.55)$ is presented in figure 4. The selected tip-speed ratios correspond to: a negative performance coefficient (C_P), a low positive C_P in the high slope zone, a high C_P where the slope is decreasing to approach the maximum and a C_P past the maximum with increasing slope, respectively. Vector representation was chosen for downstream velocity, normalized with the velocity at the inlet, to enhance visual interpretation of the data and downstream velocity angle is also shown independently in each sub-figure. The dotted blue lines indicate the position of the turbine; it rotates in the counterclockwise direction, so in the graphs, the leeward half corresponds to the negative normalized positions and the windward half to the positive ones.

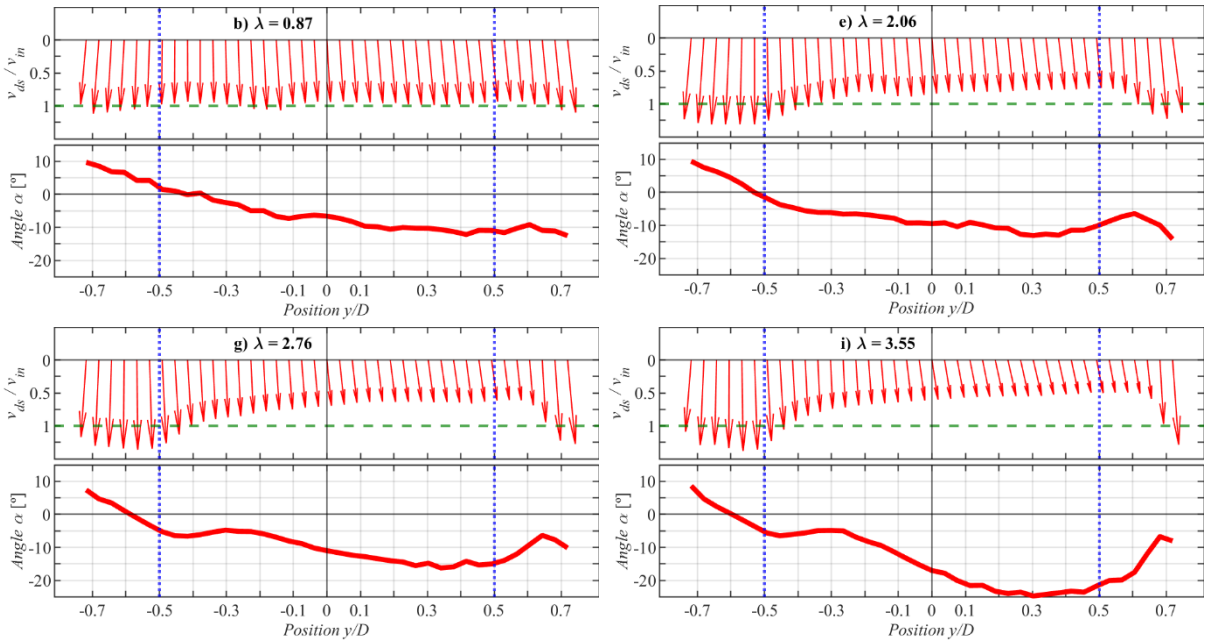

Figure 4. Selection of 4 downstream velocity profiles, showing the normalized downstream velocity in vector form and the velocity angle, over the normalized position.

- The velocity profile at $\lambda = 0.87$ shows a very light influence of the turbine rotation, with mean downstream velocities very close to the reference velocity. Incidence angles have the typical shape of an opening jet with a slight offset to the negative due to the effect of the turbine rotation.
- In the velocity profile at $\lambda = 2.06$ a marked increase in the velocity around the turbine can be appreciated, especially in the leeward zone, while the wake shadow starts to be noticeable. Incidence angle is not very different from the previous velocity profile, except from the zone corresponding to the gap between the turbine and wall in the windward side. There, the important increase in streamwise velocity, possibly because of the strong solid blockage in the area, produces a strong decrease in the absolute magnitude of the incidence angle.
- The velocity profile at $\lambda = 2.76$ exhibits the same trend as the previous ones, with minimum and maximum velocities greater than ±0.25 times the reference velocity. Regarding the incidence angle, there is an overall increase in the absolute value towards the negative direction.
- Finally, the velocity profile at $\lambda = 3.55$ shows a clear wake shadow region, revealing an important increase in the absolute value of the incidence angle towards the negative direction. This noticeable increase is the result from the combination of strong solid blockage with its consequent decrease in streamwise velocity, and the increase in turbine rotational speed.

For a more general approach, downstream streamwise velocity and incidence angle measurements from every tip-speed ratio are shown in a contour plot in figure 5. Turbine position is indicated with black dashed lines.

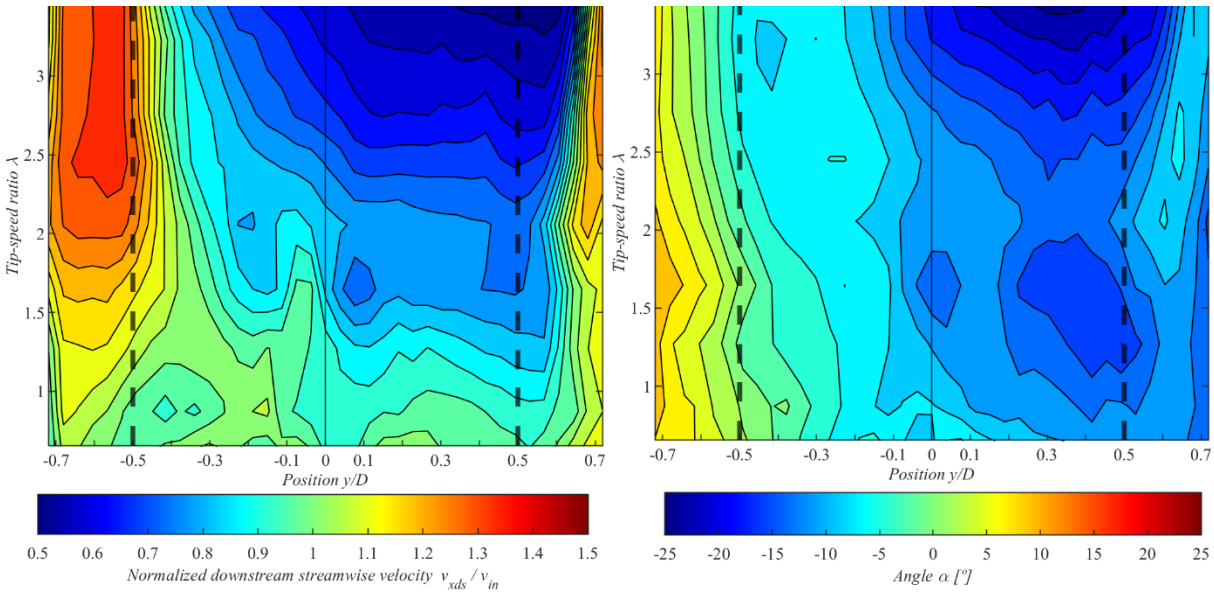

Figure 5. Contour plot of the downstream streamwise normalized velocity and the incidence angle.

A general common trend can be observed among all the measurements. There is a progressive increase of the streamwise component of the downstream velocity, around the turbine, in the leeward half, as tip speed ratio increases. On the other hand, in the same zone of the windward half, the opposite effect is appreciated, with a strong decrease in the streamwise component of the downstream velocity. A clear shadow of the wake can be observed as a decrease of the streamwise component of the downstream velocity, both in the leeward and windward halves, though stronger in this last one.

The incidence angle of the leeward side experiences a slight decrease in the absolute value, responding to a greater increase in streamwise velocity than that of the spanwise component, throughout the tip-speed ratio range. However, in the windward side, there is a strong increase in the incidence angle towards the negative direction, due to both the stronger relevance of the spanwise component induced by the turbine rotation, and the high blockage zone and its consequential decrease in streamwise velocity component.

Although the observed behavior matches the expected, the difference between the streamwise velocity from the reference velocity, and the magnitude of the incidence angle are really notable, indicating a strong influence of the wind tunnel-prototype interaction in the flow field.

6. Conclusions

Preliminary aerodynamic measurements were performed on a small-scale H-VAWT prototype in a confined environment featuring high solid blockage level, but free wake expansion, for a wide range of tip-speed ratios.

These preliminary measurements have given an initial insight on the aerodynamic relationships between turbine performance and flow patterns. Those measurements will be a starting point to complement ongoing investigations on blockage correction.

The 3-hole pressure probe developed in earlier works turned out to be a great tool to measure mean velocity profiles close to the turbine, due to its wide range, its simplicity, and the relatively low uncertainties of the measurements.

Likewise, the modular test chamber devised offers and interesting approach, permitting the study of solid blockage detached from wake blockage.

In future works, downstream velocity profiles will be measured with the same methodology and equipment at different heights, focusing specially on the lower and upper gaps. Additionally, the combination of these measurements and those from the other pressure sensors in the test chamber will allow an estimation of the turbine performance through the control volume theory. Moreover, the modular test chamber allows easy wall removal, which will be useful to perform future measurements in an unconfined environment and obtain and interesting comparison.

Further tests for different blockage conditions will shed more light on how the wind tunnel conditions are affecting turbine performance and, therefore, allow a deeper understanding of the obtained results.

Acknowledgments
The authors wish to thank the support of: MINECO, Spain [ENE 2017-89965], Principality of Asturias [GRUPIN-IDI/2018/000205], University Institute of Industrial Technology of Asturias (IUTA) and Ayto. Gijón [SV-18-GIJON-1-05, SV-19-GIJON-1-15, SV-20-GIJON-1-17].

References

[1] Kumar R, Raahemifar K and Fung A S 2018 A critical review of vertical axis wind turbines for urban applications *Renewable and Sustainable Energy Reviews* **89** 281–91
[2] Hand B, Kelly G and Cashman A 2021 Aerodynamic design and performance parameters of a lift-type vertical axis wind turbine: A comprehensive review *Renewable and Sustainable Energy Reviews* **139** 110699
[3] Battisti L, Persico G, Dossena V, Paradiso B, Raciti Castelli M, Brighenti A and Benini E 2018 Experimental benchmark data for H-shaped and troposkien VAWT architectures *Renewable Energy* **125** 425–44
[4] Glauert H 1933 Wind Tunnel Interference on Wings, Bodies and Airserews *Aeronautical Research Committee Reports and Memoranda*
[5] E. C. Maskell 1963 A Theory of the Blockage Effects on, Bluff Bodies and Stalled Wings in a Closed Wind Tunnel *Reports and Memoranda*
[6] J.J. Harper, Pope A 1966 *Low Speed Wind Tunnel Testing* (John Wiley & Sons)
[7] Alexander A J and Holownia B P 1978 Wind tunnel tests on a savonius rotor *Journal of Wind Engineering and Industrial Aerodynamics* **3** 343–51
[8] Ross I and Altman A 2011 Wind tunnel blockage corrections: Review and application to Savonius vertical-axis wind turbines *Journal of Wind Engineering and Industrial Aerodynamics* **99** 523–38
[9] Sørensen J N, Shen W Z and Mikkelsen R 2006 Wall correction model for wind tunnels with open test section *AIAA Journal* **44** 1890–4
[10] Battisti L, Zanne L, Dell'Anna S, Dossena V, Persico G and Paradiso B 2011 Aerodynamic measurements on a vertical axis wind turbine in a large scale wind tunnel *Journal of Energy Resources Technology, Transactions of the ASME* **133** 1–9
[11] Dossena V, Persico G, Paradiso B, Battisti L, Dell'Anna S, Brighenti A and Benini E 2015 An experimental study of the aerodynamics and performance of a vertical axis wind turbine in a confined and unconfined environment *Journal of Energy Resources Technology, Transactions of the ASME* **137**
[12] Jeong H, Lee S and Kwon S D 2018 Blockage corrections for wind tunnel tests conducted on a Darrieus wind turbine *Journal of Wind Engineering and Industrial Aerodynamics* **179** 229–39
[13] Carbó Molina A, De Troyer T, Massai T, Vergaerde A, Runacres M C and Bartoli G 2019 Effect of turbulence on the performance of VAWTs: An experimental study in two different wind tunnels *Journal of Wind Engineering and Industrial Aerodynamics* **193**
[14] Claessens M C 2006 The design and testing of airfoils for application in small vertical axis wind turbines *Masters Thesis* 1–137

[15] Rodríguez Lastra M, Fernández Oro J M, Galdo Vega M, Blanco Marigorta E and Santolaria Morros C 2013 Novel design and experimental validation of a contraction nozzle for aerodynamic measurements in a subsonic wind tunnel *Journal of Wind Engineering and Industrial Aerodynamics* **118** 35–43
[16] Díaz K M A, Oro J M F and Marigorta E B 2008 Extended angular range of a three-hole cobra pressure probe for incompressible flow *Journal of Fluids Engineering, Transactions of the ASME* **130** 1014011–6
[17] Argüelles Díaz K M, Fernández Oro J M, Blanco Marigorta E and Barrio Perotti R 2010 Head geometry effects on pneumatic three-hole pressure probes for wide angular range *Flow Measurement and Instrumentation* **21** 330–9

3D flow compensation for a 2D CFD numerical model of a VAWT in confined environments with high blockage

Luis Santamaría, Katia María Argüelles Díaz, Mónica Galdo Vega
Sandra Velarde-Suárez, Bruno Pereiras García and José González Pérez*
Área de Mecánica de Fluidos. Departamento de Energía Universidad de Oviedo, C/Wifredo Ricart s/n, Gijon, Asturias, 33204, SPAIN

INTRODUCTION

The world energetic framework is continuously evolving, motivated by global policies and increasingly promotes the use of sustainable energy. In this context, vertical axis wind turbines (VAWT) are called to have an important role, as they are good candidates for urban environments, microgeneration, and deep-water offshore installations. The development of such turbines is still a research topic, using the Computational fluid dynamics (CFD) and also in experimental set-ups. Adequately modeling the flow in a realistic way would require 3D CFD simulations. However, this would entail massive mesh sizes for achieving reliable results, translating to an unaffordable computational cost. Hence, the development of a methodology to correct 2D CFD simulations to compensate for 3D flow effects is inherently interesting. Experimentally, as progress is made in the study of the fluid-machine interactions, the turbines are tested in wind tunnels, as the one presented in this work, which is a high-blockage, semi-confined set-up.

This work presents a methodology to achieve the 3D flow compensation using 2D CFD simulations of VAWT in confined environments with high blockage. This methodology has been applied to a real set-up results and good agreement has been finally achieved.

CFD MODELING AND SCALING

To replicate the experimental set-up results, a full 2D URANS model of the VAWT turbine positioned on the extended casing of the wind tunnel nozzle has been developed, more details about the experimental set-up can be found in [1]. As recommended in the literature [2], the k-ω SST turbulence modelling has been used. Special care has been paid to the spatial discretization of wall-adjacent mesh, with up to 450 nodes in the streamwise direction of the airfoil and further refinement in the normal direction to guarantee $y^+ = 1$, according to [3]. The resulting mesh is a [450×40] O-mesh distribution over the blades and a total number of 350,000 cells for the whole domain (Fig. 1). The two main dimensions of the set-up are H = 0.6 m and L = 1 m. The sliding mesh technique was employed to resolve the rotational motion of the turbine, with a variable time-step size equivalent to 0.25º of angular displacement for every tip-speed ratio. At least, five complete rotations of the turbine were necessary to assure the periodic response of the aerodynamic torque.

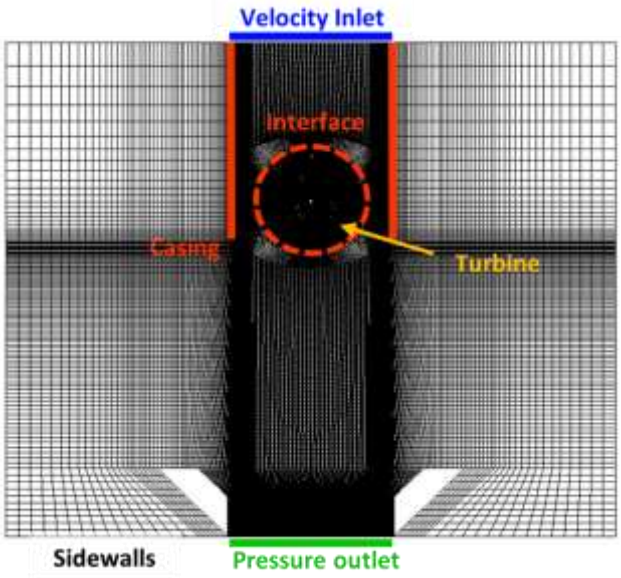

FIG 1. Numerical 2D model of the rotating turbine.

The experimental set-up is shown in Figure 2. Above and below the turbine there is a considerable gap (0.33H). Thus, at high tip-speed ratios, the flow is prone to avoid the turbine. This is shown in Fig. 2, by the mean velocity vectors measured in the mid-plane and the center of the gap, with a 3-hole pressure probe. The tip-speed ratio corresponds to the maximum power coefficient point.

To account for this effect, some scaling factors are introduced. Calculating the ratio of the volumetric flow rates in both 2D and 3D situations (in 2D, the flow rate is per unit length; whereas in 3D it is considering the real transversal section), and assuming that it must be similar, a scaling factor for the tip-speed ratios between the 2D and 3D cases is obtained. On the other hand, considering the cubic dependence of the power coefficient with respect to the bulk velocities, a scaling factor for the power values can be also derived, yielding to the following equations:

$$\lambda_{3D} = \lambda_{2D}\frac{H}{L} \quad (1) \qquad C_{p,3D} = C_{p,2D}\left(\frac{H}{L}\right)^3 \quad (2)$$

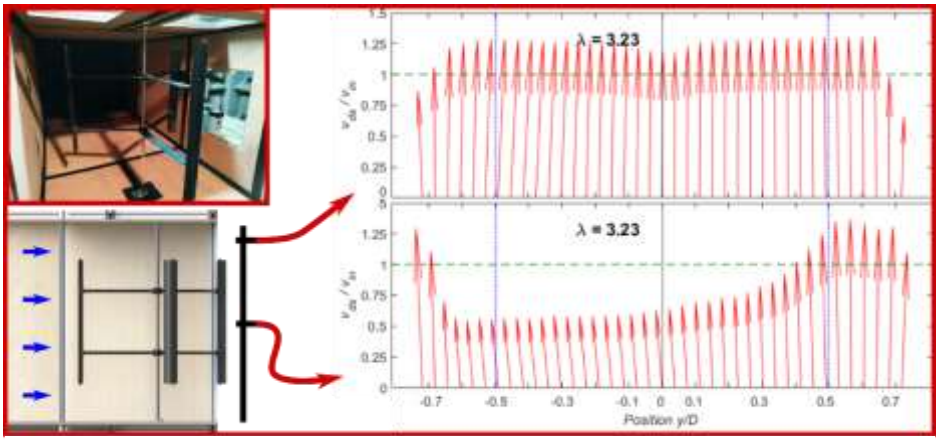

FIG 2. Experimental set-up and normalized mean velocity profiles in the mid plan and gap center, measured with a 3-hole pressure probe.

A complete range of equivalent tip-speed ratios, going from 1.5 to 3.9, have been simulated for an inlet velocity of 7.5 m/s, to obtain the aerodynamic power curve of the turbine.

RESULTS

Some examples of the normalized mean streamwise velocity contours obtained in the CFD simulations are shown in Fig. 3. As expected, as the tip speed ratio increases, the flow differs from the reality, exhibiting a major velocity increase in the sides.

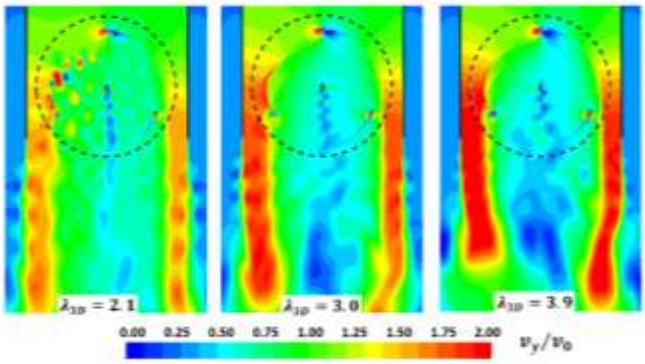

FIG 3. Normalized mean streamwise velocity contours from CFD simulations at 3 equivalent tip-speed ratios.

The raw and corrected CFD performance curves, considering Eqs. (1) and (2), are plotted in Fig. 4 and compared with the experimental results. It is clear that the raw CFD magnitude of tip-speed ratio and performance is far off from the reality. However, after the scaling is performed, following the method proposed, the corrected CFD curve matches remarkably well the experimental performance curve. This confirms the validity of the suggested 3D flow compensation procedure, allowing the achievement of realistic results without the huge computational costs of a complete 3D simulation.

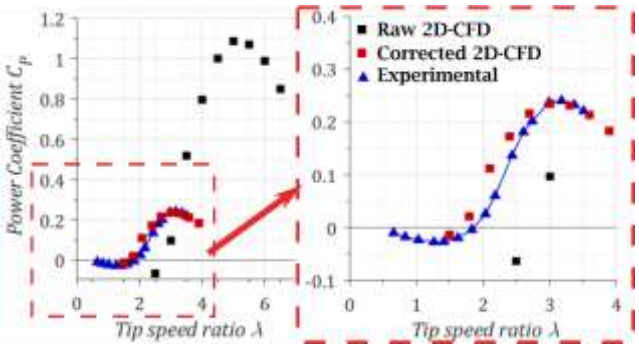

FIG 4. Raw and corrected CFD performance curves against experimental results.

CONCLUSIONS

In the present article, a numerical approach to modify the 2D CFD simulations for a VAWT, trying to account for the 3D effects, is presented. The turbine has also been experimentally tested in a confined environment, with high blockage, which is resembled by the numerical model. Velocity profiles of both CFD and experimental results have been compared, justifying the need of the procedure. Finally, after considering the proposed method, good agreement has been found between the corrected CFD and the experimental performance curve.

—

*aviados@uniovi.es

[1] Luis Santamaría, Jesús Manuel Fernández Oro, Katia María Argüelles Díaz, et al. Novel methodology for performance characterization of vertical wind turbines (VAWT) prototypes through active driving mode. Energy Conversion and Management. (In press)
[2] Rezaeiha A, Montazeri H, Blocken B. Towards accurate CFD simulations of vertical axis wind turbines at different tip speed ratios and solidities: Guidelines for azimuthal increment, domain size and convergence. Energy Conversion and Management 2018;156:301–16 https://doi.org/10.1016/j.enconman.2017.11.026.
[3] Castelli MR, Masi M, Battisti L, Benini E, Brighenti A, Dossena V, et al. Reliability of numerical wind tunnels for VAWT simulation. Journal of Physics: Conference Series 2016;753. https://doi.org/10.1088/1742-6596/753/8/082025.

ANEXO II

TRABAJOS EN CURSO

Anexo II.I. Desarrollo, ensayo y validación de un sistema modular automatizado de posicionamiento de sondas (MAPPS) de hilo caliente (HW) para ensayos en túnel de viento.

Los ensayos experimentales en túnel de viento son una parte muy importante del desarrollo de todo tipo de productos, como vehículos, turbomáquinas o construcciones civiles e industriales. Dentro de este tipo de ensayos, se encuentran los que se centran en caracterizar el flujo, con tecnologías como la velocimetría con hilo caliente (HW). Sin embargo, este tipo de medidas suelen ser tediosas y difíciles de ejecutar, ya que requieren gran precisión en el posicionamiento de las sondas y gran cantidad de puntos de medida. Esto limita enormemente su aplicación, y generalmente se opta por realizar únicamente medidas en dos dimensiones y con mallas de puntos con poca resolución espacial.

Para dar respuesta a este problema, en el marco de esta tesis y de la línea de investigación sobre VAWT, se ha planteado un diseño conceptual de un sistema modular automatizado de posicionamiento de sondas (MAPPS) para el Área de Mecánica de Fluidos de la Universidad de Oviedo, que permitirá realizar medidas automatizadas en 3 dimensiones y que cuenta con un gran espacio de trabajo.

Para la ejecución del proyecto se ha emprendido una colaboración con el Área de Ingeniería de Fabricación de la Universidad de Oviedo. Gracias a esta colaboración, el diseño conceptual ha evolucionado al actual diseño, ya construido y que se encuentra en pruebas (**Figura II.I**).

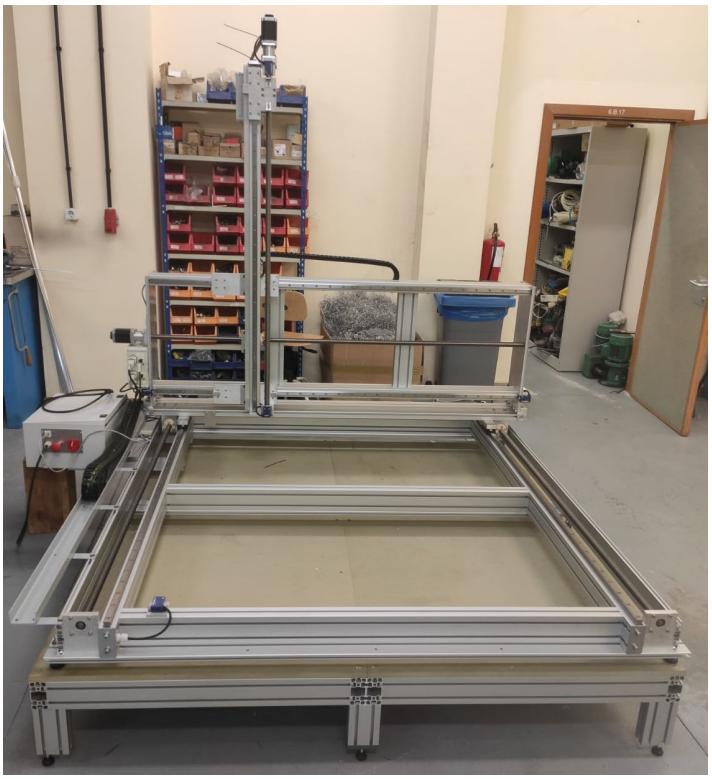

Figura II.I. Sistema modular automatizado de posicionamiento de sondas (MAPPS) en 3 dimensiones.

El primer trabajo previsto es la realización de un Trabajo Fin de Grado, cuyo objetivo será caracterizar el flujo 3D en la estela de un cilindro. Este trabajo permitirá probar, mejorar y validar el sistema gracias a la sencillez de la forma estudiada y al alto grado de caracterización disponible en la bibliografía.

Una vez validado el equipo, está previsto utilizarlo para caracterizar el flujo no estacionario en la estela de prototipo de VAWT estudiado en este trabajo.

Anexo II.II. Optimización y reducción de la incertidumbre de una balanza aerodinámica para ensayos en túnel de viento

Tras la campaña experimental que dio lugar a la publicación del Capítulo 2, se identificaron ciertas áreas de mejora, tanto en la metodología como en el equipamiento experimental. Como resultado, el montaje ha experimentado una importante evolución.

En primer lugar, se ha implementado un sistema de orientación de la balanza con motor paso a paso (BOSS) (**Figura II.II, (a)**). Este sistema está basado en la articulación inferior de un brazo robótico industrial de pequeño tamaño, y permite variar la posición angular con gran precisión y repetibilidad. Además, incluye un sensor Hall de posición que asegura una posición de referencia común en todos los ensayos. El control del sistema se ha elaborado utilizando un controlador de impresora 3D basado en Arduino Mega y el firmware Open-Source Marlin.

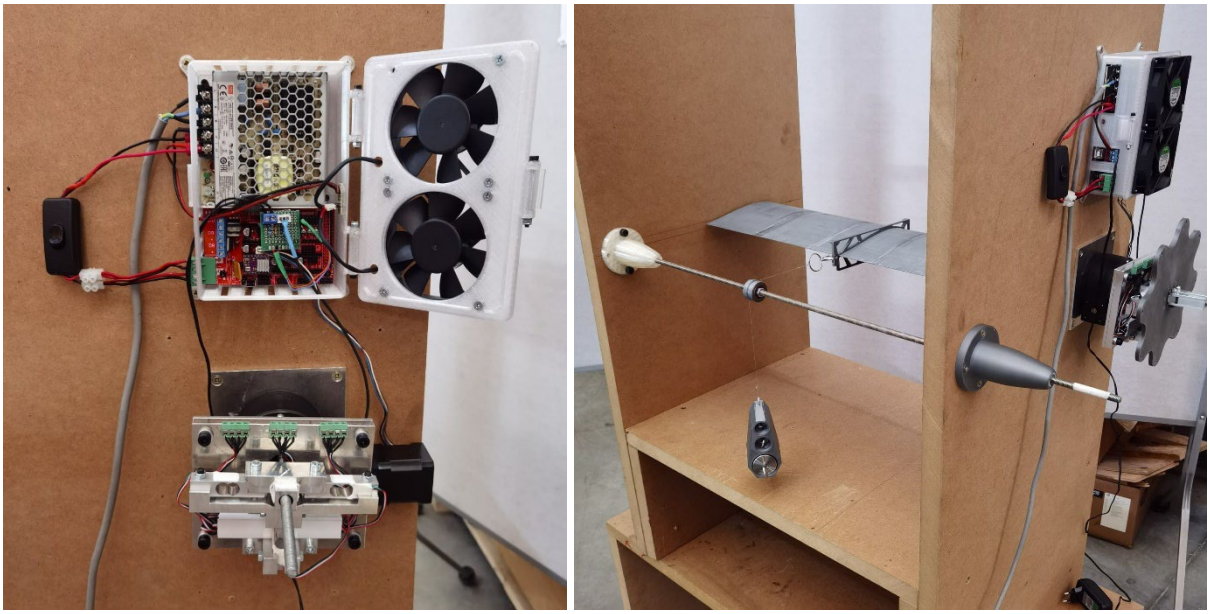

(a) (b)

Figura II.II. (a) Sistema de orientación de la balanza mediante motor paso a paso (BOSS). (b) Sistema de cargas de calibración con pesos, calibrados y utillajes de calibración.

Adicionalmente, se ha rediseñado el sistema de cargas de calibración para minimizar la incertidumbre asociada a este proceso. Se han adquirido pesos calibrados de laboratorio y se han fabricado utillajes específicos para combinar varios pesos y cubrir el rango de las balanzas disponibles en el laboratorio (**Figura II.II, (b)**).

Finalmente, se están estudiando las metodologías de calibración disponibles para implementar una solución que permita realizar una calibración de amplio rango con un número reducido de cargas. Esto es del máximo interés, porque las fuerzas de arrastre y sustentación varían sustancialmente con el ángulo de ataque, por lo que obtener una caracterización precisa en todo el rango es una tarea compleja. A partir de las mejoras planteadas y, sobre todo, del trabajo sobre metodologías de calibración, se está preparando una publicación.

Anexo II.III. Ensayos a escala real y optimización de un prototipo de VAWT para entornos urbanos

Partiendo de la base de conocimiento generada durante los años de realización de esta tesis, actualmente se está preparando una campaña experimental sobre un prototipo a escala real. El prototipo, de 2 kW de potencia nominal, tiene un diámetro de 2.2 m, una altura del rotor de 3.2 m y una altura de torre de 5 m aproximadamente (**Figura II.III**).

En una primera fase de los experimentos se evaluará el rendimiento y la producción de energía del rotor de referencia comercial provisto por el fabricante. Asimismo, también se realizarán ensayos aero-acústicos, ya que este tema es de gran importancia en esta aplicación. Posteriormente se modificará el rotor aplicando la experiencia y conocimientos adquiridos en la tesis, buscando obtener una mejora significativa de las prestaciones de la turbina. Una vez modificado el rotor, se repetirán los ensayos y se elaborarán las conclusiones pertinentes. Aunque este trabajo va dirigido hacia la parte de transferencia de conocimiento, también se prevé generar una publicación.

(a) (b)

Figura II.III. (a) Prototipo a escala real de VAWT recién recibido. (b) Prototipo montado sobre una sección de tubería y probado frente a un túnel de viento abierto.

Universidad de Oviedo